A Genetic Interaction Analysis Identifies Novel Cancer Driver Modifiers and a Combination Therapy

A genetic interaction analysis identifies novel cancer driver modifiers and a combination therapy

A dissertation presented

by

Sida Liao

To

The Division of Medical Sciences

In partial fulfillment of the requirements

for the degree of

Doctor of Philosophy

in the subject of

Biological and Biomedical Sciences

Harvard University

Cambridge, Massachusetts

April 2019

Dissertation Advisor: Dr. Stephen J. Elledge Sida Liao

A genetic interaction analysis identifies novel cancer driver modifiers and a combination therapy

Abstract

A large number of cancer drivers have been identified through tumor sequencing efforts but how they interact and the degree to which they can substitute for each other has not been systematically explored. To comprehensively investigate how cancer drivers genetically interact, I searched for modifiers of EGFR dependency by performing CRISPR, shRNA and expression screens in a non-small cell lung cancer model. I elucidated a broad spectrum of TSGs and OGs that can genetically modify proliferation and survival of cancer cells when EGFR signaling is altered. I found that mutation of *PBRM1*, a subunit of the SWI/SNF complex, attenuates the effects of EGFR inhibition in part by sustaining AKT signaling. I also found that mutation of Capicua (*CIC)*, a transcriptional repressor, suppresses the effects of EGFR inhibition by partially restoring the EGFR-promoted gene expression program including the sustained expression of Ets transcription factors like *ETV1*. Together, my data provide strong support for the hypothesis that many cancer drivers can substitute for each other in certain contexts and broadens our understanding of EGFR regulation.

I further applied this strategy of searching for cancer driver modifiers to another cancer disease model to test its generality. Bromodomain and extraterminal domain inhibitors (BETis) show efficacy on NUT midline carcinoma (NMC). However, not all NMC patients respond, and responders eventually develop resistance and relapse. Using CRISPR and ORF expression screens,

I systematically examined the ability of cancer drivers to mediate resistance of NMC to BETis and uncovered six general classes/pathways mediating resistance. Among these, I found that *RRAS2* attenuated the effect of JQ1 in part by sustaining ERK pathway function during BRD4 inhibition. Furthermore, overexpression of Krüppel-like factor 4 *(KLF4)*, mediated BETi resistance in NMC cells through restoration of the E2F and MYC gene expression program. Finally, I found that expression of cyclin D1 or an oncogenic cyclin D3 mutant or *RB1* loss protected NMC cells from BETi-induced cell cycle arrest. Consistent with these findings, cyclin-dependent kinase 4/6 inhibitors showed synergistic effects with BETis on NMC *in vitro* as well as *in vivo*, thereby establishing a potential two-drug therapy for NMC.

Table of Contents

Acknowledgments

Words cannot express my gratitude to my thesis advisor, Dr. Stephen J. Elledge. For the past five years, Steve has taught me how to think critically, how to think as a geneticist, how to think outside of the box, and how to attend to detail. His intelligence, passion and curiosity for science, broad knowledge and critical thinking is an everyday inspiration for me – he is not only my mentor but also a role model for me. I also want to thank Steve for his kind and generous support outside of the lab during the downs in my personal life.

I feel lucky to have the chance to work with Steve and all the talented people in the Elledge lab. There is no single person from whom I have not learned in the Elledge lab. I would like to thank Teresa Davoli, Mohammad Haj Dezfulian, Tomasz Kula and Kamila Naxerova for numerous inspirational conversations and valuable research advice. I would like to thank Kristen Mengwasser and Laura Sack for their mentorship when I first joined the lab. I would like to thank Yumei Leng, Mamie Li and Anthony Liang for generating the libraries I used in my screens and their help in my experiments. I would like to thank Eric Wooten for his help with my computational analyses. I would like to thank anyone with whom I crossed paths in this lab – it is because of each and every one of you that Elledge lab is such a joyful workplace for me. I would like to thank my collaborator, Ophélia Maertens, for helping me with the mouse experiments.

I would like to thank the members of my Dissertation Advisory Committee: Dr. Alex Toker, Dr. Karen Cichowski, and Dr. Myles Brown. Their insightful feedback and guidance were extremely valuable in the progression of my projects. I would also like to thank Dr. Christopher

A. French, Dr. Michael T. Hemann, Dr. Matthew L. Meyerson, and Dr. Alex Toker for their generosity in taking the time to serve as my dissertation defense examiners.

I would like to thank my undergraduate mentors, Dr. Hong Zhu, Dr. Bo Yang, and Dr. Qiaojun He, for inspiring me to embark on this journey to become a biomedical researcher.

Finally, I would like to thank my parents for their unwavering love and support throughout my life – words cannot express my gratitude to them.

Chapter 1

Introduction

Cancer is a complex family of diseases. It is characterized by an abnormal growth of cells caused by the accumulation of genetic and epigenetic changes. While the tissue of origin and molecular mechanisms of tumorigenesis vary according to different types of cancers, the overall result is dysregulated balance of cell proliferation and cell death that ultimately evolves into a populations of cells that can invade tissues and metastasize to distant sites, causing significant morbidity and, if untreated, death of the host (1).

Genetic basis of cancer

The earliest insights into the genetic basis of cancer could be traced back over a century ago. Using microscopy, David von Hansemann (2) and Theodor Boveri (3) observed the aberrant segregation of chromosomes during mitoses and postulated that cancer is a disease caused by defects in chromosomes. Later it was shown that carcinogens that damage DNA and generate mutations, such as ionizing radiation, can cause cancer (4), further solidifying the genetic basis of cancer.

The first experimental proof of the causal link between DNA and tumorigenesis is that total genomic DNA isolated from human cancers was able to transform normal NIH-3T3 mouse cells into cancer cells (5, 6). This was followed by identification of the specific gene responsible for this transforming activity – a single base substitution in the *HRAS* gene (c.35G> T; p.G12V) (7, 8). This is the first report that a single mutation of a normal cellular proto-oncogene can result in its activation and oncogenic activity. Since then, more and more oncogenes (OGs), activation of

which contributes to tumorigenesis, and tumor suppressor genes (TSGs), whose loss of function (LOF) contributes to tumorigenesis, have been discovered (9, 10).

We now know that various genetic alterations can result in the activation of OGs, including missense mutations, gain of chromosomes and chromosomal segments, translocations, overexpression etc. While inactivation of TSGs can be caused by nonsense or missense mutations, splice mutations, frameshifts, deletions, epigenetic silencing, or downregulation (11).

Cancer Genomics

Once it was established that cancers are caused by the accumulation of genomic alterations, a key goal of cancer research has been to analyze the cancer genome and to elucidate the underlying molecular mechanisms by which the cancer genome alterations contribute to cancer pathogenesis, then to use this information to improve cancer diagnosis and treatment.

Introduction of next-generation sequencing (NGS) technology has allowed cancer genomics studies to move from candidate-gene sequencing to an unbiased genome-wide level. The first whole cancer genome sequence was reported in 2008, where an acute myeloid leukemia genome and its matched normal counterpart obtained from the same patient's skin were described (12). Since then, the whole genomes of various tumor types have been sequenced and the number of sequenced cancer genome is further expanded by large-scale projects that compare tens of thousands of cancer and normal genomes, such as The Cancer Genome Atlas (TCGA) (https://cancergenome.nih.gov), the Catalogue Of Somatic Mutations In Cancer (COSMIC) (http://cancer.sanger.ac.uk), the International Cancer Genome Consortium (http://icgc.org), and

the Pediatric Cancer Genome Project (http://explore.pediatriccancergenomeproject.org). The end result of these sequencing efforts is a catalog of genomic alterations across the major human cancer types.

Cancer Drivers and Passengers

It is now clear that certain basic conditions related to the classic hallmarks of cancer must be satisfied during tumor initiation and progression (13). These include: 1) self-sufficiency in growth signals; 2) insensitivity to anti-growth signals; 3) evading apoptosis; 4) limitless replicative potential; 5) sustained angiogenesis; 6) tissue invasion and metastasis development; 7) abnormal metabolic pathways; and 8) evading the immune system. One key goal of cancer research is to identify the genes that actively facilitate these hallmark processes – the cancer driver genes. Identification of cancer driver genes is crucial to the understanding of the molecular mechanism underlying tumor pathogenesis and can be translated into diagnostic and therapeutic strategies. These large datasets of genome-wide mutations across various cancer types enable the potential to identify cancer drivers bioinformatically based on their mutational signature. While the cancer genome can harbor a large number of random mutations through carcinogen-induced DNA damage and genomic instability (14, 15), the genetic alterations of cancer driver genes will undergo Darwinian selection during tumor evolution and thus their relative enrichment and recurrence in tumors will occur relative to the passenger genes. Therefore, it remains an ongoing effort to distinguish cancer driver genes from passenger genes, and the frequency of mutagenesis of individual drivers is likely to vary in a tissue specific manner, requiring tumor-type stratification to identify such drivers.

Various computational tools have been developed to identify these cancer driver genes. Some are based on the frequency of mutations in an individual gene compared with the background mutation rate in the specific nucleotide context (16, 17). Other methods are based on the predicted functional significance of the amino acid changes caused by the mutations, as inferred from protein structure studies (18, 19).

We previously developed an algorithm called TUSON Explorer to identify known and putative cancer drivers using human tumor sequencing data (20). This method quantifies the likelihood that a gene is a cancer driver based on the distortion of its mutational signature from the pattern expected for a "neutral" gene. For example, TSGs will have a higher ratio of LOF to benign mutations than neutral genes, while OGs will have a higher ratio of missense to benign mutations than neutral genes, and these missense mutations tend to cluster together (Fig. 1).

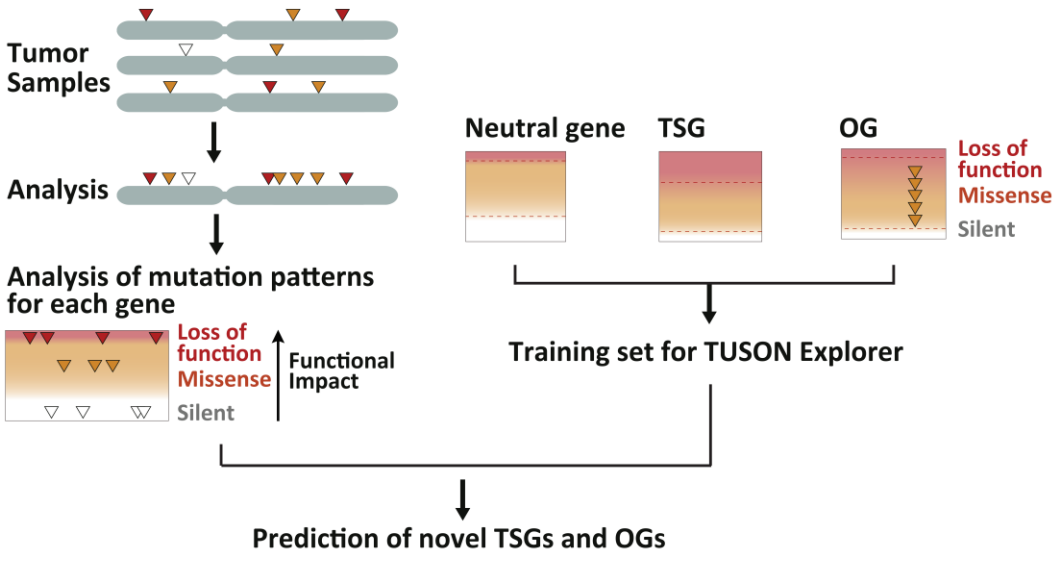

Figure 1. Schematic of the pipeline used by TUSON Explorer to predict TSGs and OGs.

Attempts to identify these cancer drivers based on patterns of mutagenesis in tumors have uncovered a bewilderingly large number of genes that bear the signature of genetic selection in tumors. Rather than a defined number of cancer drivers, there exists a continuum of genes that appear with increasingly lower frequency and potency in pan-cancer analyses. For the majority of cancer types, the overall genomic mutational landscape consists of a small number of "mountains" (commonly altered genes detected in a high percentage of tumors) and a much larger number of "hills" (genes altered in a limited cases), plus a "long tail" of massive amount of rare mutations (21-24).

Unraveling how the genes in this large network contribute to tumorigenesis poses a significant challenge for geneticists. First, while it is clear that certain basic conditions related to the classic hallmarks of cancer (e.g., immortalization and dysregulated proliferation) must be satisfied during tumor development (13), it is currently unclear if and how many cancer genes operate to achieve these conditions.

Furthermore, bioinformatic analysis of the cancer genome encounters many challenges and there are many situations where passenger events are difficult to distinguish from *bona fide* cancer drivers, thus creating "false positives". For example, cancers that have defects in mismatch-repair (MMR) genes carry tens of thousands of small insertions and deletions in short tandem repeats (known as microsatellites) (25). Such clusters of passenger mutations make it particularly challenging to distinguish mutated cancer genes from passenger genes. A similar problem arises when there is an increased mutation rate restricted to a small region of the genome. For example, many loci in the genome are intrinsically fragile and are associated with a high frequency of chromosome breakage. Genes in those fragile regions thus frequently display mutational patterns

such as rearrangements and deletions that are similar to, thus difficult to be distinguished from, those found in certain recessive TSGs, e.g. PTEN (26, 27). Another example is that while point mutations only affect a single gene, genomic alterations such as copy-number changes can affect many genes at a given genomic locus, making it difficult to deprioritize the passenger genes whose copy-number changes are simply due to chromosomal linkage to neighboring *bona fide* cancer drive genes. Therefore, the validity of the novel cancer driver genes identified through bioinformatical approaches still require experimental verification.

Finally, while the selection pressure on those putative cancer drivers based on *in silico* analysis suggests they play a role in cancer development, their biological functions in tumorigenesis and the underlying molecular mechanisms remain largely unknown, especially for the large number of genes that fall on the "long tail" side of the cancer driver landscape. It is an ongoing effort to characterize the biological function of these putative cancer drivers.

Genetic Screens for Cancer Driver Discovery

Traditionally, researchers have to study the functional impact and phenotypes of genetic alterations one at a time. The basic procedure of this approach involves generating the mutant gene through cloning, site-directed mutagenesis or knock-down/knock-out methods and comparing the effect of the mutant with the wild type in various cancer-related phenotypic assays, such as biochemical properties, signaling pathway activation/inhibition, anchorage-independent growth, *in vivo* tumorigenesis, or invasion and migration. Such an approach has facilitated the

identification and characterization of many cancer driver genes; however, it is time-consuming and not readily scalable.

Advances in the genetic screening technologies have allowed geneticists to determine the genetic basis responsible for a phenotype in an unbiased, high-throughput and genome-scale manner. To identify which genes contribute to a specific biological phenotype without prior knowledge of the potential candidates, geneticists use forward genetic screens. The basic procedure of this approach involves modifying or modulating the expression of many genes, screening or selecting for the cells or organisms with the phenotype of interest, and then characterizing the mutations that result in these phenotypic changes (28). A survey of some of the major tools currently used in forward genetic screens is described as follows.

RNA Interference

RNA Interference (RNAi) is a conserved endogenous pathway in which RNA molecules inhibit gene expression or translation and neutralize targeted mRNA molecules on the basis of sequence complementarity (29, 30). Two types of reagents – small interfering RNAs (siRNAs), and small hairpin RNAs (shRNAs) – are typically used in mammalian cell screens (31). A major drawback of RNAi screening technology is its frequent off-target activity, making it difficult to interpret screen results and requiring significant use of reagent redundancy. It remains an ongoing effort to design robust and on-target RNAi reagents and to develop better screen data analysis tools (31).

CRISPR–Cas9

The clustered regularly interspaced short palindromic repeats (CRISPR)–CRISPR associated protein 9 (Cas9) system is an RNA-guided nuclease system that was initially discovered in bacterial as an adaptive immune system (32-34). Later it was adapted for genome editing and LOF screens in many eukaryotic models (35, 36). Cas9 nuclease is directed to its target site by a short single guide RNA (sgRNA) that is complementary to the target DNA and creates a double-stranded break (DSB) in its target. The break is then repaired by one of the two endogenous DNA repair mechanisms – homology-directed repair (HDR) or non-homologous end joining (NHEJ), which is an error-prone repair mechanism that introduces indel mutations at the repair site. When a DSB is repaired by NHEJ, indel mutations can lead to early frameshift mutations or large in frame deletions, resulting in a partial or fully non-functional protein (37). CRISPR screens have many fewer off target issues than RNAi screens (28).

Using modified forms of Cas9, the CRISPR–Cas9 system can also be employed to cause transcriptional repression or activation in a non-mutagenic manner (38), further expanding its application in genetic screens.

Comparison of RNAi & CRISPR

CRISPR and RNAi have different mechanisms and off targets, thus providing complementary means of assessing the functional contribution of a given gene. Genes that retain function at low expression levels are likely to be missed in RNAi screens due to their incomplete depletion. In contrast, genes that are essential for cell viability cannot be readily assessed in CRISPR screens. Partial depletion by RNAi will be useful in these cases. In addition, as gene

regulatory networks are highly interconnected and contain multiple feedback loops, the response to knockout and depletion can be markedly different (28).

Open Reading Frame screen

To date, functional genetic screens have largely been done using a LOF approach. However, gain-of-function (GOF) screen that utilizes Open Reading Frame (ORF) expression libraries has a unique advantage in cancer driver discovery. Proteins that perform redundant functions are likely to be missed in LOF screens (39). Furthermore, customized mutagenesis of the ORFs allows direct assessment of the functions and phenotypes of not only the wild-type proto-oncogenes but most importantly, their recurring mutant alleles seen in tumors (40-42). However, one must keep in mind that the consequences of overexpression can sometimes be complicated; for example, overexpression may cause a dominant negative and deleterious effect if the stoichiometry of a protein complex is disrupted by overexpression of one of its members (43). Alternatively, overexpression can lead to promiscuous molecular interactions, resulting in phenotypes that are not physiologically relevant (44).

Taken together, LOF and GOF screen each have their own unique strengths and weaknesses. Combination of the two provides a powerful tool to interrogate the biological functions of cancer drivers.

Targeted Therapy

One major goal of cancer research is to develop effective and non-toxic cancer therapies. Traditional cytotoxic chemotherapy and ionizing radiation therapy work primarily through the inhibition of cell division with additional benefits derived from promoting priming of the immune system (45). Because these drugs act on dividing cells, normal tissues such as hair, gastrointestinal epithelium, and bone marrow are also affected. The poor therapeutic window thus results in severe side effects (46). Cancer cells can develop resistance to chemotherapy through various mechanisms such as drug inactivation, drug target alteration, drug efflux, DNA damage repair, cell death inhibition, etc. (47).

Over the past several decades, our increasing knowledge of the hallmark capabilities and vulnerabilities acquired by cancer cells during tumorigenesis and their underlying molecular mechanisms have informed the development of novel and promising therapies.

Cancer cells are dependent on certain OGs for both the establishment and maintenance of the oncogenic state. This phenomenon is called “oncogene-addiction” (48). Though may be present in normal tissues, these oncoproteins are often mutated or overexpressed in tumors. Targeted therapies that inhibit these oncoproteins thus achieve more precise and selective killing of cancer cells, resulting in less system toxicity and side effects, compared with traditional chemotherapies. The two major types of targeted therapies are small molecule inhibitors and monoclonal antibodies (mAb) (46).

The molecular pathways most often targeted in the tumors are those of the growth factor signaling. Among the earliest ones are trastuzumab (HER2), gefitinib (epidermal growth factor

receptor; EGFR), and imatinib (BCR-ABL). Angiogenesis represents another target. The concept that tumor growth is angiogenesis-dependent and that inhibition of angiogenesis could be therapeutic was first proposed by Judah Folkman in the early 1970s (49). In 2004, the first angiogenesis inhibitor, bevacizumab which targets vascular endothelial growth factor (VEGF) was approved. However, its efficacy might not fully result from preventing angiogenesis (50).

Drug Resistance

The major challenge for targeted therapies is that not all patients respond to the therapies and most responders inevitably develop resistance and relapse. Therefore, there is an urgent need to identify the underlying resistance mechanisms in order to improve clinical outcomes for patients through developing combination therapies or alternative regimens after treatment progression. Two examples of the promising targeted therapies and the challenges they are facing are discussed below.

EGFR inhibitors

One of the best-characterized examples of oncogene addiction in cancer biology is EGFR in lung cancer. EGFR belongs to a family of a receptor tyrosine kinase (RTK), called ERBB family. Binding to its ligands such as EGF triggers homodimerization or heterodimerization of this receptor with other ERBB family members, resulting in receptor phosphorylation. Subsequently, the phosphorylated EGFR further activates downstream signaling pathways such as phosphoinositol-3-kinase (PI3K)/AKT, RAS/RAF/MEK/ERK, and JAK/STAT, leading to increased cell proliferation and survival (51). Activating *EGFR* mutations occur in ~10%–30% of tumors of patients with non-small cell lung cancer (NSCLC), a leading cause of cancer-related

deaths (52). Activating *EGFR* mutations mostly cluster in the tyrosine kinase domain and enable the EGFR to activate the downstream signaling pathways in a ligand-independent manner (53-55). As a consequence, the tumor cells are addicted to the EGFR signaling pathway and are sensitive to EGFR inhibition.

The first-generation EGFR inhibitors (EGFRis), such as gefitinib and erlotinib, were developed in the 1990s – before the activating *EGFR* mutations were discovered. They were all initially intended to target the wild-type receptor, which was shown to be overexpressed in many epithelial cancer types (56). In early clinical trials, EGFRis showed disappointing and minimal efficacy when used either as monotherapy after the failure of standard chemotherapy or in combination with chemotherapy as first-line regimens. in patients with advanced NSCLC (57-63); However, subgroup analysis indicates that a significant survival benefit was associated with adenocarcinoma histology, East Asian ethnicity, a history of never smoking cigarettes and female gender (64, 65). It was until 2004, when mutations in the EGFR kinase domain were first discovered, that it was found that these mutations are associated with sensitivity to EGFRis and better survival benefit in retrospective studies (66-68). The efficacy of EGFRis both in terms of response rates and progression-free survival in *EGFR*-mutant NSCLC patients were further confirmed by two landmark randomized prospective Phase III studies (the Iressa Pan-Asia Study (IPASS) and WJTOG3405) and several other studies (64, 69-71).

Although *EGFR*-mutant NSCLCs typically respond dramatically to EGFRis, these responses are not universal, as the overall response rate is ~71%. Even among the initial responders, most inevitably develop acquired resistance to EGFR inhibitor therapies within a year of treatment (69, 71, 72). One major resistance mechanism is the development of a “gatekeeper”

mutation in EGFR itself (p.T790M) that alters the relative affinity of ATP/ drug to the target, thus abrogating the activity of EGFRis (73). Later-generation EGFRis such as Osimertinib that binds to EGFR in an irreversible manner and are selective for both the EGFRis-sensitizing and T790M resistance mutations have demonstrated clinical benefit in patients who progress on first generation inhibitors and harbor the T790M gatekeeper mutation (74); However, the responders inevitably develop resistance to Osimertinib again through various mechanisms (75). Activation of a bypass signaling pathway through mutations or overexpression of genes in redundant signaling pathways can also cause resistance. Examples include amplification of the *MET* RTK (76), amplification of the *HER2* (*ERBB2*) RTK (77), and activation of *KRAS*, *PIK3CA, BRAF*, and *MAPK1* (ERK) (78-82). Furthermore, mechanisms involving blocking EGFRis-mediated apoptosis, such as intronic deletion polymorphism in the gene encoding BCL2-like 11 (*BIM*) have also been reported (83). Finally, some patients originally diagnosed with *EGFR*-mutant NSCLC can display histologic transformation to small cell lung cancer or an epithelial-mesenchymal transition (EMT) at the time of relapse (84, 85). Despite the ongoing efforts to characterize the resistance mechanisms, these resistance mechanisms are still unknown in up to 30% of patients (86).

Over the past decade, immune checkpoint blockade therapies including mAb that targets the programmed cell death protein-1 (PD-1) pathway have radically transformed the therapeutic landscape of NSCLC. Anti-PD-1 immunotherapy produced significant improvements in overall survival compared with single-agent docetaxel delivered in the second-line setting, effectively establishing a new standard of care in NSCLC (87-89); However, notably, patients with activating *EGFR* mutations generally do not respond to PD-1 pathway blockade (89, 90). Therefore, EGFRis still represent the best regimen for *EGFR*-mutant NSCLC patients and there is an urgent need to identify treatment options for those patients after EGFR inhibition therapy progression.

Bromodomain and extraterminal domain inhibitors

Chromatin structure is tightly regulated through epigenetic posttranslational modifications of histone tails. Histone acetylation relaxes chromatin and is associated with active transcription. The encoding and decoding of the epigenetic state of chromatin is achieved through the action of so-called chromatin "readers," "writers," and "erasers" (91). Bromodomain and extraterminal (BET) proteins are a family of epigenetic readers, including ubiquitously expressed BRD2, BRD3, and BRD4 and the testis-restricted BRDT. Structurally, they are characterized by the presence of two tandem bromodomains (BD1 and BD2), an extraterminal domain, and a C-terminal domain (92). They can recognize and read acetyl-histone marks associated with open active chromatin (93).

BET proteins are localized at promoters and especially at enhancers of active genes. BRD4 participates with the Mediator complex and facilitates transcriptional elongation (94, 95). The important role of BET proteins in cancer is evidenced by the fact that they were recurrently identified as genes on which cancer cells depend for their survival through genetic screens performed in different tumor types (96-99). Small molecule bromodomain and extraterminal domain inhibitors (BETis) that target and inhibit BRD4's association with chromatin have shown anti-cancer efficacy on a variety of cancers (92). The selective inhibition of BETis on cancer cells is surprising given the ubiquitous regulation of BET proteins on transcription. BRD4 and Mediator were found to co-occupy thousands of enhancers associated with active genes. Exposure of tumor cells to BETis led to preferential loss of BRD4 at super-enhancers and consequent transcription elongation defects that preferentially impacted genes with super-enhancers, including *MYC*. Super-enhancers were found at key oncogenic drivers in many tumor cells, BETis can thus achieve

precise inhibitory effects on cancer-specific gene expression and create a therapeutic window (100).

BETis are currently being evaluated in clinical trials for patients with solid tumors and hematologic malignancies and preliminary results have provided evidence of their antitumor potential in a subset of patients (92). However, as is often the case with other single-agent therapies, cancer cells can develop resistance to BETis through a variety of mechanisms, such as: increased WNT/β-catenin signaling in adult acute myeloid leukemia (AML) (101, 102); GLI2-dependent c-Myc (encoded by *MYC*) upregulation in pancreatic cancer (103); hyper-phosphorylation of BRD4 through decreased activity of PP2A that results in bromodomain-independent binding of BRD4 to chromatin in triple-negative breast cancer (104); kinome reprogramming in ovarian cancer (105); AMPK–ULK1-mediated autophagy (106) or MCL1 upregulation (107) in AML; up-regulation of transforming growth factor-β (TGF-β) through loss of *TRIM33* in colorectal cancer (108); *PIK3CA* mutations in breast cancer (96); *SPOP* mutations that result in decreased degradation of the BET proteins in prostate cancer (109).

NUT midline carcinoma

Despite the dependency of many types of cancers on BET proteins, NUT midline carcinoma (NMC) is the only type of tumor that actually harbors an oncogenic form of BRD4 or BRD3. NMC is an aggressive subtype of squamous cell cancer. Genetically, it is defined by the fusion of most of the coding sequence of the testes-specific gene NUT on chromosome 15 to several other genes – most frequently the BRD4 gene on chromosome 19 (BRD4-NUT) (110, 111). The oncogenic role of BRD4-NUT in NMC represents another classical example of oncogene addiction.

The oncogenic function of BRD4-NUT protein is the combined function of the two moieties of the fusion protein thus the mechanism by which the fusion protein drives NMC tumorigenesis is different from the function of BRD4 itself in other types of cancers. The BRD4 moiety functions as an epigenetic reader that binds to acetyl-histone. Fusion to the NUT protein results in recruitment of p300/CBP, a histone acetyl-transferase, leading to regional histone hyperacetylation. Such acetylation further recruits BRD4-NUT in a feed-forward manner, eventually creating massive regions of acetylated chromatin that covers individual topologically associating domain across the genome (112). The transcription of oncogenic proteins such as c-Myc and its regulators within these regions is thus stimulated, blocking cellular differentiation and promoting uncontrolled growth of carcinoma cells (112, 113).

NMC is a particularly lethal cancer that does not benefit from conventional chemotherapy and has an overall survival of only ~ 7 mo (111, 114). Thus, it represents a model disease for the clinical testing of BETis given the direct oncogenic driver role that BRD4-NUT plays in NMC and the urgent need for novel therapeutic approaches. A clinical proof of concept for BETis in NMC was demonstrated recently (115). Two of four NMC patients receiving BRD4 inhibition therapy showed increased overall survival (19 and 18 mo, respectively), which was notably longer than the median survival of ~7 mo reported in the largest retrospective series of patients with NMC (114). Despite the initial response, all of the NMC patients developed resistance to the BETis and eventually relapsed. Therefore, there is an urgent need to identify the underlying mechanisms of resistance to BRD4 inhibition in NMC in order to develop combination therapies or alternative regimens after BRD4 inhibitor progression.

Strategies to overcome drug resistance

Understanding of the drug resistance mechanisms provides information on what pathway(s) can genetically modify and compensate for the dependency of the cancer cells on the cancer driver. One strategy for overcoming targeted therapy resistance is to suppress the emergence of resistant clones by deploying rational upfront polytherapy that targets both its driver OG and a common resistance mechanism (116). The success of such an approach has been demonstrated in several preclinical and clinical studies. Previous study has shown that acquired resistance to the irreversible EGFR inhibitor WZ4002 that targets both the EGFRis-sensitizing and T790M mutations can occur through genomic alterations that activate ERK1/2 signaling (78, 117). Concomitant inhibition of ERK1/2 by the MEK inhibitor trametinib prevents ERK1/2 reactivation, enhances WZ4002-induced apoptosis, and inhibits the emergence of resistance in WZ4002-sensitive models known to acquire resistance via both T790M-dependent and T790M-independent mechanisms (118). Similar findings were observed in EML4-ALK-positive lung cancer. It was shown that RAS-MAPK dependence as a hallmark of EML4-ALK lung adenocarcinoma and upfront treatment of EML4-ALK positive lung tumors with both an ALK inhibitor and a MAPK pathway inhibitor can significantly delay or even prevent the onset of resistance (119). Another clinical example is that in a phase II clinical trial, combination of BRAF inhibitor dabrafenib and MEK inhibitor trametinib in patients with $BRAF^{V600E}$-mutant NSCLC achieved higher overall response and longer median progression-free survival compared indirectly with dabrafenib monotherapy (120).

Early pre-clinical and clinical data suggest it might be critical to combat resistance by treating it before it truly emerges – once a tumor has recurred on a macroscopic level, it appears

to be less sensitive to inhibitors targeting its resistance mechanism as when a tumor is initially co-treated with inhibitors targeting both its driver OG and a common resistance mechanism (116, 121, 122).

Another drug combination strategy involves the addition of immunotherapies. As discussed above, targeted therapies generally induce a high response rate but the responses are transient. On the other hand, immune checkpoint blockade therapies have been associated with unprecedented long-lasting responses but only in a limited number of patients. Therefore, there are a lot of efforts ongoing for the clinical testing of the efficacy of combinations of these two therapeutic approaches in various cancer types with the hope that immunotherapy can transform the important tumor responses achieved with targeted therapies to durable and long-lasting remissions (123). However, multiple lines of preclinical and clinical evidence suggest that the benefit from immunotherapies in NSCLC patients with *EGFR* mutations is doubtful. First, as mentioned above, *EGFR* mutations are associated with low response rates to PD-1 pathway blockade in patients with NSCLC (89, 90). In preclinical models, no synergistic tumor cell killing effect was observed when EGFRis were combined with anti-PD-1 therapies (124). Furthermore, EGFRis-resistant lung cancer cells with EMT features have decreased expression of PD-L1 (125), which is generally associated with low response rates to PD-1 pathway blockade (126-128). Therefore, as there are not enough data from the clinical trials yet, it is currently too early to be optimistic about the benefit of such a combination approach (123).

In this thesis, I will use LOF and GOF screens to identify novel cancer drivers that modify the dependency of NSCLC cancer cells on EGFR (Chapter 2). I will further utilize the same

screening strategy to uncover novel resistance mechanisms of NMC cancer cells to BETis, a promising targeted therapy currently being tested in clinical trials (Chapter 3).

Chapter 2

A genetic interaction analysis identifies cancer drivers that modify EGFR dependency

Note: This entire chapter, was published in the article: Liao S, Davoli T, Leng Y, Li MZ, Xu Q, Elledge SJ. A genetic interaction analysis identifies cancer drivers that modify EGFR dependency. Genes Dev. 2017;31(2):184-96.

Introduction

Cancer is driven by a number of distinct genetic alterations including gain or loss of chromosomes and chromosomal segments, translocations, frameshifts, and point mutations that result in inactivation of TSGs or activation of OGs. Attempts to identify those cancer drivers based on patterns of mutagenesis in tumors have uncovered a bewilderingly large number of genes that bear the signature of genetic selection in tumors. Rather than a defined number of cancer drivers, there exists a continuum of genes that appear with increasingly lower frequency and potency in a pan-cancer analysis (20). This has also been referred to as mountains and hills and the "long tail" of cancer drivers (21-23).

Unraveling how the genes in this large network contribute to tumorigenesis poses a significant challenge for geneticists. While it is clear that certain basic conditions related to the classic hallmarks of cancer (e.g. immortalization and dysregulated proliferation) must be satisfied during tumor development (13), it is currently unclear how many cancer genes operate to achieve these conditions. From a theoretical perspective, it makes sense that many cancer drivers may perform similar functions and be partially interchangeable during tumor evolution. They may act either to genetically modify a shared central oncogenesis pathway or in parallel pathways that provide the cell with equivalent functions to drive tumorigenesis. Thus, it is likely that many genes on these TSG and OG lists will genetically interact to modify common conditions of oncogenesis.

One of the most extensively studied oncogenic pathways is the RTK–RAS–PI3K pathway. This pathway is activated in the majority of solid tumors and has been examined extensively both biochemically and genetically. Among RTKs, perhaps the most studied is EGFR. EGFR activates cellular signaling pathways such as PI3K/AKT, RAS/RAF/MEK/ERK, and JAK/STAT, leading

to increased cell proliferation and survival (51). Activating *EGFR* mutations occur in ~10%–30% of tumors of patients with NSCLC, a leading cause of cancer-related deaths (52). These mutations confer sensitivity to EGFRis such as gefitinib and a variety of later-generation inhibitors (66, 67, 129). Although *EGFR*-mutant NSCLCs typically respond dramatically to EGFRis, these responses are not universal, as the overall response rate is ~71%. Even among the initial responders, most inevitably develop acquired resistance to EGFRi therapies within a year of treatment (69, 71, 72). The resistance mechanism is unknown in up to 30% of patients (86).

Given its central role in driving oncogenesis, the existing knowledge of the pathway, and the many tools available, the EGFR pathway is well suited for examining genetic interactions with other known and putative cancer drivers. This is supported by existing evidence of genetic interactions of EGFR with other drivers of tumorigenesis (130). For example, patients bearing *EGFR* mutations are known to evolve resistance to EGFRi therapies by virtue of mutations in other cancer drivers. In addition to mutations in *EGFR* itself, low expression of *NF1* (131) or *PTEN* (132, 133), amplification of the *MET* RTK (76), amplification of the *HER2* (*ERBB2*) RTK (77), and activation of *KRAS*, *PIK3CA, BRAF*, and *MAPK1* (ERK) (78-82) can confer EGFRi resistance. Thus, it is likely that additional drivers will also genetically interact with the EGFR pathway.

To test the hypothesis that cancer drivers can genetically interact and substitute for one another to drive proliferation and survival, we investigated TSG and OG drivers for their ability when mutated to partially replace EGFR in EGFR-dependent tumor cells by performing CRISPR, shRNA, and ORF expression screens in parallel in an NSCLC model. We took advantage of an algorithm called TUSON Explorer to identify TSGs and OGs (20). Here, we show that this genetic approach successfully recovered previously validated TSGs and OGs that interact genetically with

the EGFR pathway. We also identified novel TSGs that have not been linked previously to EGFRi resistance. We further characterized the mechanisms underlying gefitinib resistance mediated by several novel TSGs. Among these, we showed that mutation of *PBRM1*, a subunit of the SWI/SNF complex, attenuated the effect of gefitinib in part by sustaining AKT pathway function during EGFR inhibition. We also showed that mutation of *CIC*, a transcriptional repressor, partially restored the EGFR gene expression program upon EGFR inhibition in NSCLC cells in part through sustained activation of *ETV1*, resulting in gefitinib resistance. These findings provide new biochemical insight into EGFR signaling and support the general notion that cancer drivers are part of a robust joint network that can compensate for the loss of any one member.

Results

The central hypothesis motivating this study is that cancer mutations often impact the same pathways or control parallel pathways that can substitute for each other. To test this notion, we investigated the RTK EGFR pathway. While EGFR has been extensively studied both biochemically and genetically, it has not been systematically probed for its interactions with all known and putative cancer drivers. To explore these interactions for genes with TSG properties, we generated both a CRISPR and an shRNA library containing 10 gRNAs or 10 shRNAs per gene to a list of ~500 genes whose LOF has been implicated in driving tumorigenesis by the TUSON Explorer algorithm. Each library also contained 1000 gRNAs or 1000 shRNAs targeting the *Escherichia coli* genome as negative controls. To explore the genetic interactions with EGFR for genes with OG properties, we generated a barcoded-ORF lentivirus library of ~50 selected genes

whose mutational signatures implicate them as potential OGs by TUSON Explorer. We set out to determine which alterations could substitute for EGFR signaling using a chemical inhibitor of EGFR, gefitinib. We performed screens using an NSCLC cell line, PC9, which harbors an activating *EGFR* mutation and is sensitive to gefitinib. CRISPR and shRNA have different mechanisms and off targets, thus providing complementary means of assessing the functional contribution of TSGs to EGFRi resistance. By performing these complementary CRISPR and shRNA screens in parallel with the ORF screen, we were able to obtain a broad genetic view of the EGFR-interacting pathways.

The schematic of the CRISPR, shRNA, and ORF screens is outlined in Figure 2 and described in detail in the Materials and Methods.

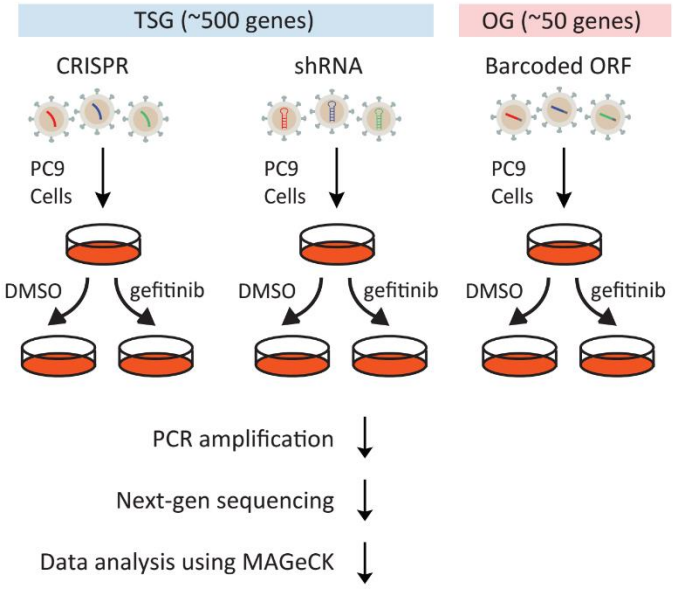

Figure 2. Outline of the genetic screening strategy of gefitinib bypass screens.

In each screen, cells were treated with either DMSO or 30 nM gefitinib for ~17 d. This intermediate concentration of gefitinib was not completely lethal but caused a significant

lengthening of the doubling time of PC9 cells, allowing more subtle suppressors of reduced EGFR function to be detected. We used the MAGeCK (model-based analysis of genome-wide CRISPR–Cas9 knockout) scoring algorithm (134) to rank the performance of individual genes. For TSG screens, the negative controls were incorporated in the MAGeCK analysis to generate null distributions and calculate the *P*-value and false discovery rate (FDR) for each gene. The top 15 hits from each screen are shown in Figure 3A. For TSG screens, each screen successfully recovered previously validated TSGs that impact sensitivity to EGFR inhibition, including *NF1* and *PTEN*, as well as novel TSGs that have not been linked previously to EGFR pathway function. The rank and FDR of each gene in the two TSG screens are summarized in Supplemental Table S1. The top 30 genes based on the combined rank of the two screens (combined FDR < 0.001) are marked in red. The rank and FDR of each gene in the OG screen are shown in the Supplemental Table S1. This screen identified a number of key regulators in the EGFR pathway previously implicated in EGFRi resistance including *EGFR* itself, *ERRB2*, *NRAS*, *HRAS*, *BRAF*, *MAP2K1*, as well as two canonical cell cycle regulators *CDK6* and *CCND1*. Since the majority of the strong interactions with EGFRi resistance were known previously, we focused the rest of our efforts on characterizing the novel TSG hits.

The top-scoring genes from the TSG screen showed a significant overlap between CRISPR and shRNA screens (Fig. 3B). For example, the number of overlapping genes in the top 20 of CRISPR and the top 20 of shRNA is 10 ($P = 1.1 \times 10^{-10}$).

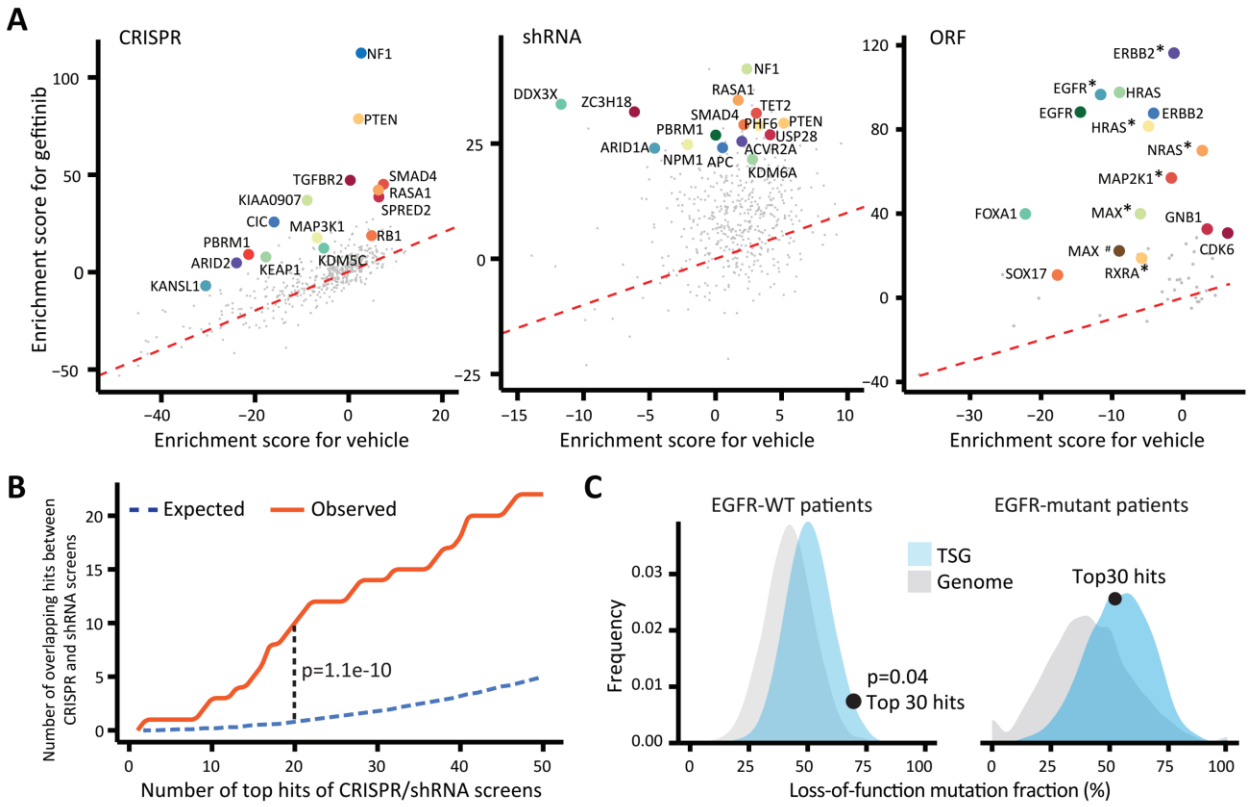

Figure 3. Genetic screens identify modifiers of the cellular response to reduced EGFR signaling. (A) Enrichment score (Z-score determined by MAGeCK) of gefitinib treatment plotted against vehicle (DMSO) treatment for genes in the CRISPR, shRNA, and ORF screens. The top 15 genes of each screen (FDR< 0.05) are highlighted. One outlier in the shRNA screen, *AAMP* (enrichment score for gefitinib >100, FDR = 0.96) was excluded in the plot of shRNAs. (*) Mutant form; (#) mutant form 2. (B) The number of overlapping genes observed between the top hits of the CRISPR and shRNA screens compared with the number expected for a random overlap. (C) Distribution of the pooled LOF mutation fraction based on a permutation of a group of 30 genes from the TSG library (combined FDR > 0.1 in the screens; blue) or whole genome (excluding genes in the TSG library; gray) in *EGFR* mutant or *EGFR* wild-type tumors. The dot represents the behavior of the top 30 hits from our screen mapped on the distribution of the TSGs. The *P*-value was calculated based on the relative distribution of the TSG library.

If the top TSG hits in this screen perform a function equivalent to that of *EGFR* mutants, they would be expected to be largely epistatic and would lack selective power in an *EGFR* mutant background. To examine this, we calculated the LOF fraction (the ratio of nonsense, frameshift, and high-impact missense mutations vs. total mutations) for a group of the top 30 TSG hits (combined FDR < 0.001) using the lung adenocarcinoma TCGA data set. The higher the LOF fraction, the more selective pressure is on those mutations in a given tumor set. In tumors bearing

a wild-type, but not mutant, *EGFR* gene, the LOF fraction of the top 30 hits was much higher than the average of all the genes in the TSG library (Fig. 3C; $P = 0.04$). This suggests that the top TSG hits are more strongly selected in *EGFR* wild-type tumors. Such selective pressure suggests that they act like activating *EGFR* mutations and theoretically could, when mutant, impact EGFR signaling in *EGFR* mutant tumors when treated with an EGFRi.

We also identified three genes among our top 30 hits whose focal deletion/LOF mutations are mutually exclusive with activating *EGFR* mutations (Supplemental Fig. S1). Two of these, *NF1* and *KEAP1*, were previously known to be involved in EGFRi resistance, while the third, *THRAP3*, is novel. The mutual exclusivity between the inactivation of these TSGs and activating *EGFR* mutations observed in patients further suggests that such events operate in the same or functionally redundant pathways.

Down-regulation of *PBRM1* Attenuates the Effect of Gefitinib by Sustaining AKT Pathway Activation During EGFR Inhibition

A prominent candidate that emerged from the screens is the SWI/SNF complex. Six genes encoding subunits of SWI/SNF complexes have been ranked among the top 500 TSGs by the TUSON algorithm and were represented in our libraries. Among those, *PBRM1*, *ARID2*, and *ARID1A* scored in the top 30 of both CRISPR and shRNA screens (combined FDR < 0.001), while *ARID1B* and *SMARCB1* scored only in the CRISPR screen (FDR < 0.001) (Fig. 4A).

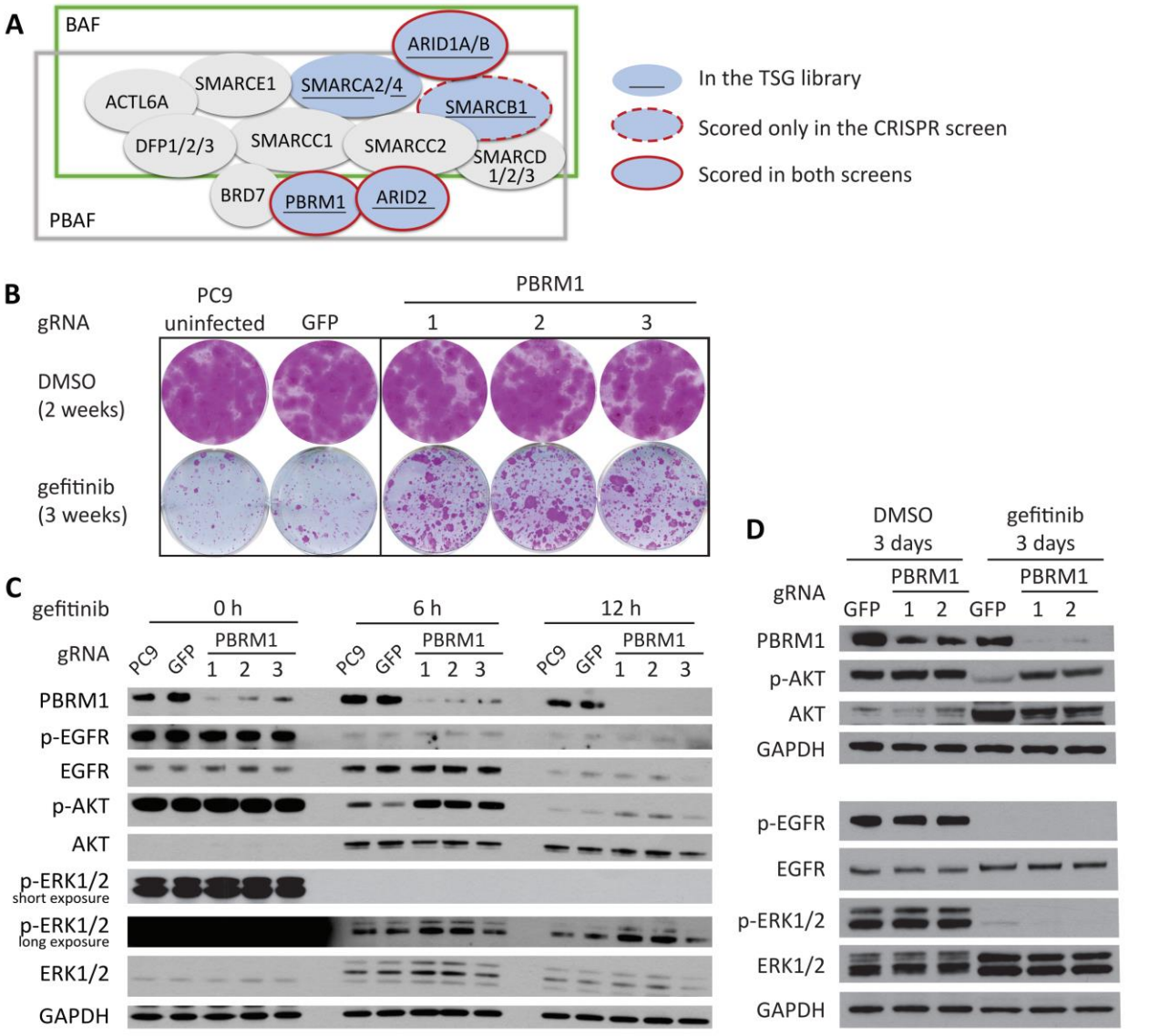

Figure 4. Multiple subunits of the SWI/SNF complex scored as modifiers of EGFR pathway function. (A) Schematic of the BAF and PBAF complexes showing which subunits scored in our screens as modifiers of EGFR dependency. (B) *PBRM1* down-regulation enhances survival of PC9 cells in long-term colony formation assays. Cells were fixed and stained after treatment with DMSO or 30 nM gefitinib for the indicated times. Uninfected PC9 cells and GFP gRNA-expressing PC9 cells were used as controls. (C) Immunoblot analysis of *PBRM1* mutant PC9 cells treated with 30 nM gefitinib for 0, 6, and 12 h. Cells were incubated with medium containing 0.5% serum 18 h before and during drug treatment. (D) Immunoblot analysis of *PBRM1* mutant PC9 cells treated with 30 nM gefitinib for 3 d with the indicated antibodies.

SWI/SNF complexes interact with transcription factors, coactivators, and corepressors and are capable of mobilizing nucleosomes at target promoters and enhancers to modulate gene expression. The mechanism by which mutation of each individual subunit promotes oncogenesis

and the function of mutated SWI/SNF complexes in cancer are now active areas of investigation (135).

The mechanistic role of *PBRM1* in tumorigenesis remains elusive. *PBRM1* is required for p21 expression and cell cycle arrest in breast cancer cells upon TGF-β treatment (136). However, in primary mouse embryonic fibroblasts (MEFs), *PBRM1* suppresses p21 expression, and deletion of *PBRM1* triggers cell cycle arrest and cellular senescence (137). Direct links between EGFR signaling and *PBRM1* or other SWI/SNF components have not yet been established.

To validate the effects of *PBRM1* loss on the phenotype of EGFR pathway impairment, we performed colony formation assays in which cells were cultured in the presence of gefitinib for 3 wk. *PBRM1* mutation using three different gRNAs substantially enhanced cell survival in these assays (Fig. 4B). *PBRM1* mutation also enhanced the survival of PC9 cells treated with erlotinib or third-generation EGFRi AZD9291 but had no effect on cisplatin treatment (Supplemental Fig. S2A). Given the role of *PBRM1* on p21 regulation in other cellular contexts, we examined the p21 levels of *PBRM1* gRNA-expressing and control gRNA-expressing PC9 cells treated with DMSO or gefitinib. *PBRM1* mutation did not affect the basal level of p21 in PC9 cells or reduce the induction of p21 by gefitinib treatment (Supplemental Fig. S2B). Because two other SWI/SNF subunits, *SMARCE1* and *ARID1A*, have been reported to negatively regulate *EGFR* mRNA levels (138), we sought to examine whether loss of *PBRM1* also affects *EGFR* expression. *PBRM1* mutation by CRISPR in PC9 cells did not affect the level of EGFR or phosphorylation of EGFR (p-EGFR) in the absence or presence of gefitinib (Fig. 4C).

We next examined the phosphorylation status of several downstream signaling proteins of EGFR. We found that treatment of PC9 cells with gefitinib quickly induced the levels of AKT

while reducing its phosphorylation (p-AKT). We found that *PBRM1* mutant cells showed slower rates of reduction of p-AKT than parental and control gRNA-expressing cells after 6 and 12 h of gefitinib treatment (Fig. 4C), but then the levels of p-AKT fully rebounded to untreated levels by 3 d (Fig. 4D). Gefitinib completely abolished ERK1/2 phosphorylation (p-ERK1/2), and that effect did not rebound by 3 d of treatment. These results indicate that *PBRM1* loss attenuates the effects of gefitinib on the downstream AKT pathway, which is likely to ameliorate the effects on EGFR pathway inhibition.

Loss of *CIC* Confers Resistance of NSCLC Cell Lines to EGFRis

Among the novel hits that scored in both the CRISPR and shRNA screens, *CIC* (combined FDR = 0) stood out because a related gene has been reported to transcriptionally repress EGFR target genes during *Drosophila* development. In *Drosophila,* LOF of the *CIC* ortholog Capicua bypasses the requirement for EGFR signaling in vein cell determination (139). *CIC* mutations increase the rate of cell proliferation without affecting cell size and bypass the requirement for EGFR signaling in imaginal discs (140). However, the potential role of *CIC* loss in drug resistance has not been investigated.

To validate that *CIC* loss mediates gefitinib resistance, we performed a multicolor competition assay in which PC9 cells labeled with GFP were infected with a virus encoding Cas9 and a gRNA to *CIC* (referred to here as *CIC* knockdown cells) and were mixed with control Cas9-gRNA-infected cells labeled with mRuby in a 50:50 ratio. After DMSO or gefitinib treatment, the percentage of *CIC* knockdown cells was then quantified as the percentage of GFP cells using

FACS. Knockdown of CIC protein was confirmed by immunoblotting (Fig. 5A). The percentage of *CIC* knockdown cells remained ~50% under DMSO treatment, indicating that *CIC* does not regulate basal proliferation of PC9 cells. However, when treated with gefitinib, *CIC* knockdown cells were selectively enriched (Fig. 5B). *CIC* knockdown also enhanced survival of PC9 cells treated with erlotinib or the third-generation EGFRi AZD9291 (Supplemental Fig. S3A). We confirmed the effects of *CIC* knockdown in another NSCLC cell line, H1975. H1975 cells harbor an activating *EGFR* mutation (L858R) and the gatekeeper mutation T790M, which confers resistance to gefitinib and erlotinib but not AZD9291. *CIC* knockdown using two different gRNAs substantially enhanced cell survival under AZD9291 treatment in the colony formation assays (Fig. 5C,D), suggesting that the role of *CIC* is cell type- and EGFRi-independent.

To further characterize the resistance mechanism, we examined apoptosis and cell cycle distribution of *CIC* knockdown cells under gefitinib treatment using propidium iodide (PI) staining and BrdU labeling respectively. Unlike loss of *NF1*, impairing *CIC* function did not protect PC9 cells from gefitinib-induced apoptosis (Supplemental Fig. S3B). However, while gefitinib induced G1/S cell cycle arrest in control cells, impairing *CIC* function reduced the effects of gefitinib on cell cycle arrest (Fig. 5E), suggesting that *CIC* loss causes gefitinib resistance in part through promoting cell cycle entry. This is consistent with our observation that *CIC* loss prevents the repression of cyclin D expression by gefitinib (see Fig. 6F).

Figure 5. *CIC* LOF enhances growth of cells with impaired EGFR signaling. (A) Immunoblot analysis of the CIC protein in PC9 cells infected with lentivirus expressing Cas9 and the indicated gRNAs. (B) Viruses expressing Cas9 and CIC or GFP gRNAs were used to infect PC9 cells, infected cells were mixed in a 50:50 ratio and treated with either DMSO or 30 nM gefitinib for 10 d or DMSO or 100 nM gefitinib for 14 d, and the percentage of *CIC* mutants was quantified using FACS. (C) Immunoblot analysis of CIC protein in H1975 cells infected with lentivirus expressing Cas9 and the indicated gRNAs. The dots indicate a cross-reactive protein. (D) *CIC* mutation enhances survival of H1975 cells in long-term colony formation assays with EGFRis. Cells described in *C* were fixed and stained after treatment with DMSO or 100 nM AZD9291 for the indicated times. (E) Cell cycle profiles of CIC and GFP gRNA-expressing cells treated with DMSO or 30 nM gefitinib for 48 h. Incorporated BrdU and total DNA content (7AAD) were used to distinguish cells in the G0/G1, S, or G2/M phases of the cell cycle. Apoptotic (sub-G1) cells are not shown. (F) Competition assays as in *B*. After 10 d of treatment with either DMSO, 1 μM palbociclib, 30 nM gefitinib, or a combination of 1 μM palbociclib and 30 nM gefitinib, the percentage of CIC gRNA-expressing cells was quantified using FACS. Data are the means ± SD. n = 3 in all panels. (*) $P < 0.05$; (**) $P < 0.01$; (***) $P < 0.001$.

Figure 5 (Continued)

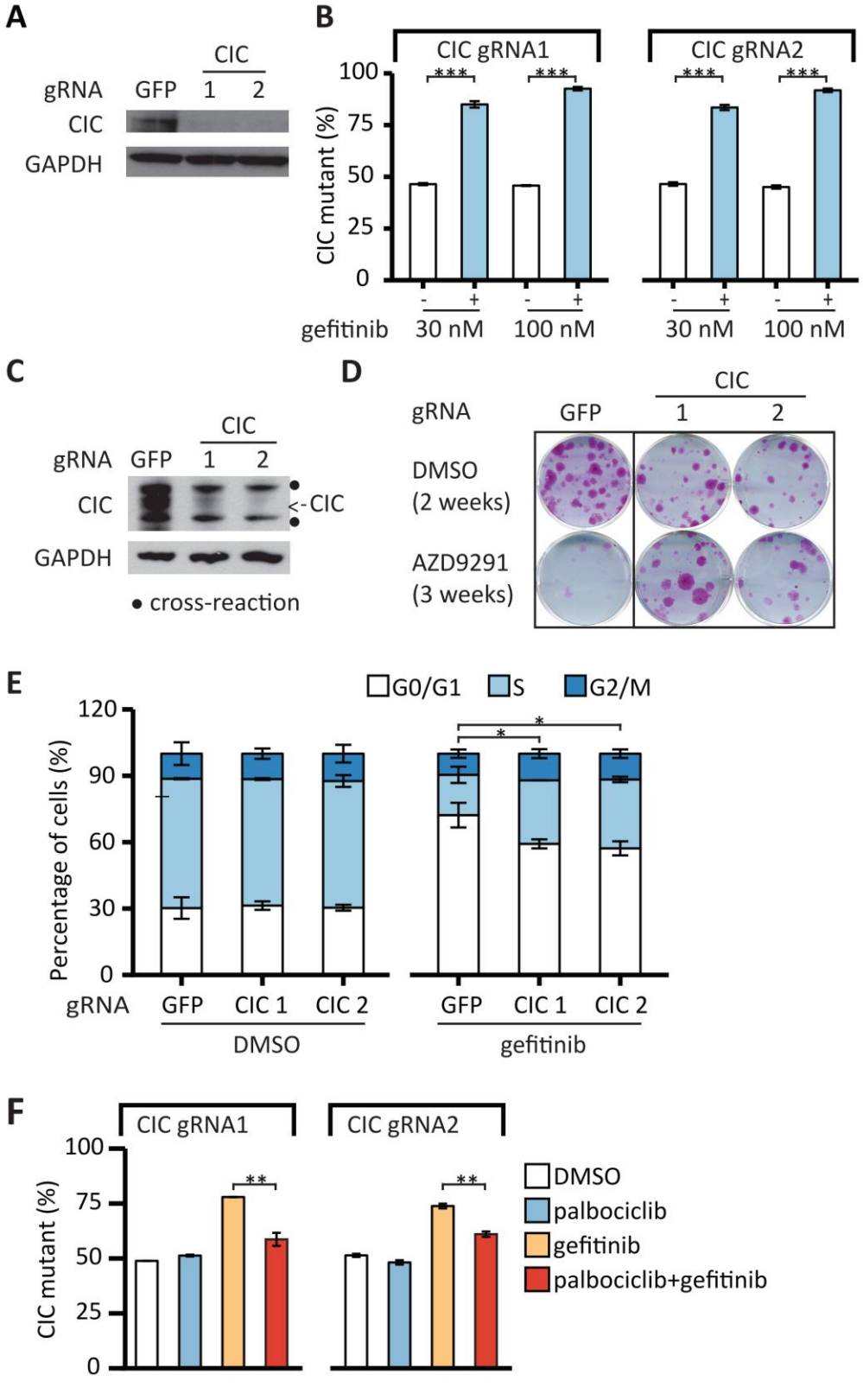

Cyclin D binds and activates the cyclin-dependent kinases CDK4 and CDK6 to promote cell proliferation. If this mechanism contributes to gefitinib resistance, one might expect that reducing CDK4/6 function would restore gefitinib sensitivity of *CIC* knockdown cells. We tested this hypothesis and found that the selective outgrowth of *CIC* impaired cells treated with gefitinib could be inhibited by cotreating with a CDK4/6 inhibitor, palbociclib (Fig. 5F). The effects appear to be specific to gefitinib treatment because palbociclib had little effect on these cells in the absence of gefitinib.

CIC Loss Mediates Sustained Activation of EGFR Target Genes During EGFR Inhibition

To identify the effectors that are induced upon loss of CIC in the EGFRi resistance setting, we performed RNA sequencing (RNA-seq) using two replicates for control gRNA and three different gRNAs of CIC as three replicates. Cells were treated with DMSO or 30 nM gefitinib for 6 h (Fig. 6A). Knockdown of CIC was confirmed by immunoblotting (Fig. 6B). The full analyses of differentially expressed genes (DEGs) across different conditions are shown in Supplemental Table S2. Gene set enrichment analysis (GSEA) revealed that the EGFR target genes identified by Kobayashi et al. (141) comprised the highest-ranking up-regulated gene set in CIC knockdown cells compared with control cells during gefitinib treatment (Fig. 6C), indicating that CIC knockdown cells were able to partially sustain EGFR signaling during gefitinib treatment. Protein-protein interaction (PPI) hub analysis indicated that MAPK1/3 (ERK1/2) and EGFR were the most significantly enriched hubs of DEGs between *CIC* knockdown cells and control cells during gefitinib treatment (Fig. 6D). However, *CIC* knockdown cells did not exhibit differential p-EGFR or p-ERK1/2 compared with control cells with or without gefitinib treatment (Supplemental Fig.

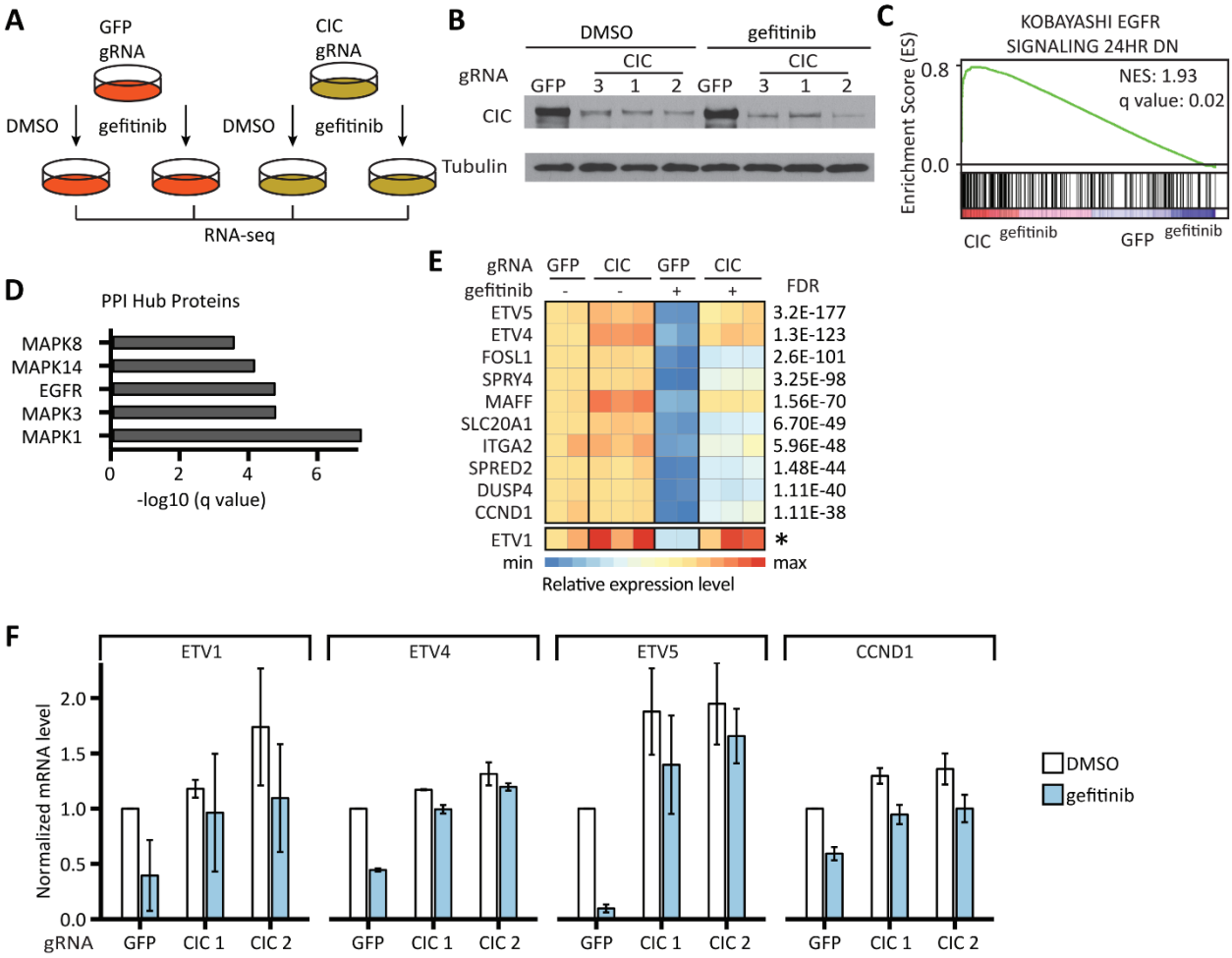

Figure 6. Identification and functional evaluation of genes regulated by CIC. (A) Schematic of the RNA-seq analysis. Cells were treated with DMSO or 30 nM gefitinib for 6 h. Differentially expressed genes (DEGs) were identified using edgeR. (B) Confirmation of *CIC* knockout in PC9 cells using immunoblots. (C) EGFRi resistance signature enrichment plot (using Kobayashi EGFR Signaling 24hr DN signature data sets obtained from the gene set enrichment analysis [GSEA]). The plot indicates a significant up-regulation of EGFR signatures in CIC gRNA-expressing PC9 cells compared with GFP gRNA-expressing PC9 cells during gefitinib treatment. (NES) Normalized enrichment score. (D) Protein–protein interaction (PPI) hubs among the DEGs between CIC gRNA-expressing and GFP gRNA-expressing PC9 cells during gefitinib treatment. (E) Heat map of expression levels (Z-scores) of the top up-regulated genes in CIC gRNA-expressing compared with GFP gRNA-expressing PC9 cells during gefitinib treatment. Each sample was normalized to the basal condition (GFP gRNA-infected, DMSO-treated sample 1). FDRs were calculated by comparing CIC gRNA-expressing cells with GFP gRNA-expressing cells during gefitinib treatment. The asterisk for *ETV1* indicates that we were unable to calculate an FDR, as the total read counts were too low, but it ranks in the top 10 by fold change. (F) RT-qPCR analysis of mRNA expression of the indicated genes in CIC gRNA-expressing or GFP gRNA-expressing PC9 cells treated with DMSO or 30 nM gefitinib for 6 h. Data are the means ± SD. n = 3.

S4A), suggesting that *CIC* regulates *EGFR* target genes downstream from EGFR-ERK1/2

functioA heat map of the top 10 up-regulated genes in the CIC knockdown cells compared with

control cells during gefitinib treatment is shown in Figure 6E. The top two up-regulated genes were ETV4 and ETV5. ETV1, ETV4, and ETV5 are members of the PEA3 (polyoma enhancer activator 3) subfamily of Ets transcription factors. The three PEA3 Ets transcriptional activators function as oncoproteins in several tumor types and promote cell proliferation (142). Notably, ETV1 was shown previously to restore the RAS/MAPK gene expression program upon MEK inhibition in prostate cancer cells (143). ETV1 was not included in the transcriptional analysis due to low read counts detected in RNA-seq but was significantly up-regulated in the CIC knockdown cells compared with control cells during gefitinib treatment and ranks in the top three genes when considering fold change (Fig. 6E). Using RT-qPCR, we further confirmed the mRNA levels of the three PEA3 Ets transcription factors as well as CCND1, which is of interest given that CIC knockdown bypassed cell cycle arrest induced by gefitinib. The mRNA levels of these genes were significantly reduced in response to gefitinib in control cells but remained high in CIC knockdown cells (Fig. 6F).

The CIC-Regulated Oncogenic Ets Factor ETV1 Can Enhance Cell Growth in NSCLC Cells When the EGFR Pathway Is Impaired

Given that mRNA levels of the PEA3 Ets transcription factors were sustained in CIC knockdown cells upon gefitinib treatment, we sought to determine whether these genes contribute to the resistance caused by loss of CIC. We individually expressed ORFs of ETV1, ETV4, and ETV5 in PC9 cells and examined the effects on gefitinib resistance using the multicolor competition assay. Ectopic expression of ETV4 was toxic to PC9 cells. The percentage of GFP-

labeled ETV4-expressing cells decreased to ~0% after DMSO treatment for 10 d (Fig. 7A); thus, its role in promoting drug resistance could not be evaluated.

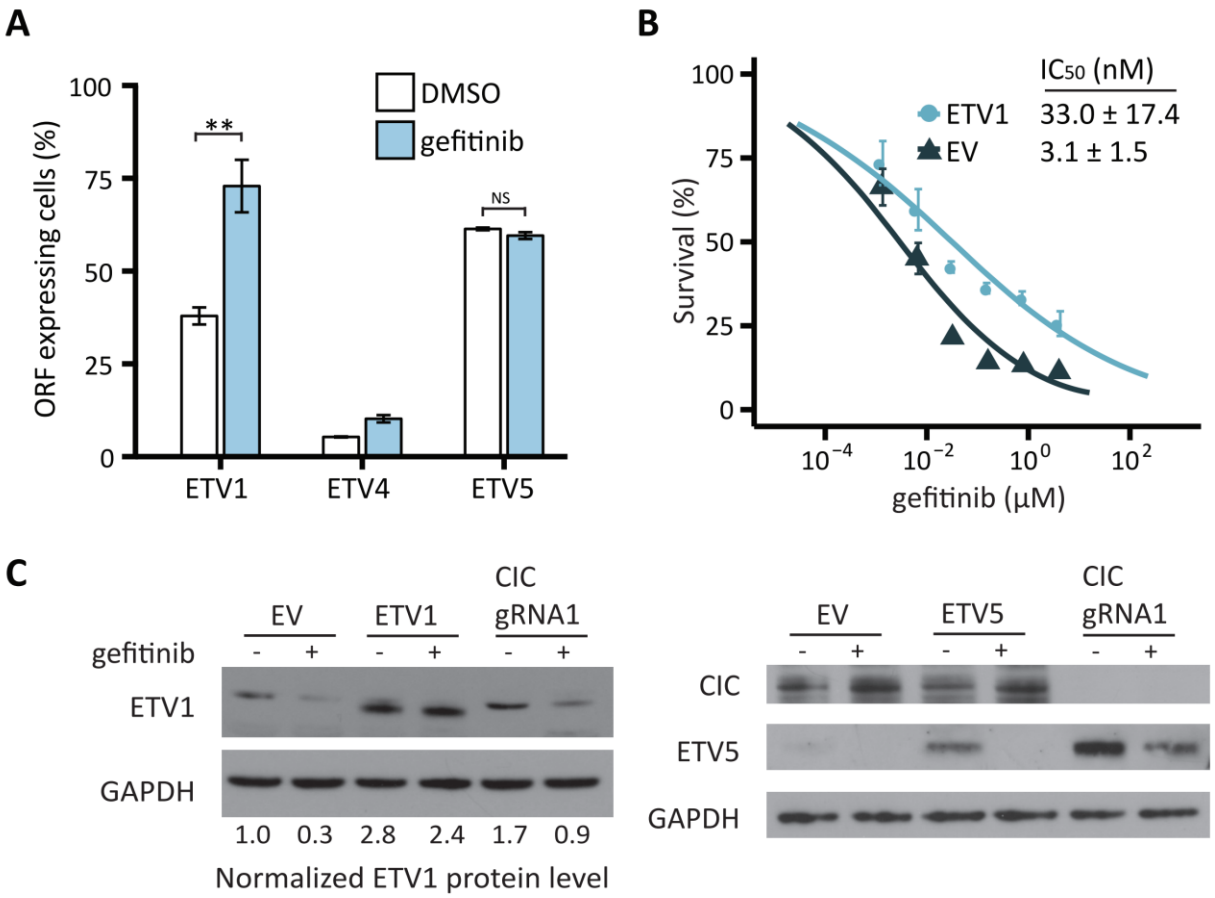

Figure 7. The CIC-regulated oncogenic Ets factor ETV1 can enhance cell growth when the EGFR pathway is impaired. (A) PC9 cells containing virus expressing the indicated ORFs were mixed with cells containing the empty vector (EV) in a 50:50 ratio. After 10 d of treatment with DMSO or 30 nM gefitinib, the percentage of GFP-labeled ORF-expressing cells was quantified using FACS. Data are means ± SD. n = 3. (NS) Not significant; (**) $P < 0.01$. (B) PC9 cells expressing *ETV1* or EV were treated with the indicated concentrations of gefitinib for 72 h before cell viability was measured using an SRB assay and normalized to untreated controls. Data are means ± SD. n = 3. (C) Immunoblot analysis of PC9 cells overexpressing EV or the indicated ORFs or infected with CIC gRNA and treated with 30 nM gefitinib for 12 h.

While not promoting the basal proliferation of PC9 cells, ETV1 expression conferred a significant growth advantage over the empty vector (EV) during gefitinib treatment (Fig. 7A). The IC50 of gefitinib increased 10.7-fold for *ETV1*-expressing cells compared with EV-expressing

cells, as determined by the sulphorhodamine B (SRB) assay (Fig. 7B). Notably, consistent with the regulation of its mRNA levels, protein levels of ETV1 in the control cells were decreased upon gefitinib treatment, while in the *CIC* mutant cells upon gefitinib treatment, ETV1 protein levels were maintained at a level comparable with or higher than the basal level of DMSO-treated control cells (Fig. 7C; Supplemental Fig. S4B). Collectively, these results suggest that sustained activation of *ETV1* and possibly other Ets factors contribute to gefitinib resistance mediated by *CIC* loss.

ETV5 protein was expressed at low levels in PC9 cells, and these levels were reduced upon gefitinib treatment (Fig. 7C). Basal ETV5 levels were much higher in *CIC* mutant cells, and, while partially reduced by gefitinib treatment, significant levels of ETV5 still remained after gefitinib treatment and could potentially contribute to gefitinib resistance. Surprisingly, while ectopic expression of *ETV5* showed increased basal levels in untreated cells, addition of gefitinib reduced the protein to undetectable levels. Consistent with this, doxycycline (Dox)-induced expression of *ETV5* in PC9 cells had no effect on sensitivity to gefitinib treatment (Fig. 7A). Thus, the role of *ETV5* in promoting gefitinib resistance in *CIC* mutants remains to be established.

Discussion

We used LOF and GOF genetic screens to systematically investigate genetic interactions among cancer drivers with a focus on RTK pathways. The validity of this genetic interaction screen was the identification of many genes previously known to play roles in RTK signaling, although only a few had been shown previously to impact cell growth and survival in EGFR-dependent cell lines. This is illustrated by the heat map pathway shown in Figure 8.

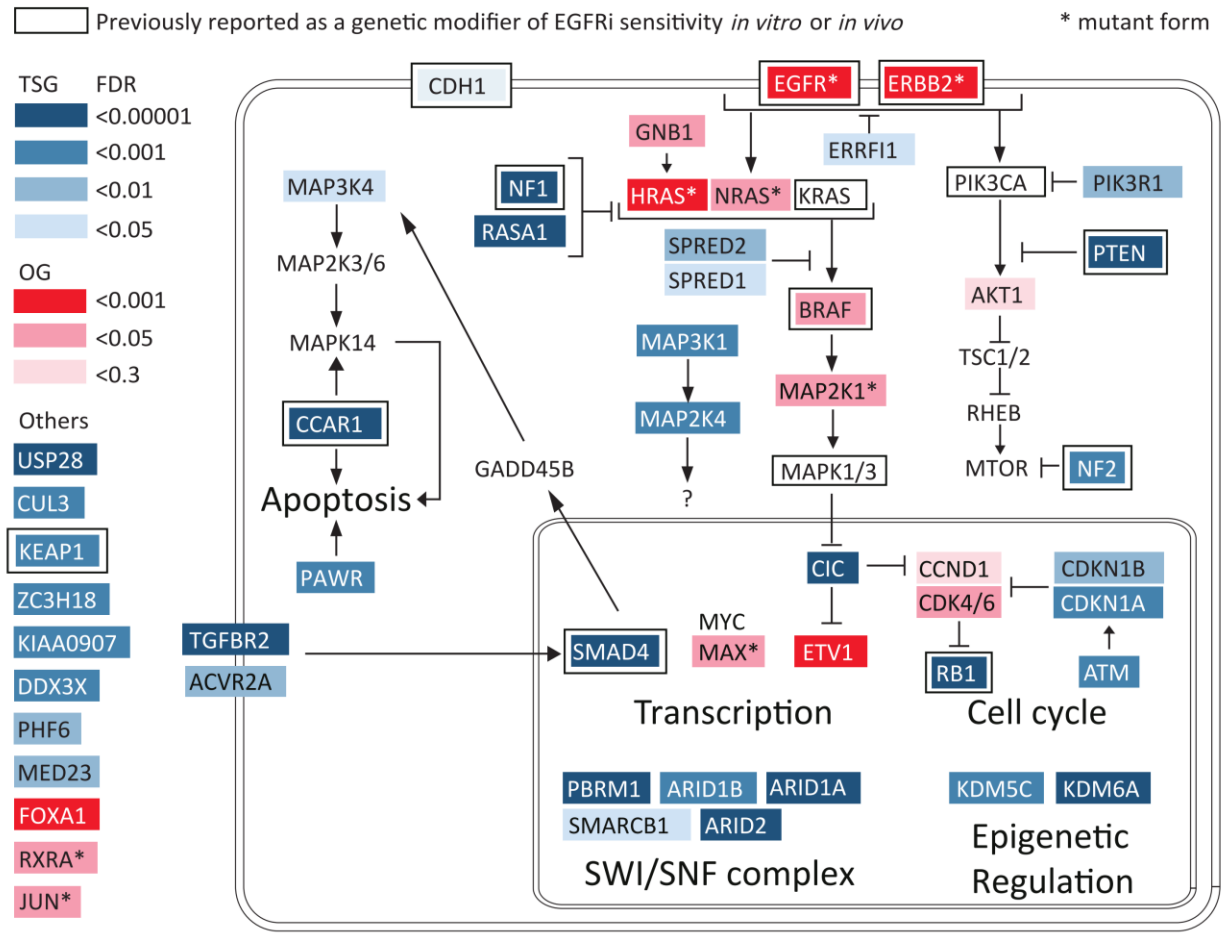

Figure 8. Summary and pathway schematic. Genetic interactions of TSGs and OGs with the EGFR pathway.

Core members of the RTK pathway, *EGFR* and *ERBB2 (HER2)* scored strongly, as did *HRAS* and *NRAS*, key downstream effectors of the RTK pathway (Supplemental Table S1). Additional regulators of RAS – the RAS-GAPs *NF1* and *RASA1* – stood out, as did *SPRED1* and *SPRED2,* known to negatively influence RAS downstream signaling. Direct effectors of RAS such as *BRAF* and *MAP2K1* also strongly scored, as did additional MAPK pathways that may function in various feedback mechanisms at play in RTK signaling. Genes involved in the PI3K pathway

that act downstream from RTKs, such as *PIK3R1*, *PTEN*, *NF2* (144), and *AKT1*, were also recovered in our screens.

We observed additional pathways whose direct connection to the RTK signaling is less clear. They may represent parallel pathways that provide equivalent functions. Perturbation of the TGF-β pathway – including the two TGF-β superfamily receptors *TGFBR2* and *ACVR2A* and their downstream effector, the transcription factor *SMAD4* – all showed phenotypes. *SMAD4* loss has been shown previously to impact resistance to EGFRis (145), but how it suppresses EGFRi sensitivity is not known. Other key pathways illustrated in the screen involved proliferation and survival. Genes involved in promoting apoptosis such as *CCAR* and *MAP3K4* (146) were also identified. Consistent with the identification of *MAP3K4*, TGF-β signaling was shown to play a role in tumor inhibition by activating MAPK14 (P38 MAPK) signaling through *SMAD4*-dependent GADD45β expression (147). This could be part of the mechanism of EGFRi resistance mediated by *SMAD4* loss. Among genes promoting proliferation are the central G1/S transition regulators such as the CDK4/6–Cyclin D genes (141) and their inhibitors, $p21^{CDKN1A}$ and $p27^{CDKN1B}$. In addition, the downstream inactivation target of the CDK4/6 kinases, the *RB1* gene (148) that is known to restrain cyclin E and other genes necessary for promoting entry into S phase was a strong hit in the screen. This central network may be a direct target of many TSG and OG drivers and has been linked to both RTK and TGF-β pathways in other contexts (149-152). Another key pathway known to regulate proliferation and survival identified in our screens was the MYC–MAX pathway. While *MAX* scored, *MYC* did not, but it is possible that MYC is already in excess, and its partner, MAX, is rate-limiting in this cell line. We also recovered *CDH1* in our screens, down-regulation of which was shown previously to up-regulate *EGFR* and promote proliferation and invasiveness in NSCLC cells (153).

Many TSGs and OGs not previously connected to RTK signaling emerged from our screens, including *USP28* and the CUL3–KEAP1 E3 ubiquitin ligase complex. Damaging mutations in *KEAP1* were previously shown to mediate EGFRi resistance (154). Among these, the SWI/SNF complex stood out, as multiple members of that complex scored as modifiers of EGFR-dependency. Two SWI/SNF subunits, *SMARCE1* and *ARID1A*, have been reported to confer resistance to MET and ALK inhibitors by regulating *EGFR* expression (138). However, we showed that loss of *PBRM1* does not affect EGFR levels. Instead, *PBRM1*-mutant NSCLC cells were able to restore activation of AKT in the presence of gefitinib after an initial inhibition. AKT signaling pathways are known to rebound in the continuous presence of PI3K inhibitors due to relief of various feedback mechanisms (155, 156), but it is unknown whether the effect of EGFR inhibition works through the same mechanism as PI3K inhibitors and, in this case, the rebound in response to gefitinib is dependent on *PRBM1* mutation. Thus, how *PBRM1* restrains AKT activation remains to be determined. The different mechanisms underlying the regulation of EGFR signaling by different subunits of SWI/SNF may be complex. Also, despite the role of *PBRM1* in regulating p21 in other cellular contexts, knockdown of *PBRM1* in PC9 cells did not affect the basal level of p21 or its level during gefitinib treatment. This may be in part because the composition of the SWI/SNF complex varies from tissue to tissue as do its transcriptional targets (135). This level of combinatorial complexity may allow for different mechanisms depending on which subunits are expressed and in which tissues they are present.

Another TSG identified and characterized in our study is *CIC*. *CIC* has been studied primarily in *Drosophila melanogaster,* where it acts downstream of EGFR during fly development. Depending on the context, EGFR signaling causes the CIC protein to decrease or to exit the nucleus and relocate to the cytoplasm (157). In some cases, neither of these events occur, but the activity

is somehow interfered with by RAS/MAPK signals (158). In PC9 cells, we did not see either induction of CIC protein or increased localization to the nucleus under gefitinib treatment (data not shown), suggesting another form of inactivation in response to EGFR signaling. Regardless, these studies suggest that the relationship between CIC and EGFR found in *Drosophila* is conserved in humans and that *CIC* loss can suppress loss of EGFR signaling in both organisms.

The mechanism through which *CIC* loss impacts EGFR signaling and resistance to gefitinib is likely its role as a transcriptional repressor of genes that affect the ability of cells to maintain cell proliferation. Among the transcriptional targets induced in PC9 cells in the absence of *CIC*, we identified a D-type cyclin (*CCND1*) and a family of Ets-related transcription factors (*ETV1*, *ETV4*, and *ETV5*). Furthermore, the CDK4/6 kinase inhibitor *CDKN2B* is induced by gefitinib in *CIC* wild-type cells, but this induction was abrogated in the absence of *CIC* (Supplemental Table S2). A functional role for regulators of the CDK4/6–Cyclin D/RB pathway in mediating part of the bypass of EGFR function in the absence of *CIC* was suggested by the enhanced sensitivity of *CIC* mutant PC9 cells to gefitinib in the presence of the CDK4/6 inhibitor palbociclib (Fig. 5F). The fact that *CDK4* and *CDK6* overproduction provided gefitinib resistance in the OG screen (Supplemental Table S1) further supports a role for cell cycle regulation in EGFR-driven cell proliferation.

The Ets factors, which have known oncogenic functions, are also likely to play an important role in the ability of *CIC* mutants to modify PC9 cells' resistance to gefitinib. Ectopic *ETV1* expression conferred gefitinib resistance to these cells. It is likely that *ETV4* and *ETV5* also play a role in mediating resistance to gefitinib in the absence of *CIC*; however, we were unable to test this because we were unable to express sufficient levels of these proteins in PC9 cells.

Unexpectedly, while we were able to express detectable levels of ETV5 from an exogenous promoter, inhibition of EGFR still extinguished ETV5 protein levels, suggesting that active EGFR is promoting the expression of *ETV5* both transcriptionally and post-transcriptionally. Nonetheless, the derepression of this family of oncogenic transcription factors is likely to play an important role in how *CIC* loss mediates resistance to *EGFR* inhibition in PC9 cells.

The present systems-level study of the genetic interactions among cancer drivers provides strong support for the hypothesis that cancer drivers can substitute for each other in some contexts. We identified a large number of TSGs and OGs that can genetically modify the growth and survival deficiencies caused by reduced EGFR signaling. In addition to the genes already known to modify resistance to EGFR inhibition and genes directly implicated in the RTK–RAS–PI3K signaling pathway, we uncovered many new TSGs and OGs that can genetically interact with EGFR signaling. These genes may play a role in augmenting the RTK–RAS–PI3K pathway or parallel pathways that can provide cells with enhanced growth and survival functions that substitute for those lacking when EGFR signaling is impaired. Many of these genes become candidates for the 30% of tumors that acquire resistance through unknown mechanisms. This type of analysis can also be performed in cells experiencing other forms of OG addiction or TSG hypersensitivity to identify OGs and TSGs that modify their function and will provide information on the role of many relatively understudied cancer drivers.

Materials and Methods

Cell culture and reagents

PC9 cells were kindly provided by Dr. J. Engelman (Massachusetts General Hospital Cancer Center and Harvard Medical School). H1975 cells were kindly provided by K. K. Wong (Dana-Farber Cancer Institute and Harvard Medical School). 293T cells were purchased from American Type Culture Collection (ATCC). PC9 cells/ H1975 cells and 293T cells were maintained in RPMI 1640 medium (ATCC modification) and DMEM, respectively (Thermo Fisher Scientific, Inc.), supplemented with 10% heat-inactivated fetal bovine serum (FBS) (GE Healthcare HyClone), 100 IU/mL penicillin, and 100 μg/mL streptomycin in a humidified atmosphere of 95% air and 5% CO_2 at 37°C. Gefitinib, erlotinib, and AZD9291 were purchased from Selleck Chemicals. Palbociclib was a gift from Dr. K. Cichowski (Harvard Medical School).

TSG CRISPR library construction

A customized DNA oligonucleotide library with 10 gRNAs per gene for each of the 500 TSG candidates was synthesized on a microarray (Agilent). The gRNA oligonucleotide library was PCR-amplified by a set of specific primers and digested with BbsI. The digested gRNA was purified on a 10% TBE PAGE gel and cloned into BsmBI-digested pLentiCRISPR V2 (Addgene plasmid no. 52961).

TSG shRNA library construction

A customized DNA oligonucleotide library with 10 shRNAs per gene for each of the 500 TSG candidates was synthesized as above. The shRNA oligonucleotide library was PCR-amplified

by a set of specific primers and digested with XhoI and EcoRI. The digested PCR products were purified on a 3% Nusieve gel and cloned into the XhoI/EcoRI-digested vector (pMSCV-mirE-pheS) to make pMSCV-mirE libraries. The pMSCV-mirE libraries were digested with XhoI/MluI and cloned into XhoI/MluI-cut pHAGE-Ind10-mirE. The pMSCV-mirE-pheS vector was made by two steps. First, pMSCV-PM-pheS plasmid DNA was digested with EcoRI, and a pair of complementary oligonucleotides containing the 3'mirE sequences was inserted using SLIC (159) to generate pMSCV-mirE3'-pheS. Secondly, the pMSCV-mirE3'-pheS plasmid was digested with HpaI and a pair of complementary oligonucleotides containing the 5'mirE sequence was inserted using SLIC to generate pMSCV-mirE-pheS.

CRISPR and shRNA screen

The CRISPR and shRNA screens were performed in three and two replicates, respectively. Each library contained 10 gRNAs or 10 shRNAs per gene for each of the 500 TSG candidates and 1000 gRNAs or 1000 shRNAs targeting the *E. coli* genome as negative controls. PC9 cells were transduced using 4 μg/mL polybrene (Sigma) at a low multiplicity of infection ([MOI] = 0.2) with an average representation of ~1000 cells per gRNA/shRNA. Transduced cells were then selected with 1 μg/mL puromycin (Clontech) for 3 d. The shRNA library was constructed in a Dox-inducible vector. After puro selection, Dox was added 3 d prior to gefitinib treatment, allowing the targeted genes to be knocked down. For the CRISPR screen, cells were passaged for 9 d, allowing enough time for genome modification by Cas9. Cells from the initial time point were harvested, and the cells were then split into two arms and treated with either DMSO or 30 nM gefitinib for ~17 d. Cells from the end time point (DMSO treatment and gefitinib treatment for 17 d) were then harvested. Genomic DNAs containing shRNA or gRNA were amplified by PCR and subsequently

subjected to NGS. The MAGeCK scoring algorithm was used to rank the performance of individual genes based on enrichment, comparing the gefitinib treatment group with the DMSO treatment group at the endpoint. The negative controls were incorporated in the MAGeCk analysis to generate null distributions and calculate the *P*-value and FDR for each gene. Combined FDRs of the two screens were generated using combined *P*-values generated by Fisher's method and were used as the FDRs for TSGs in Figure 8.

OG barcoded-ORF library construction

OGs were individually picked from ORFeome V8.1 and Ultimate ORF libraries. Genes with mutant alleles were generated using QuikChange II XL site-directed mutagenesis kit (Agilent Technologies). All of them were sequence-verified and then were cloned into a pre-barcoded pHAGE-TRE-DEST-3'BC library via Gateway LR Clonase II (Invitrogen). The resulting lentiviral library contains a list of ~ 50 3'barcoded OGs under the control of a Dox-inducible TRE promoter and the rtTA gene. Sequencing was performed to link the barcodes with genes. There are on average about 5 barcodes per gene.

OG screen

The OG screen was performed in three replicates. PC9 cells were transduced with the OG barcoded-ORF library using 4 μg/mL polybrene (Sigma) at a low MOI (MOI = 0.2) with an average representation of ~1000 cells per barcode. Transduced cells were then selected with 1 μg/mL puromycin (Clontech) for 3 d and grown for 7 d. Dox (1 μg/mL) was added, and cells were grown for 3 d, allowing the genes to be expressed. Next, either DMSO or 30 nM gefitinib was

added, and cells were grown for ~17 d in medium containing Dox. DNA was harvested, processed, and analyzed as described above.

Analysis of the somatic mutation data set and focal deletion data set

The data sets of somatic mutations and focal deletions of lung adenocarcinoma patients were from TCGA (http://cancergenome.nih.gov). We classified patients harboring the following activating mutations in *EGFR* as *EGFR* mutant patients: p.L858R, p.TSPKANKE751del, p.KANKEI754del, p.LREAT747del, p.ELR746del, p.ELREA746del, p.G719A, p.G719C, p.G719S, p.V765A, p.T783A, and p.L861Q. After excluding patients with mutations > 1000, we ended up with 50 *EGFR* mutants and 443 *EGFR* wild-type patients.

We used the PolyPhen2 Hum-Var prediction model (160) to weigh the functional impact of each missense mutation. Based on the possible or probable damage in the Hum-Var prediction by PolyPhen2, we defined missense mutations with a Hum-Var score > 0.447 as damaging. We defined LOF mutations as nonsense, frameshift, and "damaging missense" (corresponding to possibly or probably damaging in the Hum-Var prediction with a score > 0.447). We defined a gene as focally deleted if its $\log_2$ copy number change was lower than -0.2.

Because of the low number of *EGFR* mutant tumors in our data set, most genes had few mutations and could not be analyzed individually. Therefore, we pooled 30 genes as a group to reduce noise and gain statistical power. We then calculated the average percentage of LOF mutations (L^{Top30}) for our top 30 TSG hits in *EGFR* mutant and wild-type patients as follows:

$$L^{Top30} = \frac{\sum_{gene=1}^{30} \sum_{patient=1}^{n} (\text{Nonsense} + \text{Frameshift} + \text{Missense}^{HVar>0.447})}{\sum_{gene=1}^{30} \sum_{patient=1}^{n} (\text{All mutations})} * 100\%$$

We then performed 10,000 permutations using a random group of 30 genes to get the distribution of L^{TSG}(using genes in the TSG library with rank position > 65 in the screens, FDR > 0.1) or L^{genome} (using all genes in the genome, excluding the ones in the TSG library). The *P*-value of L^{Top30} was calculated based on the distribution of L^{TSG}.

The analysis of mutual exclusivity of each gene with activating *EGFR* was performed using the Fisher exact test (one-tailed test) based on 447 patients who had both mutation and focal deletion data.

Western blot analysis

Cells were lysed in 1× NuPAGE LDS sample buffer (Thermo Fisher Scientific) supplemented with 1× Bond-Breaker TCEP (Life Technologies) and 1× Halt protease and phosphatase cocktail (Life Technologies) on ice. The whole-cell lysates were sonicated briefly to break down the chromatin. Samples were boiled for 5 min at 95°C and then loaded to 4-12% Bis-Tris Protein Gels (Novex) and transferred to iBlot Transfer Stack nitrocellulose membranes (Novex). Membranes were incubated with primary antibodies overnight at 4 °C then with horseradish peroxidase-coupled secondary antibodies at 1:5000 dilution at room temperature for 1 h. Proteins were visualized using an enhanced chemiluminescence kit (PerkinElmer).

The antibodies used were Tubulin (1:2500; Cell Signaling, 2128S), GAPDH (1:2500; Cell Signaling, 8884), PBRM1 (1:500; Bethyl Laboratories, A301-591A-M), p21 (1:1000; Cell Signaling, 2947S), phospho-EGFR (Tyr1068; 1:1000; Cell Signaling, 2236S), EGFR (1:1000; Cell Signaling, 2232S), phospho-ERK1/2 (T202/Y204; 1:1000; Cell Signaling, 4370P), total ERK1/2 (1:1000; Cell Signaling, 4695P), phospho-AKT (S473; 1:1000; Cell Signaling, 4060P), total AKT

(1:1000; Cell Signaling, 2920S), ETV1 (1:1000; Abcam, ab184120), ETV5 (1:1000; Abcam, ab54704), and CIC (1:5000; a gift from Dr. Huda Zoghbi).

Multicolor competition assay

GFP-labeled PC9 cells were transduced with the indicated gRNA/ORFs, and mRuby-labeled PC9 cells were transduced with GFP gRNA/EV. After puromycin selection and 3 d of 1 μg/mL Dox treatment for ORF-expressing cells, GFP-labeled PC9 cells were mixed with mRuby-labeled PC9 cells in a 50:50 ratio in six-well plates. After treatment of DMSO or the indicated dose of the drug, the drug and medium were replaced every 2 d, and the percentage of GFP-labeled gRNA/ORF-expressing cells was quantified using FACS (BD, LSR II).

Colony formation assay

Single-cell suspensions were seeded into six-well plates (200 cells per well) and incubated overnight before continuous treatment of DMSO for 2 wk or 30 nM gefitinib for 3 wk, with drug and medium replaced every 2 d. At the end of treatment, cells were fixed with 10% trichloroacetic acid, washed, and stained with SRB as described previously (161).

Cell viability assay

The effects of gefitinib on cell proliferation were determined by SRB as described previously (161).

Apoptosis and cell cycle analysis

Cells seeded in six-well plates (5×10^4 cells per well) were treated with DMSO or 30 nM gefitinib for 48 h. For apoptosis analysis, cells were then fixed with 70% (v/v) cold ethanol overnight at −20°C and stained with PI solution (20 μg/mL PI [Sigma-Aldrich], 0.1% Triton X-100, 8 μg/mL RNase). For cell cycle analysis, cells were pulsed with BrdU (10 μM final concentration) for 1 h prior to fixation. BrdU labeling and staining were performed using the APC BrdU flow kit (BD Biosciences) according to the manufacturer's instructions. Samples were analyzed by flow cytometry (BD, LSR II).

Quantitative RT-qPCR

Total RNA was isolated using the RNAeasy mini kit (Qiagen), and cDNA was synthesized using SuperScript IV (Invitrogen) according to the manufacturer's instructions. Quantitative RT-qPCR was performed in triplicate using the TaqMan gene expression master mix (Invitrogen) with TaqMan gene expression assay (Life Technologies) on an Applied Biosystems Fast 7500 machine using GAPDH as the endogenous normalization control. The IDs for the TaqMan assays used were as follows: GAPDH (Hs99999905_m1), ETV1 (Hs00951951_m1), ETV4 (Hs00383361_g1), ETV5 (Hs00927557_m1), and CCND1 (Hs00765553_m1).

Gene expression profiling

PC9 cells were transduced with pLentiCRISPR V2 with gRNA targeting GFP or CIC. Infected cells were selected using 1 μg/mL puromycin (Clontech) for 3 d. One week after transduction, cells were treated with DMSO or 30 nM gefitinib for 6 h. Total RNA was isolated using the RNAeasy mini kit (Qiagen). RNA-seq libraries were generated using NEBNext ultra

RNA library preparation kit (New England Biolabs). RNA-seq was performed using two replicates for control GFP gRNA and three different gRNAs of CIC as three replicates. 50bp single end sequencing was performed using an Illumina HiSeq 2500. Reads were aligned to the hg19 genome using HiSat2 (162); transcripts and frequencies were assessed from the aligned data by subread (163), and edgeR (164) was used to identify DEGs and generate the counts per million expression values used for GSEA (http://www.broadinstitute.org/gsea/) (165). PPI hubs were identified using Enrichr (166). Z-scores were used to generate a heat map of relative expression levels. Each sample was normalized to the basal condition (GFP-gRNA-infected, DMSO-treated sample 1) by subtracting the Z-score of the basal condition from the Z-score of each sample for each gene as $Z^{\text{nomalized to basal}} = Z^{\text{sample}} - Z^{\text{GFP gRNA, DMSO sample 1}}$.

Plasmids, cloning and viral transduction

gRNAs were cloned into pLentiCRISPR V2 (Addgene, plasmid no. 52961) as described previously (167).

The sequences targeted by the gRNAs used were as follows (if the first base of the targeted sequence is not G, it was changed to G during cloning for expression under U6 promoter): GFP, GGGCGAGGAGCTGTTCACCG; PBRM1_1, CGAGACTATAAGGATGAACA; PBRM1_2, GCAATGGTCTTGAGATCTAT; PBRM1_3, TCATTAGGGCACCAAAGCGA; CIC_1, GCAACCTGCCAGCCACCCAG; CIC_2, GGGGTACACAGCCTGGACGG; CIC_3, GGGGCGGCAGTGGGTAAAGG; and NF1, GAGAGAAAATAAAACCCCAG. cDNA for ETV4 was from PlasmID. cDNAs for ETV1 and ETV5 were from the human ORFeome library version 8.1. Stop codons were added using QuikChange II XL site-directed mutagenesis kit

(Agilent Technologies). cDNAs were subcloned into pHAGE-TREx-BC-Dest vector via LR recombinase reaction (Invitrogen).

To produce lentiviruses, 293T cells were transfected with vector DNA, pRev, pTat, pHIV Gag/pol, and pVSVG. Viruses were harvested 48 h after transfection and filtered (45-μm pore size). TransIT-293 (Mirus) was used to transfect 293T cells.

Cells were transduced with 4 μg/mL polybrene, and infected cells were selected using 1 μg/mL puromycin (Clontech) for 3 d. pLentiCRISPR-V2-infected cells were subjected to multicolor competition assay, cell viability assay, colony formation assay, or immunoblot analysis 1 wk after infection to allow for genome modification by Cas9. Cells expressing ORFs were treated with 1 μg/mL Dox for 3 d prior to subsequent experiments for ORF expression and maintained in medium containing 1 μg/mL Dox during subsequent experiments.

Statistical analysis

Data are presented as the mean ± SD, and significance was analyzed using the Student's *t*-test. Differences were considered significant when $P < 0.05$.

Chapter 3

Genetic modifiers of the BRD4-NUT dependency of NUT midline carcinoma uncovers a synergism between BETis and CDK4/6is

Note: This entire chapter, was published in the article: Liao S, Maertens O, Cichowski K, Elledge SJ. Genetic modifiers of the BRD4-NUT dependency of NUT midline carcinoma uncovers a synergism between BETis and CDK4/6is. Genes Dev. 2018;32(17-18):1188-200.

Introduction

NUT midline carcinoma (NMC) is an aggressive subtype of squamous cell cancer. Genetically, it is defined by the fusion of most of the coding sequence of the testes-specific gene NUT on chromosome 15 to several other genes – most frequently the BRD4 gene on chromosome 19 (BRD4-NUT) (110, 111). BRD4 is an epigenetic reader that binds to acetyl-histone. Fusion to the NUT protein results in recruitment of p300/CBP, a histone acetyl-transferase, leading to regional histone hyperacetylation. Such acetylation further recruits BRD4-NUT in a feed-forward manner, eventually creating massive regions of acetylated chromatin that covers individual topologically associating domain across the genome (112). The transcription of oncogenic proteins such as c-Myc (encoded by *MYC*) and its regulators within these regions is thus stimulated, blocking cellular differentiation and promoting uncontrolled growth of carcinoma cells (112, 113).

Small molecule bromodomain and extraterminal (BET) domain inhibitors (BETis) that target and inhibit BRD4's association with chromatin have shown anti-cancer efficacy on a variety of cancers, including NMC, in preclinical models and are currently being evaluated in clinical trials (92). A clinical proof of concept for BETis in NMC was demonstrated recently (115). Two of four NMC patients receiving BRD4 inhibition therapy showed increased overall survival (19 and 18 mo, respectively), which was notably longer than the median survival of ~7 mo reported in the largest retrospective series of patients with NMC (114). However, as is often the case with other single-agent therapies, cancer cells can develop resistance to BETis through a variety of mechanisms (96, 101, 103-106, 108, 109, 168, 169). Despite the initial response, all of the NMC patients developed resistance to the BETis and eventually relapsed. Therefore, there is an urgent

need to identify the underlying mechanisms of resistance to BRD4 inhibition in NMC in order to develop combination therapies or alternative regimens after BRD4 inhibitor progression.

Cancer is driven by a number of distinct genetic alterations including gain or loss of chromosomes and chromosomal segments, translocations, frameshifts, and point mutations that result in inactivation of TSGs or activation of OGs. We previously developed an algorithm called TUSON Explorer to identify known and putative cancer drivers using human tumor sequencing data (20). We and others have shown that cancer drivers can genetically interact and substitute for one another to drive proliferation and survival in *EGFR* mutant NSCLCs and other cancer models (40, 130, 170, 171), suggesting that it might be a general notion that cancer drivers can form a function network and genetically modify the dependency of each other. Thus, the TSGs and OGs identified by TUSON Explorer could serve as an ideal list to survey for the genetic modifiers that can partially replace the cancer driver of interest – BRD4-NUT, in the case of NMC.

To systematically identify the TSGs and OGs that can partially replace BRD4-NUT in BRD4-NUT-dependent NMC tumor cells, we performed CRISPR and OG/ proto-oncogene expression screens in parallel using an *in vitro* NMC model. Here, we show that this genetic approach successfully recovered previously validated cancer drivers that mediate BETi resistance, such as *MYC*, in addition to novel cancer drivers not previously linked to BETi resistance in NMC. We further characterized the mechanisms underlying BETi resistance mediated by several novel OGs. Among these, we showed that mutation of *RRAS2*, a member of the R-Ras subfamily of Ras-like small GTPases, attenuated the effect of JQ1 in part by sustaining ERK pathway function during BRD4 inhibition. We also showed that overexpression of Krüppel-like factor 4 *(KLF4)*, a transcriptional factor, mediated JQ1 resistance in NMC cells through restoring the E2F and MYC

gene expression program upon JQ1 treatment. Finally, we showed that expression of cyclin D1 and mutant cyclin D3 or loss of *RB1* protected the NMC cells from JQ1-induced cell cycle arrest. In accordance with this observation, CDK4/6 inhibitors showed synergistic effects with JQ1 on NMC *in vitro* as well as *in vivo*, revealing the central role of cell cycle regulation in mediating JQ1 response. These findings provide new biochemical insight into the resistance mechanisms to BETis in NMC as well as a rationale for combination therapy of BETis and CDK4/6 inhibition on NMC.

Results

To investigate the question of which drivers could substitute for BRD4-NUT in NMC, we used a CRISPR library containing 10 gRNAs per gene to a list of ~500 putative TSGs implicated using the TUSON Explorer algorithm (Fig. 1). In addition, we expanded a Dox-inducible barcoded-ORF library of putative OGs (40) to a total of ~400 constructs that contained ~150 both wild-type proto-oncogenes and their recurring mutant alleles identified by TUSON. We also included genes that are frequently amplified in cancers (172), identified in the Cancer Gene Census (27), or implicated in cancer hallmarks such as cell proliferation (173), anchorage-independent growth (174), epithelial-to-mesenchymal transition (175) etc., as well as ~40 "neutral genes" that behaved in a neutral fashion in a previous genetic screen that looked for cell proliferation regulators (173). We used these libraries to determine which alterations could substitute for BRD4-NUT signaling using a chemical inhibitor of BET proteins: JQ1. We performed screens using an NMC cell line (NMC1015) that harbors a BRD4-NUT fusion and is sensitive to JQ1 (113).

The schematic of the CRISPR and ORF screens is outlined in Figure 9 and described in detail in the Materials and Methods.

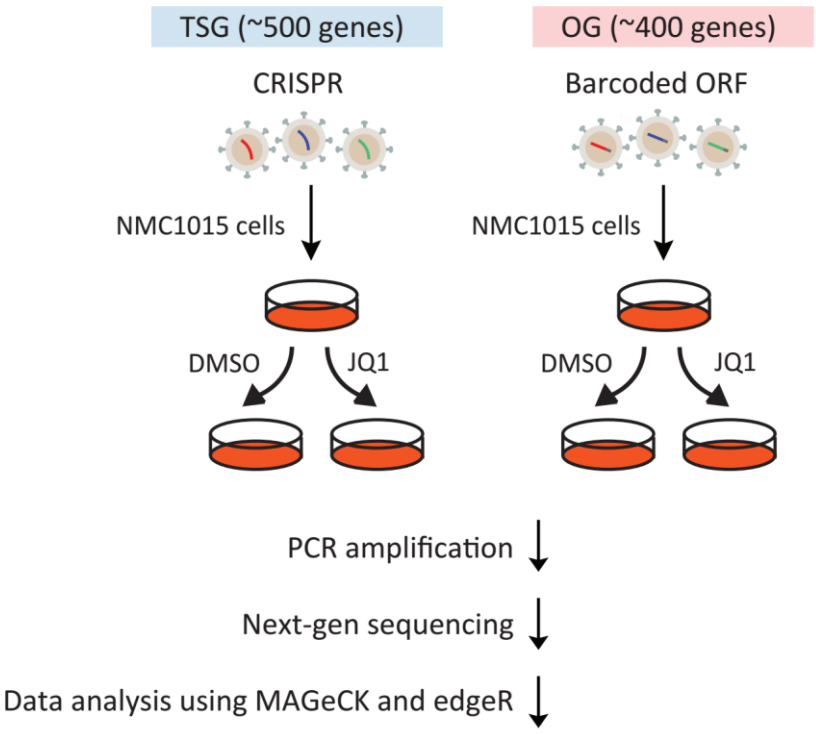

Figure 9. Outline of the genetic screening strategy of JQ1 bypass screens.

In each screen, cells were treated with either DMSO or 200 nM JQ1 for ~17 d. We used the MAGeCK scoring algorithm (134) and edgeR analysis (164) to rank the performance of individual genes in the CRISPR and ORF screen respectively based on enrichment comparing the JQ1 treatment group with the DMSO treatment group. The rank and FDR of each gene in the two screens are summarized in Supplemental Table S3. The top 10 hits (FDR < 0.05) from the CRISPR screen and top 20 hits (FDR < 0.05) from the ORF screen are shown in Figure 10A and B. An immediate validation of our screen approach is that, *MYC*, a major downstream target of BRD4-

NUT that can replace its function to prevent differentiation/arrested proliferation induced by the knockdown of BRD4-NUT (113), scored as the number one hit in the OG screen.

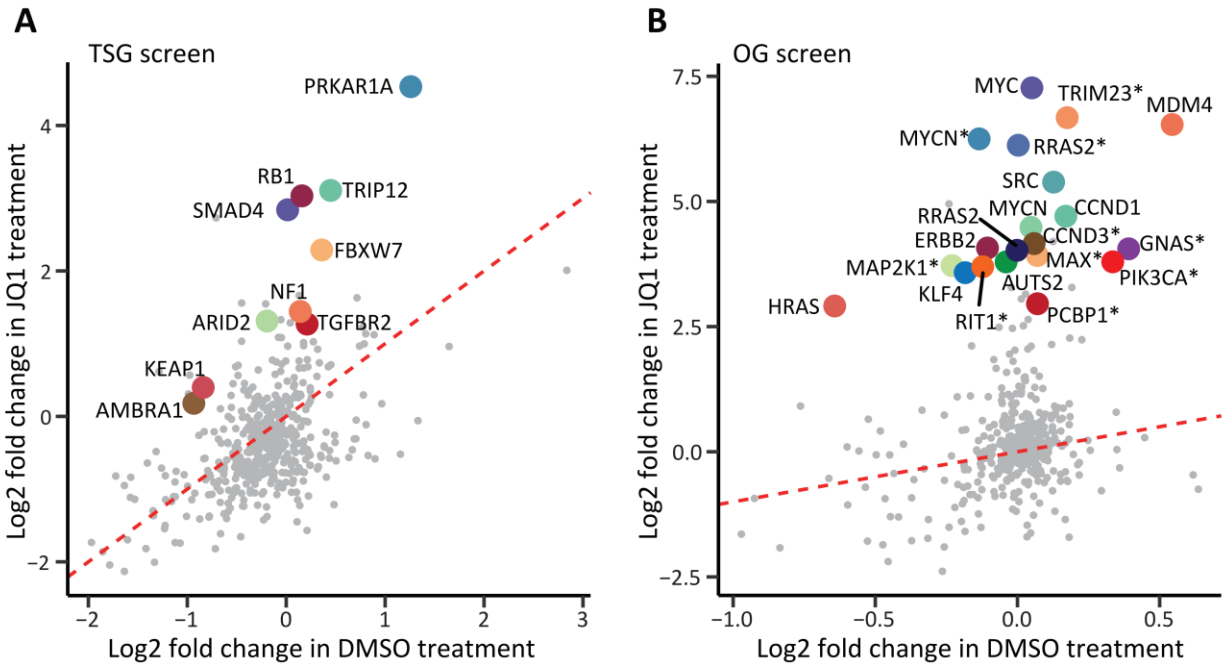

Figure 10. Genetic screens identify modifiers of the cellular response to reduced BRD4-NUT signaling. (A,B) Log_2 fold change comparing end time point (day 17) with start time point (day 0) of JQ1 treatment plotted against vehicle (DMSO) treatment for genes in the CRISPR and ORF screens, respectively. The top 10 genes of the CRISPR screen and the top 20 genes of the ORF screen (FDR <0.05) are highlighted. The asterisk indicates a mutant form of the gene.

Notably, the novel cancer drivers we identified largely fall into the following five categories: (1) MYC-related genes: *MYCN* (wild type and c.131C > T; p.P44L), *MAX* (c.179G > A; p.R60Q), and *FBXW7*; (2) RTK signaling pathway: *ERBB2*, *SRC*, *RRAS2* (wild type and c.216A > C; p.Q72H), *HRAS*, *NF1*, *MAP2K1* (c.371C > A; p.P124Q), and *PIK3CA*(c.3140A > G; p.H1047R); (3) cell cycle regulation: *CCND1*, *CCND3* (c.869T > G; p.I290R), and *RB1*; (4) the G-protein-coupled receptor (GPCR)/cyclic AMP (cAMP)/cAMP-dependent protein kinase A (PKA) signaling pathway: *GNAS* (c.2530C > T; p.R844C) and *PRKAR1A*; and (5) TGF-β pathway: *SMAD4* and *TGFBR2*.

Given the stronger phenotype (larger fold change) induced by the OGs compared with TSGs, we primarily focused our efforts on characterization of the novel OG hits.

Mutant RRAS2 Attenuates the Effect of JQ1 by Sustaining ERK Pathway Activation During BRD4-NUT Inhibition

One of the top hits identified in our OG screen is RRAS2, a Ras-related GTPase with transforming potential (176, 177). Downstream effectors of RRAS2 include three members of the mitogen-activated protein kinases (MAPKs); namely, ERK1/2, c-Jun N-terminal kinase, and p38 MAPK as well as PI3K (177-180). The amino acid Q72 of RRAS2 is conserved in K-Ras, H-Ras, and N-Ras (Q61) in humans (Fig. 11A). Q61 mutations in KRAS are commonly found in human cancers and mutations such as Q61L have been shown to increase KRAS activity through higher affinity to RAF kinase compared with wild type (181). Consistent with this, both wild-type and Q72H-mutant RRAS2 scored in our screen, and the mutant form showed a stronger phenotype (larger fold change) in the screen (Fig. 10B).

To explore how RRAS2 impacts JQ1 resistance in NMC cells, we first validated the effect of expression of Q72H-mutant RRAS2 on JQ1 resistance using an independent NMC cell line, NMC797 cells (182). As seen with NMC1015 cells, expression of mutant RRAS2 significantly increased the survival of NMC797 cells in response to JQ1 treatment, as measured by SRB assay (Fig. 11B). To identify the downstream effectors of mutant RRAS2, we examined the two signaling kinases that have been reported previously to be responsible for RRAS2-induced cell transformation: ERK and PI3K.

Figure 11. Mutant RRAS2 attenuates the effect of JQ1 by sustaining ERK pathway activation during BRD4-NUT inhibition. (A) Protein sequence alignment of human RRAS2 (UniProt entry P62070), KRAS (UniProt entry P01116), HRAS (UniProt entry P01112), and NRAS (UniProt entry P01111) using UniProt. An asterisk indicates positions that have a single fully conserved residue. A colon (:) indicates conservation between groups of strongly similar properties (roughly equivalent to scoring >0.5 in the Gonnet PAM 250 matrix). A single dot indicates conservation between groups of weakly similar properties (roughly equivalent to scoring between 0 and 0.5 in the Gonnet PAM 250 matrix). (B) NMC797 cells containing an empty vector (EV) or expressing the $RRAS2^{Q72H}$ mutant were treated with the indicated concentrations of JQ1 for 72 h before cell viability was measured using an SRB assay and normalized to untreated controls. Data are means ± SD. n = 3. (C) Immunoblot analysis of NMC1015 cells containing an empty vector (EV) or expressing the $RRAS2^{Q72H}$ mutant treated with 200 nM JQ1 for the indicated time period and probed with the indicated antibodies. (D) Immunoblot analysis of NMC1015 cells containing an empty vector (EV) or expressing the $RRAS2^{Q72H}$ mutant treated with DMSO or 200 nM JQ1 and the indicated concentrations of SCH772984 for 72 h and probed with the indicated antibodies. (E) Immunoblot analysis of NMC1015 cells containing an empty vector (EV) or expressing the $RRAS2^{Q72H}$ mutant treated with DMSO or 200 nM JQ1 and the indicated concentrations of GDC-0068 for 72 h and probed with the indicated antibodies. (F) NMC1015 cells containing an empty vector (EV) or expressing the $RRAS2^{Q72H}$ were treated with 200 nM JQ1 plus DMSO or 1 μM SCH772984 for 72 h before cell viability was measured using an SRB assay. Results were normalized to untreated controls. Data are means ± SD. n = 3. (**) $P < 0.01$; (NS) not significant.

Figure 11 (Continued)

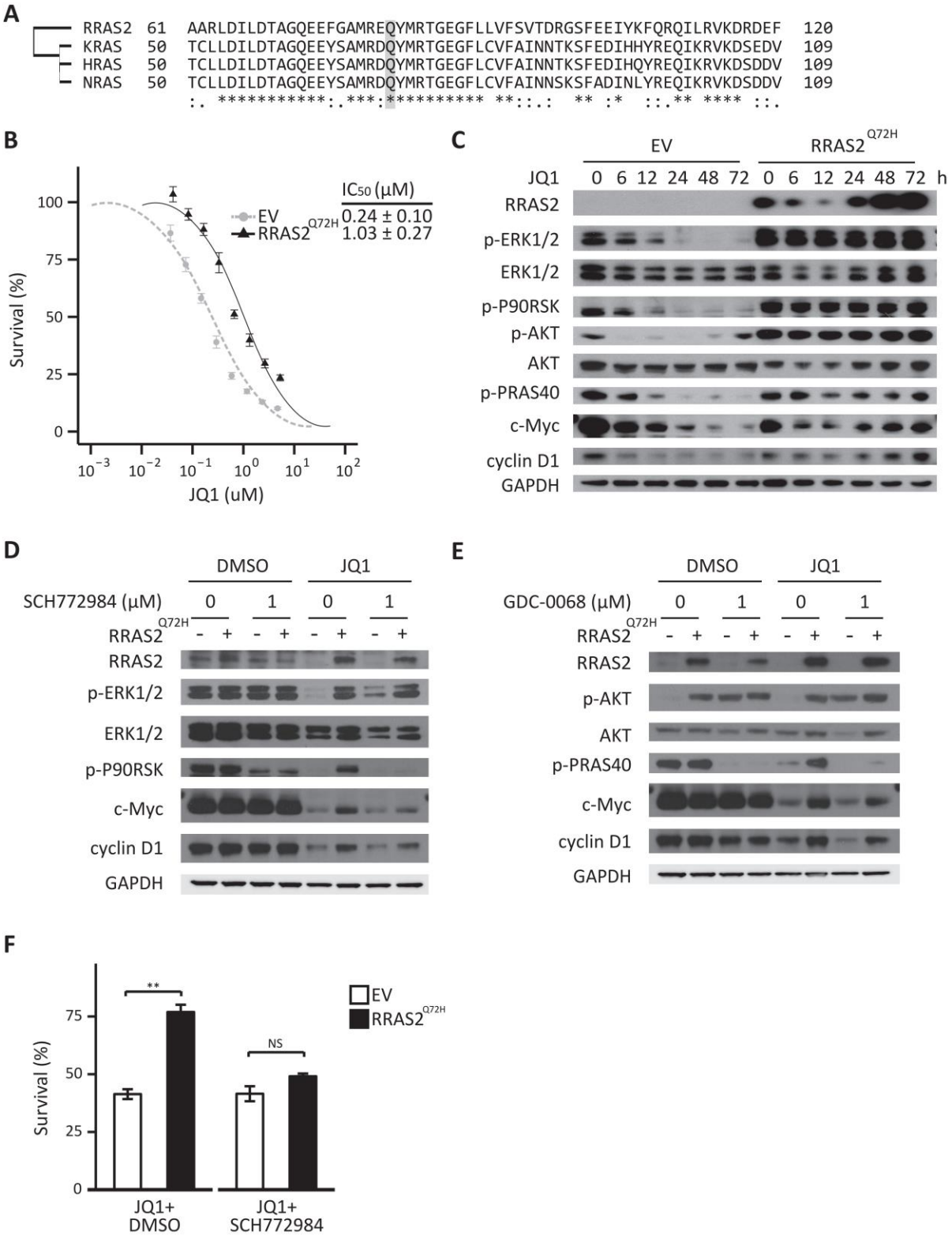

Surprisingly, JQ1 treatment inhibited ERK signaling measured by ERK1/2 phosphorylation (p-ERK1/2) and phosphorylation of its downstream effector, P90RSK (p-P90RSK), starting as early as 6 h and reduced the phosphorylation of these two proteins to nearly undetectable levels by 24 h in NMC1015 cells (Fig. 11C). However, expression of RRAS2^{Q72H} abolished the effect of JQ1 on ERK signaling (Fig. 11C). JQ1 also decreased the phosphorylation of AKT (p-AKT) and phosphorylation of its downstream effector, PRAS40 (p-PRAS40), at 6 h, and phosphorylation was barely detectable at 24 h (Fig. 11C). Expression of RRAS2^{Q72H} activated AKT and restored PRAS40 phosphorylation in the presence of JQ1, demonstrating that RRAS2 ^{Q72H} can rescue both of these signaling arms.

We note that JQ1 reduced the protein level of c-Myc (a known JQ1 target) and cyclin D1 (another gene identified in our screen in NMC1015 cells) with kinetics similar to its effect on ERK and AKT signaling. Cells expressing mutant RRAS2 also showed higher levels of c-Myc and cyclin D1, providing an attractive mechanism of action (Fig. 11C). Because ERK and AKT can regulate both of these pathways, we investigated their contributions to c-Myc and cyclin D1 expression downstream from RRAS2. Cells were cotreated with JQ1 and an ERK inhibitor (SCH772984) or an AKT inhibitor (GDC-0068). As noted above, JQ1 suppressed p-ERK and p-P90RSK and dramatically reduced the expression of c-Myc and cyclin D1, whereas RRAS2 largely restored ERK and P90RSK phosphorylation and increased c-Myc and cyclin D1 expression levels. Notably, SCH772984 reversed the effects of RRAS2 on p-ERK and p-P90RSK (Fig. 11D). Interestingly, the higher levels of c-Myc and cyclin D1 in mutant RRAS2-expressing NMC1015 cells during JQ1 treatment were also reduced to that of control cells by SCH772984 treatment. SCH772984 did not further reduce the p-P90RSK level of control NMC1015 cells, suggesting JQ1 alone potently inhibited ERK signaling in these cells.

As expected, GDC-0068 reduced p-PRAS40 levels of mutant RRAS2-expressing cells to that of control cells treated with JQ1 alone. However, it had less of an effect on c-Myc and cyclin D1 in mutant-RRAS2-expressing cells than the ERK inhibitor (Fig. 11E). Together, these results suggest that the RRAS2 mutant attenuates the suppressive effect of JQ1 on c-Myc and cyclin D1 levels, primarily through sustained ERK signaling, although sustained AKT may also contribute to a lesser extent.

The observation that ERK inhibitors could effectively reverse the effects of RRAS2 on these important downstream signals in JQ1 treated cells, suggested that ERK inhibitors might also negate the resistance conferred by RRAS2 in JQ1-treated cells. Consistent with signaling changes, while SCH772984 did not further reduce the viability of JQ1-treated control cells, SCH772984 resensitized mutant RRAS2-expressing cells to JQ1 (Fig. 11F). The contribution of ERK signaling to JQ1 resistance is further supported by the fact that the upstream kinase of ERK1/2, MEK1 (encoded by *MAP2K1*), also scored highly in the OG screen (Fig. 10B). Thus, sustained ERK signaling significantly contributes to the ability of RRAS2 to overcome JQ1's effect on survival.

KLF4 Mediated JQ1 Resistance in NMC Cells through Restoring the E2F and MYC Gene Expression Program upon JQ1 Treatment

Another novel hit identified in our OG screen is the Yamanaka factor *KLF4*. KLF4 is a zinc finger-containing transcription factor that plays a critical role in regulating a variety of cellular processes such as proliferation, differentiation, development, maintenance of normal tissue homeostasis and apoptosis. It can function as a TSG or OG in different cancers depending on the

cellular context (183). As an OG, KLF4 has been shown to mediate resistance to a variety of therapies such as chemotherapy and Her2 inhibition (184, 185). However, how it might modulate BRD4-NUT dependency is unclear.

We first validated the effect of *KLF4* expression on JQ1 resistance in NMC cells using a 3-d SRB assay. Surprisingly, expression of *KLF4* did not provide NMC cells with resistance to JQ1 as measured by this short-term viability assay (Supplemental Fig. S5A,B). However, when we examined the effect of *KLF4* expression on JQ1 resistance using a longer-term colony formation assay which is more reflective of the initial screen, *KLF4* expression significantly enhanced the colony formation of NMC1015 cells in the presence of JQ1 (Fig. 12A). One possible explanation is that KLF4 may take substantial time to remodel the cell state like Yamanaka factors have been suggested to work (186). Therefore, we pretreated *KLF4*-infected NMC797 and NMC1015 cells with Dox for 4 wk and measured their sensitivity to JQ1 using the 3-d SRB assay. Again, KLF4-expressing NMC cells did not show differential sensitivity to JQ1 (data not shown), suggesting that it is not the length of time of *KLF4* expression but the length of time of JQ1 exposure that determines the ability of *KLF4*-expressing cells to mediate JQ1 resistance.

To identify the effectors that are induced by KLF4 in the JQ1 resistance setting, we performed RNA-seq on empty vector or *KLF4*-expressing NMC1015 cells. Cells were treated with DMSO or 200 nM JQ1 for 6 h, 24 h, or 7 d (Fig. 12B). The full analyses of DEGs across different conditions are shown in Supplemental Table S4. Among the top genes that are differentially expressed comparing *KLF4*-expressing and control cells under JQ1 treatment, *MYC*; its downstream target, *TERT*; and several long noncoding RNAs (lncRNAs) such as *CCAT1* and *CASC19* stood out (Fig. 12C). Notably, the transcriptional down-regulation of these genes by JQ1

is attenuated by *KLF4* expression only at late (7 d) but not early (6 and 24 h) time points, which is consistent with the observation that *KLF4*-expressing cells manifest a resistant phenotype only in long-term, but not short-term, survival assays.

CCAT1 and *CASC19* are near the *MYC* locus, and *CCAT1* has been reported to play oncogenic roles through transcriptional up-regulation of *MYC* (187, 188). Previously, Alekseyenko et al. had shown that *CCAT1* and *CASC19* are among the few genes that are within BRD4-NUT megadomains that overlap in multiple NMC cell lines, including NMC797 and NMC1015 cells, and whose expression is significantly reduced by JQ1 treatment (112). We validated the RNA-seq results using RT-qPCR (Fig. 12D). Our data indicate that expression of *KLF4* prevents the down-regulation of *CCAT1* and *CASC19* by JQ1, which might result in higher *MYC* levels and thus resistance to JQ1. Indeed, GSEA revealed that E2F targets, MYC targets, and G2M checkpoint genes comprised the top-ranking gene sets when comparing the *KLF4*-expressing NMC1015 cells with control cells under JQ1 treatment at day 7 (Fig. 12E–G). In agreement with this, *KLF4*-expressing cells exhibited higher levels of E2F1, c-Myc, and cyclin D1 during JQ1 treatment compared with control cells (Fig. 12H). Taken together, these data suggest that KLF4-expressing cells are able to sustain the MYC and E2F gene expression programs under JQ1 treatment and bypass the cell cycle arrest induced by JQ1, providing a second distinct mechanism of resistance involving these same pathways.

Figure 12. KLF4 mediated JQ1 resistance in NMC cells through restoring the E2F and MYC gene expression program upon JQ1 treatment. (A) *KLF4* expression enhances survival of NMC1015 cells in long-term colony formation assays with JQ1. NMC1015 cells containing control (EV) or *KLF4* expression vectors were fixed and stained after treatment with DMSO for 1 wk or 200 nM JQ1 for 6 wk. Colony numbers of each condition were quantified using ImageJ and normalized to control cells under DMSO treatment. Data are means ± SD. n = 3. (**) $P < 0.01$. (B) Schematic of the time course for the RNA-seq experiment. NMC1015 cells containing control (EV) or *KLF4* expression vectors were treated with 200 nM JQ1 for the indicated times. DEGs were identified using edgeR. (C) Log_2 fold change of normalized gene expression level (counts per million) as measured using RNA-seq of the indicated genes in NMC1015 cells containing control (EV) or *KLF4* expression vectors treated with 200 nM JQ1 for the indicated times. Data are the means ± SD. n = 2. (D) RT-qPCR analysis of mRNA expression of the indicated genes in NMC1015 cells containing control (EV) or *KLF4* expression vectors treated with DMSO or 200 nM JQ1 for 7 d. Data are the means ± SD. n = 3. (E–G) Gene set enrichment analysis plots. Plots indicate a significant up-regulation of E2F targets, MYC targets, and G2M checkpoint signatures in *KLF4*-expressing NMC1015 cells compared with NMC1015 cells containing an empty vector (EV) during JQ1 treatment at day 7. (H) Immunoblot analysis of NMC1015 cells containing control (EV) or *KLF4* expression vectors treated with DMSO or 200 nM JQ1 for 7 d and probed with the indicated antibodies.

Figure 12 (Continued)

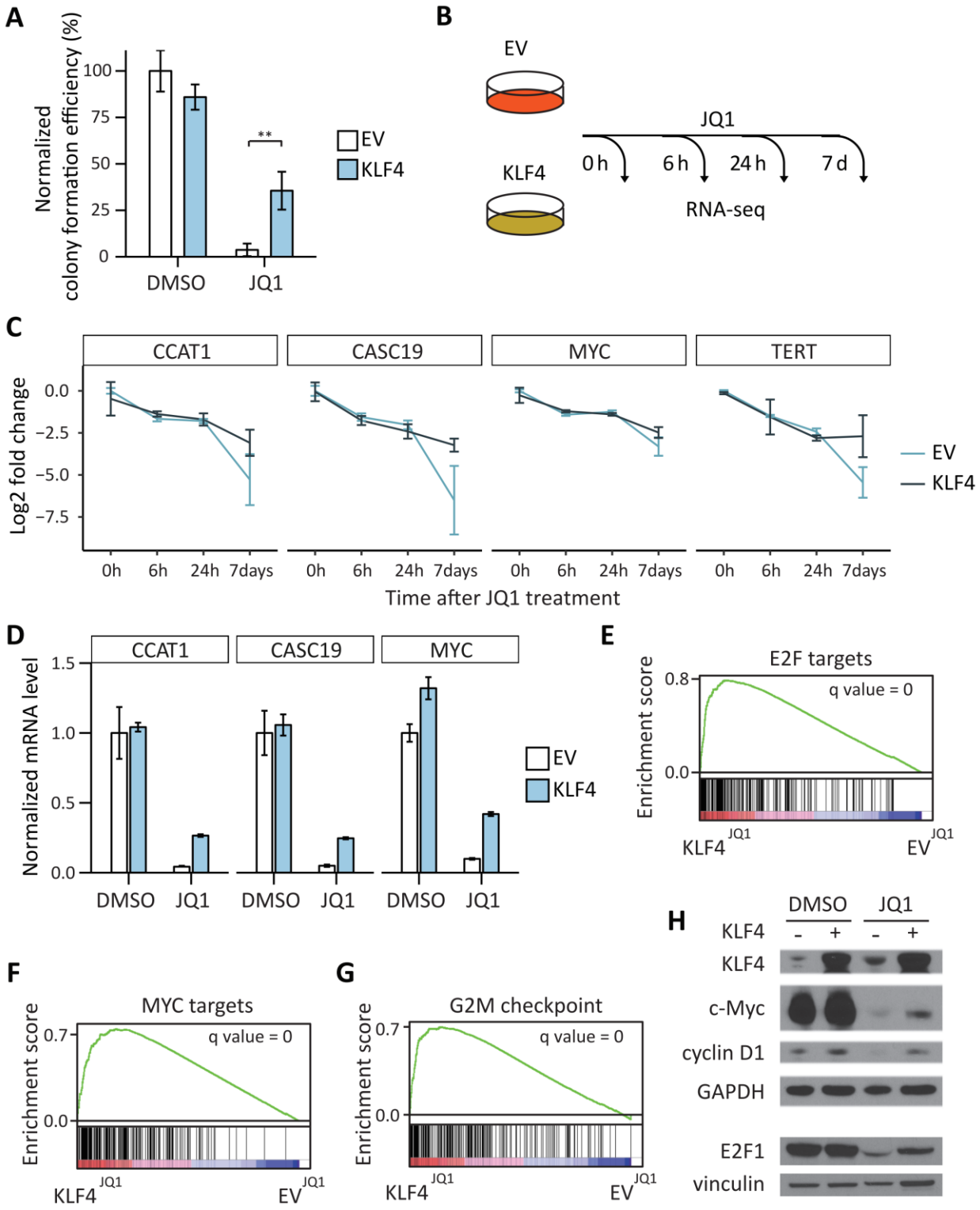

The Central Role of Cell Cycle Regulators in Mediating JQ1 Resistance

One recurring theme from our screens is cell cycle regulation. *RB1* is a TSG that negatively regulates E2F-dependent transcription and cell cycle entry (189). During G1/S cell cycle progression, CDK4 and CDK6 form a complex with their regulatory subunit, D-type cyclins, which phosphorylates the Rb protein, resulting in its dissociation from E2F and activation of transcription of genes that are important for S phase, such as cyclin A (190). Two central G1/S transition regulators – cyclin D1 and a mutant form of cyclin D3 (c.869T > G; p.I290R) that is highly stable (191), scored as top 10 hits in the OG screen. In addition, the downstream inactivation target of the CDK4/6–Cyclin D complex, the *RB1* gene, scored in the top 10 of TSG screens and FBXW7, an F-box protein that targets cyclin E and c-Myc for degradation (192-194), also scored highly in the TSG screen further implicating the cell cycle.

We first validated the effect of expression of cyclin D1 and mutant cyclin D3 on JQ1 resistance using an independent NMC cell line, NMC797 cells. As seen with the NMC1015 cells in the screen, expression of cyclin D1 or mutant cyclin D3 significantly increased the survival of NMC797 cells under JQ1 treatment (Fig. 13A,B). To validate that loss of *RB1* mediates JQ1 resistance, we used CRISPR to knock out *RB1* in NMC797 cells. Cells expressing Cas9 and two independent gRNAs targeting *RB1* showed significantly increased survival in response to JQ1 compared with cells expressing Cas9 and control gRNAs targeting *AAVS1* or *GFP* (Fig. 13C). Thus, these cell cycle regulators mediate JQ1 resistance in multiple NMC cell lines.

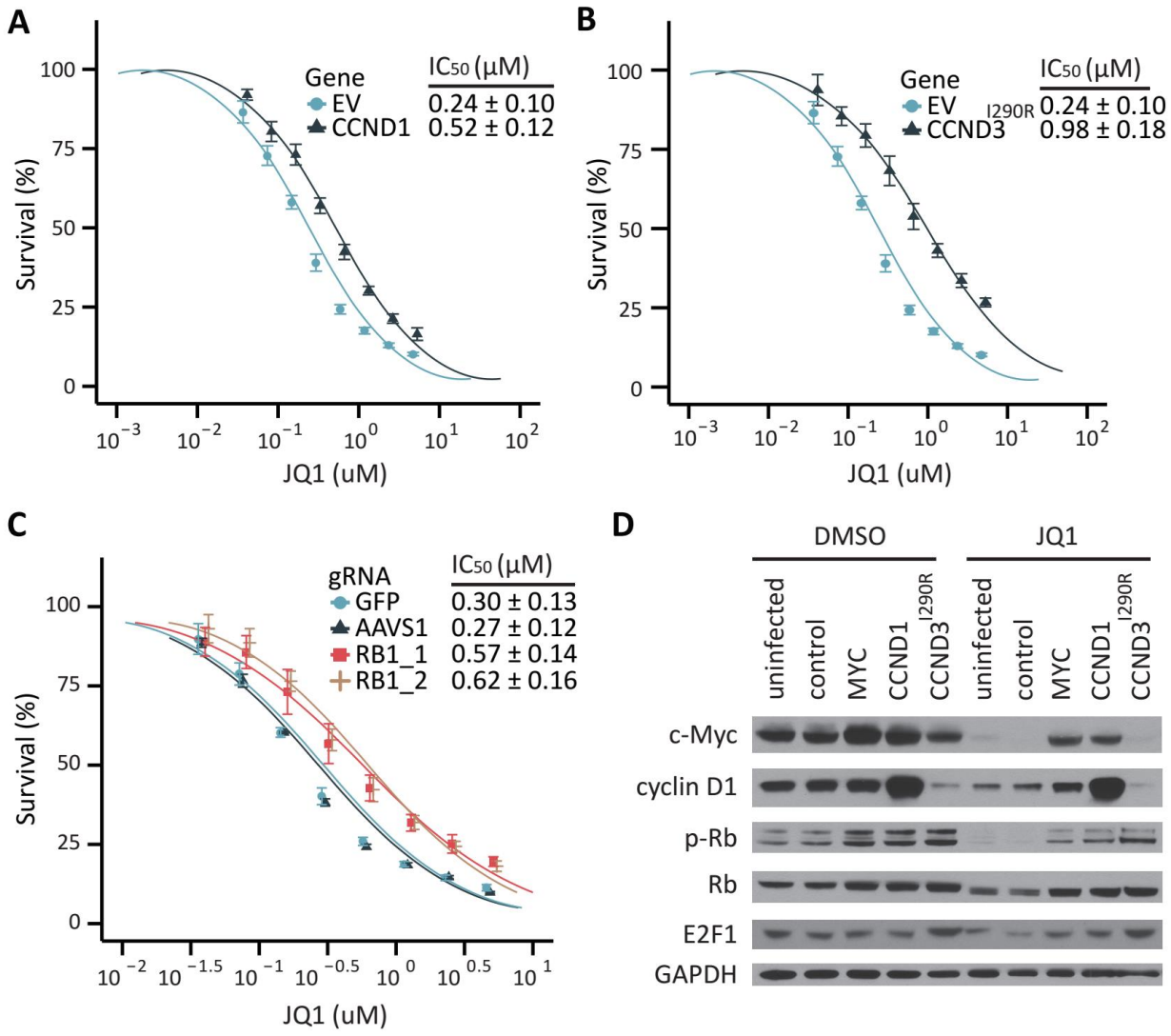

Figure 13. A central role for cell cycle regulators in mediating JQ1 resistance. (A–C) NMC797 cells expressing the indicated genes or Cas9 and gRNAs targeting the indicated genes were treated with the indicated concentrations of JQ1 for 72 h before cell viability was measured using an SRB assay and normalized to untreated controls. Data are means ± SD. n = 3. (D) Immunoblot analysis of NMC1015 cells expressing the indicted genes treated with DMSO or 200 nM JQ1 for 24 h and probed with the indicated antibodies.

We next returned to the NMC1015 cells to explore how JQ1 affects the CDK4/6–cyclin D/Rb signaling axis by examining the levels of these proteins in NMC1015 cells. JQ1 treatment reduced cyclin D1 levels, Rb phosphorylation (p-Rb) and E2F1 levels in uninfected parental or control infected NMC1015 cells (Fig. 13D). Like *MYC*, ectopic expression of D-type cyclins

restored Rb phosphorylation and E2F1 levels in the presence of JQ1. Together, our data suggest that JQ1 downregulates cyclin D1, whose reduction results in hypophosphorylation of Rb and cell cycle arrest. Blocking Rb activation by JQ1 through either *RB1* loss or upregulation of cyclin D1 or D3 is sufficient to induce JQ1 resistance.

CDK4/6 Inhibitor Synergizes with JQ1 on NMC *in vitro*

Given that c-Myc can activate expression of D-type cyclins and the ability of ectopic expression of D-type cyclins to mediate JQ1 resistance, we hypothesize that the endogenous CDK4/6–cyclin D/Rb axis may play an important role in modulating JQ1 sensitivity and that CDK4/6 inhibition should synergize with JQ1. To test this hypothesis, we cotreated NMC1015 cells with JQ1 and the CDK4/6 inhibitor palbociclib and measured cell viability. We found that the combination of JQ1 and palbociclib achieved significantly higher cell proliferation inhibition than either drug alone across a range of doses (Fig. 14A). We observed such synergism also on NMC797 cells (Fig. 14B). To further quantify the synergistic effect between JQ1 and palbociclib and rule out the possibility of an additive effect, we calculated the combination indices (CIs) of a range of different combinations of JQ1 and palbociclib on NMC1015 cells. A CI between 0 and 1 indicates a synergistic effect between two drugs, and the closer the index to 0, the stronger the synergism (195). We found that palbociclib showed strong synergism (CI < 0.3) with JQ1 across a range of doses (Fig. 14C).

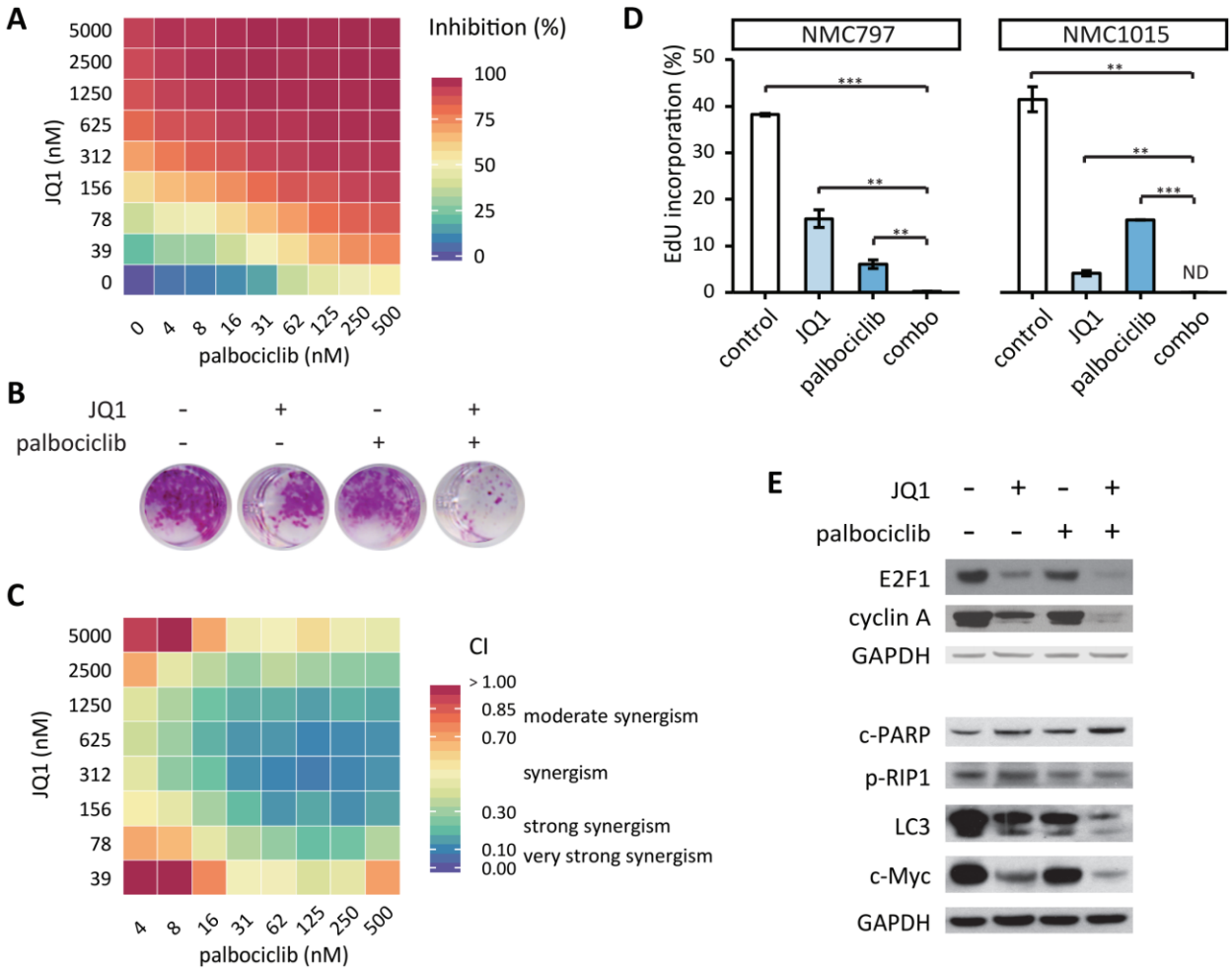

Figure 14. **CDK4/6 inhibitors synergize with JQ1 to inhibit NMC growth *in vitro*.** (A) NMC1015 cells were treated with the combination of the indicated concentrations of JQ1 and palbociclib for 72 h before cell viability and inhibition percentage were measured using an SRB assay and normalized to untreated controls. Data are means. n = 3. (B) Cell viability assays of NMC797 cells treated with either vehicle, 625 nM JQ1, 250 nM palbociclib, or the combination of both drugs for 72 h. Cells were stained using SRB after treatment. (C) CI analysis of NMC1015 cells treated with the combination of the indicated doses of JQ1 and palbociclib for 72 h based on the viability inhibition percentage in *A* using CalcuSyn. Data are means. n = 3. (D) Cell cycle profiles of NMC797 and NMC1015 cells treated with either 200 nM JQ1, 400 nM palbociclib, the combination of both drugs, or vehicle (control) for 48 h. Incorporated EdU percentage is used to indicate the percentage of cells that went into cell cycle. Data are means ± SD. n = 3. (**) $P < 0.01$; (***) $P < 0.001$; (ND) not detected. (E) Immunoblot analysis of NMC1015 cells treated with either 200 nM JQ1, 400 nM palbociclib, the combination of both drugs, or vehicle for 48 h.

To determine whether and how the combination of the two drugs may affect cell cycle, we examined cell cycle distribution under single or combinations of drug treatment using EdU

labeling. While a small percentage of cells was still able to incorporate EdU and progress through the cell cycle with treatment by single agents, cotreatment of palbociclib and JQ1 induced complete cell cycle arrest and abolishment of EdU incorporation in both NMC797 and NMC1015 cells (Fig. 14D). Consistent with this, cotreatment of palbociclib and JQ1 profoundly reduced the levels of E2F1 and its downstream target, cyclin A (Fig. 14E), which accumulates in S phase and is necessary for initiation and completion of DNA replication. Cotreatment of palbociclib and JQ1 did not induce cell death through mechanisms such as apoptosis, necroptosis, or autophagic cell death, marked by cleaved-PARP (c-PARP) and Caspase-Glo 3/7 assay (data not shown), phosphorylation of RIP1 (p-RIP1), or LC3-II/LC3-I ratio, respectively (Fig. 14E), suggesting that the profound cell viability reduction induced by the combination treatment *in vitro* was primarily due to cell cycle arrest.

CDK4/6 inhibitor Synergizes with JQ1 on NMC *in vivo*

To validate the effectiveness of the combination therapy on NMC *in vivo*, we used a xenograft mouse model. Tumors generated from NMC1015 cells were established and once they reached 200-300 mm^3, mice were randomized into one of the four following treatment groups and treated for 21 d using well-established preclinical doses and regimens: (1) vehicle, (2) JQ1 alone, (3) palbociclib alone, and (4) JQ1 plus palbociclib. Despite a small initial weight loss seen in the palbociclib and combination treatment groups, the weight of mice of both groups recovered to the start point by the end of treatment, and no other signs of toxicity were observed (Fig. S6A). A spider plot of tumor growth is shown in Figure 15A.

Figure 15. CDK4/6 inhibitor synergizes with JQ1 to inhibit NMC growth *in vivo*. (A) NMC1015 cells were injected subcutaneously into nude mice (one to two tumors per mouse). Mice were randomized into the following four groups and treated with either vehicle ($n_{mouse} = 4$; $n_{tumor} = 7$), 45 mg/kg JQ1 (intraperitoneal injection; $n_{mouse} = 5$; $n_{tumor} = 6$), 100 mg/kg palbociclib (oral gavage; $n_{mouse} = 5$; $n_{tumor} = 7$), or a combination of the two drugs ($n_{mouse} = 5$; $n_{tumor} = 7$) for 21 d. The spider plot depicts tumor growth. Each line represents an individual tumor. The left axis indicates the $\log_2$ fold change in tumor volume, and the right axis indicates the percentage in tumor volume relative to day 0 (the day of enrollment). (B,C) Waterfall plot and box plot depicting changes in tumor volume after 8 d of treatment with single or combined agents as indicated. Each bar or dot represents an individual tumor. (**) $P < 0.01$; (***) $P < 0.001$. (D) Survival of the mice is represented by a Kaplan-Meier plot. The duration of treatment is indicated at the top, and median survival per group is indicated at the right. Animals were euthanized when the tumor volume reached 1200 mm^3. For mice bearing two tumors, the fast-growing one was considered. (**) $P < 0.01$. (E) As in *A*. Mice were treated with the indicated drugs for 8 d. Tumors were harvested 1 h after the last treatment and subjected to immunohistochemical staining for Ki-67 (brown). One representative image for each group is shown. Bars, 100 μm. Ki-67-positive cells were quantified using eSlide Manager. Data are the means ± SD. n = 2. (*) $P < 0.05$, one-sided Student's *t*-test. (F) As in *E*. Tumors were subjected to immunoblot analysis using the indicated antibodies. Each sample came from an individual tumor. (Pal) Palbociclib. (G) As in *A*. Mice were treated with the indicated drugs for 3 d. Tumors were harvested 1 h after the last treatment and subjected to immunoblot analysis using the indicated antibodies. Each sample came from an individual tumor. (Pal) Palbociclib.

Figure 15 (Continued)

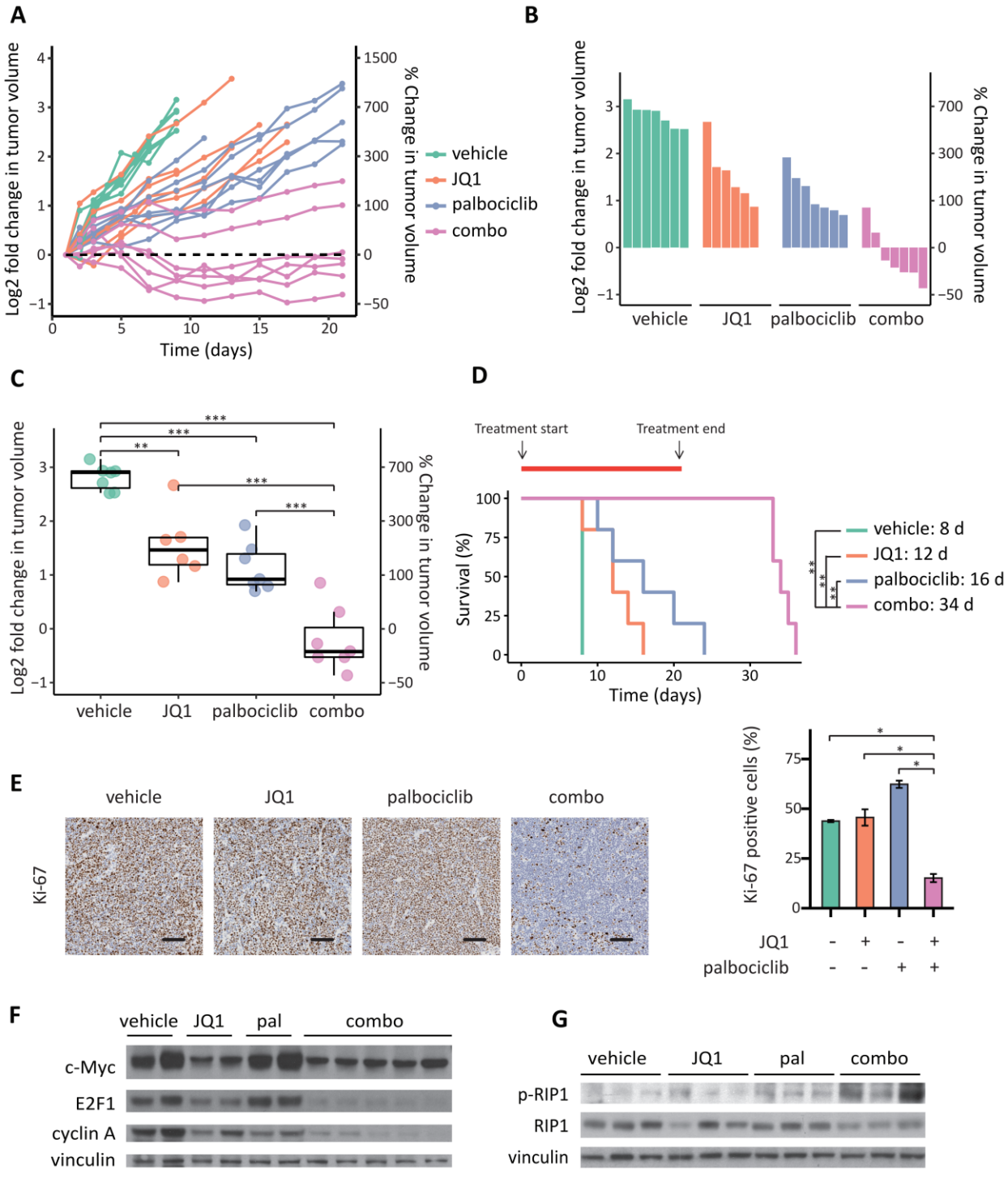

The tumors in the vehicle group grew rapidly to the maximum size threshold within 8 d, recapitulating the aggressive nature of NMC in human patients. While single treatment of JQ1 or palbociclib caused no tumor shrinkage and only slowed tumor growth, cotreatment of JQ1 and palbociclib caused tumor regression in the majority of tumors, and tumor size remained stable throughout the course of treatment. In only 8 d, when tumor size necessitated the sacrifice of vehicle-treated mice, the drug combination therapy exerted substantial effects on every tumor and induced frank regression in five out of seven tumors up to 45.1% (Fig. 15B,C). During the course of treatment (21 d), all animals treated with vehicle or single agents had to be euthanized with the exception of one in the palbociclib-alone group; however, no animals died in the presence of the combination (Fig. 15D). Even when drug treatment ceased, this drug combination significantly improved the median survival of the mice over each agent or vehicle alone (combination: 34 d; palbociclib: 16 d; JQ1: 12 d; vehicle: 8 d) (Fig. 15D).

Finally, as seen *in vitro*, palbociclib and JQ1 cotreatment profoundly reduced the expression of the cell growth marker Ki-67 and the levels of E2F1 and its downstream target, cyclin A, *in vivo* as measured by immunohistochemical staining and immunoblot analysis, respectively (Fig. 15E,F), suggesting that these agents induce a more complete cell cycle arrest compared with each agent alone. To investigate whether the tumor shrinkage induced by the combination treatment *in vivo* was due to apoptosis, we examined the c-PARP and cleaved caspase substrate levels in different treatment groups. Surprisingly, there was more apoptosis in the vehicle-treated tumors (Supplemental Fig. S6B). Such increased proliferation along with an increased apoptotic rate has been observed in other cancer types (196). However, compared with each agent alone, palbociclib and JQ1 cotreatment significantly increased the levels of p-RIP1 (Fig.

15G), suggesting the tumor shrinkage induced by the combination treatment *in vivo* was due to increased necroptosis.

Discussion

NMC is a particularly lethal cancer that does not benefit from conventional chemotherapy and has an overall survival of only ~ 7 mo (111, 114). Thus, it represents a model disease for the clinical testing of BETis given the direct oncogenic driver role that BRD4-NUT plays in NMC and the urgent need for novel therapeutic approaches. Despite the promising responses seen in some patients treated with BETis, why most patients fail to respond or why even the responders eventually relapse is unknown. Understanding which signaling pathways can modulate the sensitivity of NMC tumors to BETis could inform new therapeutic approaches to treat this deadly cancer. Here, using high-throughput LOF and GOF screening technologies, we systematically explored ~900 known drivers of tumorigenesis for their ability to impact NMC's response to BETis with the hope that some of these pathways might contribute to NMC tumorigenesis in a basal state and that inhibiting these pathways might improve the efficacy of BETi therapy.

We identified multiple cancer driver networks that can genetically modify BRD4-NUT dependency to partially compensate for it and drive proliferation and survival of NMC cancer cells during BETi treatment. Unlike the MYC locus, the regulatory regions and gene bodies of these cancer drivers do not fall in BRD4-NUT megadomains (Supplemental Fig. S7), suggesting that these cancer drivers are not the direct targets of BRD4-NUT in this disease and compensate for

BRD4-NUT inhibition in an indirect manner. Overall, those cancer drivers that we identified largely fall into six categories (Fig. 16).

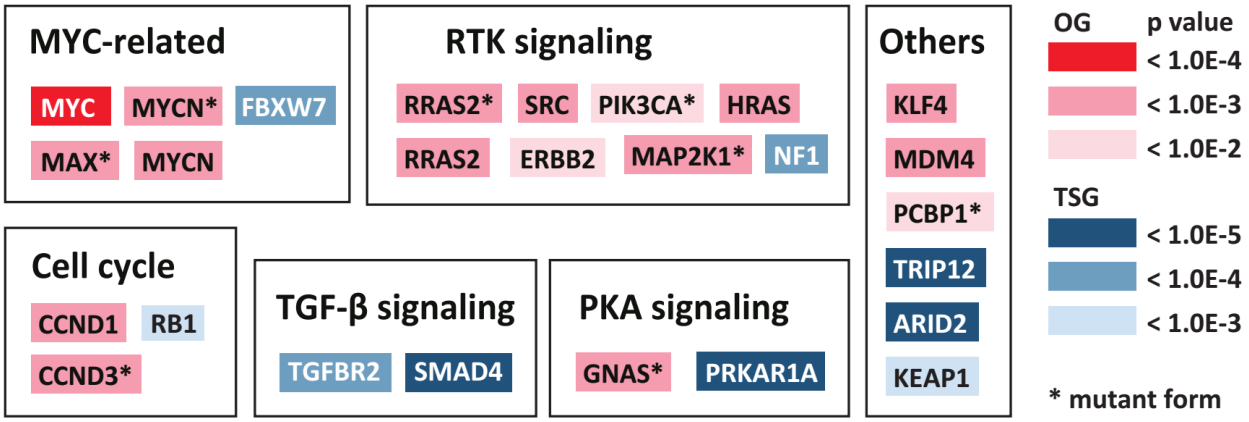

Figure 16. Summary of the cancer drivers and genetic pathways uncovered in this study. Top hits of the CRISPR and ORF screens (FDR < 0.05) are grouped based on the cell signaling pathways to which they belong.

The first category encompasses MYC and MYC-related genes such as *MYCN*, encoding N-Myc. Structurally, the coding regions of both MYC and MYCN are highly homologous. Both c-Myc and N-Myc form heterodimers with Max at consensus E-box sequences (CANNTG), and regulate transcription. Functionally, c-Myc and N-Myc are partially redundant but have several distinct spatiotemporal expression patterns and functions (197). In addition to the previously validated *MYC* gene, we recovered wild-type *MYCN* and a mutant form, *MYCN* (c.131C > T; p.P44L). The N-Myc^{P44L} mutation is recurrently identified in different cancers but remains to be characterized biochemically (197). Our results suggested that N-Myc^{P44L} is indeed an activating mutation given its stronger phenotype (i.e. greater fold change) than wild-type N-Myc in our screen. The fact that many of the mutant alleles picked up by TUSON Explorer achieved stronger phenotypes than their corresponding wild-type alleles in our OG screen (Supplemental Table S3)

confirmed the robustness of the TUSON Explorer algorithm to identify bona fide activating oncogenic mutations from passenger mutations. We also recovered a mutant form of *MAX* (c.179G > A; p.R60Q) in our OG screen. The Max^{R60Q} mutation is recurrently identified in many cancers and is suggested to be an activating mutation through inhibition of Max homodimerization, but not disruption of c-Myc/Max heterodimerization, thus shifting the balance toward c-Myc activation in proliferating cells (198). We also recovered the tumor suppressor *FBXW7* – the F-box substrate adaptor component of the SCF^{Fbx7} E3 ubiquitin ligase that targets c-Myc for degradation (193, 194), in our LOF screen. Together, our data confirmed the central role of c-Myc signaling in mediating the oncogenic function of BRD4-NUT and revealed that there are many potential ways for NMC cancer cells to sustain MYC function, thus bypassing the need for BRD4-NUT during BRD4 inhibition.

The second class of genes encompasses the RTK signaling pathway. We recovered *ERBB2*, *SRC*, *PIK3CA* (c.3140A > G; p.H1047R), and several RAS-related genes, including wild-type *RRAS2*, mutant *RRAS2* (c.216A > C; p.Q72H), and wild-type *HRAS*, in our OG screen as well as their negative regulator, *NF1* (199), in the TSG screen. We further showed that the $RRAS2^{Q72H}$ mutant mediates JQ1 resistance predominately through ERK signaling. The importance of ERK signaling was further supported by the fact that the upstream kinase of ERK1/2, *MAP2K1*, with an activating mutation (c.371C > A; p.P124Q) that harbors RAF-independent kinase activity (200) scored highly in our screen. Previous work has demonstrated that a mechanism of resistance to BETis in ovarian cancers involves the activation of RTKs and their downstream signaling pathways (105). Our results suggest that activation of RTK signaling can mediate BETi resistance in NMC cancer cells as well.

The third general class of suppressors involves the GPCR/cAMP/PKA signaling pathway. We identified *GNAS* (c.2530C > T; p.R844C) in our OG screen. *GNAS* encodes the α subunit of the stimulatory G protein that transduces signals from GPCR signaling to the cAMP/PKA pathway. Activating mutations in *GNAS* promotes tumorigenesis through activation of PKA, resulting in up-regulation of Wnt and MAPK/ERK signaling (201-203). In agreement with the GOF screen, a negative regulator of PKA, *PRKAR1A*, was one of the top-scoring TSGs recovered in our LOF screen. *PRKAR1A* encodes the type 1a regulatory subunit (RIα) of PKA. LOF mutations of *PRKAR1A* are responsible for the Carney complex (CNC) (204, 205), a multiple neoplasia syndrome. Its inactivation acts as a tumorigenic signal through increasing PKA activity, resulting in ERK signaling activation, Wnt signaling activation, c-Myc activation, up-regulation of D-type cyclins and E2F1, increased cell cycle rates and decreased apoptosis (206-212). Given the important role that ERK signaling and cell cycle entry play in BETi resistance in our screens, their up-regulation through increased PKA activity could be a plausible mechanism of *GNAS* and *PRKAR1A* loss-mediated BETi resistance in NMC and is worthy of further investigation.

The fourth class involves the TGF-β pathway. The TGF-β pathway is known to play both anti-tumorigenic and pro-tumorigenic roles in cancer biology, depending on the tumor type, stage, genetic background, and microenvironment as well as the status of Smad and other pathways (213). Up-regulation of TGF-β signaling has been proposed as a mechanism of BETi resistance in colon cancer cells (108). However, we found that loss of *SMAD4* or, with slightly less potency, *TGFBR2*, two major components of the canonical TGF-β signaling pathway, mediates BETi resistance in NMC in our screen. We also found that the TGF-β signaling is one of the top signaling pathways transcriptionally induced by JQ1 treatment in NMC1015 cells (Supplemental Fig. S8). Thus, it is

likely that activation of TGF-β signaling could mediate part of the anti-cancer effect of BETis on NMC.

A fifth class is a catchall category of several unrelated drivers such as the Yamanaka factor *KLF4*, *MDM4*, and *PCBP1* (c.299T > C; p.L100P) in the OG screen and *TRIP12*, *ARID2*, and *KEAP1* in the TSG screen. Of these, we characterized the mechanism of KLF4-mediated JQ1 resistance. We found that *KLF4*-expressing cells are able to sustain the E2F and c-Myc transcription program during BETi treatment. Given the central role that *MYC* plays in mediating the oncogenic function of the BRD4-NUT fusion protein, it is not surprising that *KLF4* and other modifiers of BETi treatment might regulate MYC function. Whether and how the other novel hits recovered in our screens impact MYC function are worthy of future investigation.

The final class of suppressors involves cell cycle regulation. Our data revealed the central role of cell cycle regulators in mediating the oncogenic function of BRD4-NUT and demonstrated that there are multiple ways for NMC cancer cells to bypass the cell cycle arrest induced by BETis – through *RB1* loss or up-regulation of D-type cyclins. This suggested that reinforcing cell cycle arrest might improve the efficacy of BETis. Critically, we showed that CDK4/6 inhibition synergizes with BETis against NMC tumors *in vitro* and *in vivo*. Importantly, CDK4/6 inhibitors such as palbociclib, ribociclib, and abemaciclib have been approved in clinics for the treatment of certain breast cancers. Therefore, the pharmacokinetic and pharmacodynamic profiles of the relevant drugs have been established. Our results on synergy and the favorable clinical properties of the relevant inhibitors of these pathways suggest that this combination forms the basis of a clinical trial for combination therapy of BETis and CDK4/6 inhibitors on NMC.

In summary, analysis of cancer drivers' effects on BRD4-NUT dependency in NMC has provided a broad picture of the genetic landscape of resistance to BETis in this cancer. These pathways now become candidates to explore in NMC tumors that evolve BETi resistance during therapy. In addition, beyond the synergism that we identified with CDK4/6 inhibitors, future therapies that reinforce other aspects of the mechanism of BETi inhibition of tumorigenesis might also show activity in combination therapy to further improve the efficacy of BETis.

Materials and Methods

Cell culture and reagents

NMC1015 and NMC797 cells were kindly provided by Dr. C. A. French (Brigham and Women's Hospital and Harvard Medical School). 293T cells were purchased from ATCC. NMC1015, NMC797 and 293T cells were maintained in DMEM-Glutamax (Thermo Fisher Scientific) supplemented with 10% heat-inactivated fetal bovine serum (GE Healthcare HyClone), 100 IU/mL penicillin, and 100 µg/mL streptomycin in a humidified atmosphere of 95% air and 5% CO_2 at 37°C. SCH772984 and GDC-0068 were purchased from Selleck Chemicals. JQ1 used *in vitro* was purchased from Sigma-Aldrich, and JQ1 used *in vivo* was a gift from Dr. J. Qi (Dana-Farber Cancer Institute and Harvard Medical School).

Plasmids, cloning and viral transduction

gRNAs were cloned into pLentiCRISPR V2 (Addgene plasmid no. 52961) as described previously (167).

The sequences targeted by the gRNAs used were GFP (GGGCGAGGAGCTGTTCACCG), AAVS1 (GGGGCCACTAGGGACAGGAT), RB1 gRNA1 (GGTTCTTTGAGCAACATGGG), and RB1 gRNA2 (GCAGTGTGATTATTCTGGAG).

cDNAs were picked from the ORFeome version 8.1 or Ultimate ORF libraries. Stop codons and mutations were introduced using the QuikChange II XL site-directed mutagenesis kit (Agilent Technologies). cDNAs were subcloned into the pHAGE-TREx-BC-DEST vector via LR recombinase reaction (Invitrogen).

To produce lentiviruses, 293T cells were transfected with vector DNA, pRev, pTat, pHIV Gag/pol, and pVSVG. Viruses were harvested 48 h after transfection and filtered (45 μm pore size). TransIT-293 (Mirus) was used to transfect 293T cells.

Cells were transduced with 4 μg/mL polybrene (Sigma), and infected cells were selected using 1 μg/mL puromycin (Clontech) for 3 d. pLentiCRISPR-V2-infected cells were subjected to cell viability assay or immunoblot analysis 1 wk after infection to allow for genome modification by Cas9. Cells expressing ORFs were treated with 1 μg/mL Dox for 3 d prior to subsequent experiments for ORF expression and maintained in medium containing 1 μg/mL Dox during subsequent experiments.

TSG CRISPR library construction

A customized DNA oligonucleotide library with 10 gRNAs per gene for each of the 500 TSG candidates was synthesized on a microarray (Agilent). The gRNA oligonucleotide library was PCR amplified by a set of specific primers and digested with BbsI. The digested gRNA was purified on a 10% TBE page gel and cloned into BsmBI-digested pLentiCRISPR V2 (Addgene plasmid no. 52961).

TSG CRISPR screen

The CRISPR screen was performed in three replicates. NMC1015 cells were transduced with the TSG CRISPR library using 4 μg/mL polybrene (Sigma) at a low MOI (MOI = 0.2) with an average representation of ~1000 cells per gRNA. Transduced cells were then selected with 1 μg/mL puromycin (Clontech) for 3 d. Cells were then passaged for 9 d, allowing for enough time for genome modification by Cas9. Cells from the initial time point were harvested and the cells

were then split into two arms, treated with either DMSO or 200 nM JQ1 for approximately 17 d. Cells from the end time point (DMSO treatment and JQ1 treatment for 17 d) were then harvested. Genomic DNAs containing gRNA were amplified by PCR and subsequently subjected to NGS. The MAGeCK scoring algorithm was used to rank the performance of individual genes based on enrichment comparing the JQ1 treatment group to the DMSO treatment group.

OG barcoded-ORF library construction

OGs were individually picked from ORFeome V8.1 and Ultimate ORF libraries. Genes with mutant alleles were generated using QuikChange II XL site-directed mutagenesis kit (Agilent Technologies). All of them were sequence-verified, arrayed and pooled together as a total of 6 pools. Each one of these pools was cloned into a pre-barcoded pHAGE-TRE-DEST-3'BC library via Gateway LR Clonase II (Invitrogen). The resulting lentiviral library contains a list of ~ 400 3'barcoded OGs under the control of a Dox-inducible TRE promoter and the rtTA gene. Sequencing was performed to link the barcodes with genes. There are on average about 5 barcodes per gene.

OG expression Screen

The OG screen was performed in three replicates. NMC1015 cells were transduced with the OG barcoded-ORF library using 4 μg/mL polybrene (Sigma) at a low MOI (MOI = 0.2) with an average representation of ~1000 cells per barcode. Transduced cells were then selected with 1 μg/ml puromycin (Clontech) for three days and grown for 7 d. Dox (1 μg/mL) was added and cells were grown for three days allowing for the genes to be expressed. Then either DMSO or 200 nM JQ1 was added and cells were grown for approximately 17 d in medium containing Dox. Genomic

DNA was harvested, processed and analyzed as described in the CRISPR screen. The read counts of different barcodes for the same gene were collapsed to the gene level and edgeR analysis was used to rank the performance of individual genes based on enrichment comparing the JQ1 treatment group to the DMSO treatment group.

Western blot analysis

Cells were lysed in 1× NuPAGE LDS sample buffer (Thermo Fisher Scientific) supplemented with 1× Bond-Breaker TCEP (Life Technologies) and 1× Halt protease and phosphatase cocktail (Life Technologies) on ice. The whole-cell lysates were sonicated briefly to break down the chromatin. Samples were boiled for 5 min at 95°C and then loaded to 4-12% Bis-Tris Protein Gels (Novex) and transferred to iBlot Transfer Stack nitrocellulose membranes (Novex). Membranes were incubated with primary antibodies overnight at 4 °C then with horseradish peroxidase-coupled secondary antibodies at 1:5000 dilution at room temperature for 1 h. Proteins were visualized using an enhanced chemiluminescence kit (PerkinElmer).

The following antibodies were from Cell Signaling: GAPDH (8884), phospho-ERK1/2 (T202/Y204; 4370P), total ERK1/2 (4695P), phospho-AKT (S473; 4060P), total AKT (2920S), phospho-p90RSK (Ser380; 9341S), c-Myc (5605S), cyclin D1 (2978S), phospho-PRAS40 (Thr246; 2997S), KLF4 (4038S), phospho-Rb (Ser780; 3590S), total Rb (9309S), E2F1 (3742S), c-PARP (9541S), cleaved caspase substrate motif (8698S), phospho-RIP1 (Ser166; 65746S), total RIP1 (3493T), and LC3B (3868T). Other antibodies used were cyclin A (Santa Cruz Biotechnology, sc-751), vinculin (Sigma, V9131), and RRAS2 (Abcam, ab182264).

Colony formation assay

Single-cell suspensions were seeded into six-well plates (200 cells per well) and incubated overnight before continuous treatment of DMSO or 200 nM JQ1 for the indicated times, with drug and medium replaced every 3 d. At the end of treatment, cells were fixed with 10% trichloroacetic acid, washed, and stained with methylene blue (Sigma-Aldrich). Colony numbers of each condition were quantified using ImageJ and normalized to control cells under DMSO treatment.

Cell viability assay

The effects of drugs on cell viability were determined by SRB (Sigma Aldrich) as previously described (161).

Cell cycle analysis

Cells seeded in six-well plates (5×10^4 cells per well) were treated with DMSO or 200 nM JQ1 for 48 h. Cells were pulsed with 10 μM EdU final concentration for 1 h using the Click-iT Plus EdU Alexa fluor 647 flow cytometry assay kit (Thermo Fisher Scientific) and then processed according to the manufacturer's instructions. Samples were analyzed by flow cytometry (BD LSR II).

Quantitative RT-qPCR

Total RNA was isolated using the RNAeasy minikit (Qiagen), and cDNA was synthesized using SuperScript IV (Invitrogen) according to ssthe manufacturer's instructions. RT-qPCR was performed in triplicate using the TaqMan gene expression master mix (Invitrogen) with TaqMan gene expression assay (Life Technologies) on an Applied Biosystems Fast 7500 machine using

GAPDH as the endogenous normalization control. The IDs for the TaqMan assays used were as follows: GAPDH (Hs99999905_m1), MYC (Hs00153408_m1), CCAT1 (Hs04402620_m1), and CASC19 (Hs04405851_g1).

Gene expression profiling

NMC1015 cells were transduced with pHAGE-TREx-KLF4 or empty vector. Infected cells were selected using 1 μg/mL puromycin (Clontech) for 3 d. Cells were then passaged for 1 wk and treated with 1 μg/mL Dox (Clontech) for 3 d to allow for gene expression. Cells were then treated with 200 nM JQ1 in medium containing 1 μg/mL Dox for 0 h, 6 h, 24 h or 7 d (two replicates for each condition). Total RNA was isolated using the RNAeasy minikit (Qiagen). RNA-seq libraries were generated using NEBNext Ultra RNA library preparation kit (New England Biolabs). Fifty-base-pair single-end sequencing was performed using an Illumina NextSeq. Reads were aligned to the hg19 genome using HiSat2 (162); transcripts and frequencies were assessed from the aligned data by subread (163), and edgeR (164) was used to identify differentially expressed genes and to generate signed LR scores used for Gene Set Enrichment Analysis (http://www.broadinstitute.org/gsea/) (165).

Xenograft mouse model

Animal procedures were approved by the Institutional Animal Care and Use Committee in Brigham and Women's Hospital in accordance with the NIH Guide for the Care and Use of Laboratory Animals and the Animal Welfare Act. 1.5 million NMC1015 cells were injected into the flanks of 6-week-old female nude mice. When tumors reached between 200 mm^3 to 300 mm^3, animals were randomly assigned to a treatment group. Mice were treated once daily with JQ1 via

i.p. injection at 45 mg/kg, palbociclib via oral gavage at 100 mg/kg, the combination of both JQ1 and palbociclib, or vehicle for 21 d. JQ1 was dissolved into DMSO, and then diluted into 10% (2-hydroxypropyl)-beta-cyclodextrin (Sigma Aldrich). Palbociclib was dissolved in 50 mM sodium lactate (pH = 4, Sigma Aldrich). Body condition and weight loss were monitored as signs of toxicity. Tumors were measured every 2 to 3 d with a digital vernier caliper. Tumor volume was calculated using the standard formula: $L \times W^2 \times 0.52$.

Statistical analysis

Data are presented as the mean ± SD and significance was analyzed using the two-sided Student's *t*-test unless specified otherwise. Differences were considered significant when $P < 0.05$.

Chapter 4

Conclusions and Perspective

In this thesis, I conducted comprehensive CRISPR, shRNA and barcoded-ORF expression screens to enable systems-level discovery of drug resistance mechanisms in multiple cancer disease models. I identified a large number of TSGs and OGs that can genetically modify the growth and survival deficiencies caused by reduced EGFR signaling in NSCLC and reduced BRD4-NUT function in NMC, respectively. The present systems-level study of the genetic interactions among cancer drivers provides strong support for the hypothesis that cancer drivers can substitute for each other in some contexts. I have gained many insights into the pros and cons of different screening technologies and discovered many novel hits and interesting biological phenomena that are worthy of following up.

Lessons learned from the present study

1) Introduction of CRISPR technology has revolutionized functional genomic screens. My results suggest that, indeed, CRISPR harbors many superior properties compared with shRNAs and could be considered as the first choice when doing LOF screens. As others have noticed (214), in my screens, CRISPR exhibited greater consistency among the gRNAs targeting the top candidate genes compared with shRNAs. For the top 20 genes, on average 62.5% of gRNAs targeting each gene ranked among the top 5% of enriched gRNAs, whereas 40.2% of shRNAs targeting each gene ranked among the top 5% of enriched shRNAs (Fig. 17A). CRISPR also induced stronger phenotype for most of the genes, reflected as larger fold-changes compared with shRNAs (Supplemental Table S1). However, my results also confirmed the notion that the shRNA screen is able to recover genes essential for cell viability that will be missed in the CRISPR screen. One example is *ZC3H18* (215), an essential gene that scored as the number one hit to modify

EGFR dependency in the shRNA screen but caused severe dropout when targeted by CRISPR and thus ranked poorly in the CRISPR screen (Fig. 17B). Notably, the top-scoring genes from the TSG screen showed a significant overlap between CRISPR and shRNA screens (Fig. 3B), suggesting that shRNA screen can serve as an orthogonal validation of the CRISPR screen results. Therefore, we suggest that ideally, if time and resources permit, performing RNAi-based screens coupled with CRISPR screens will give the most complete and comprehensive genetic landscape of the biological question of interest.

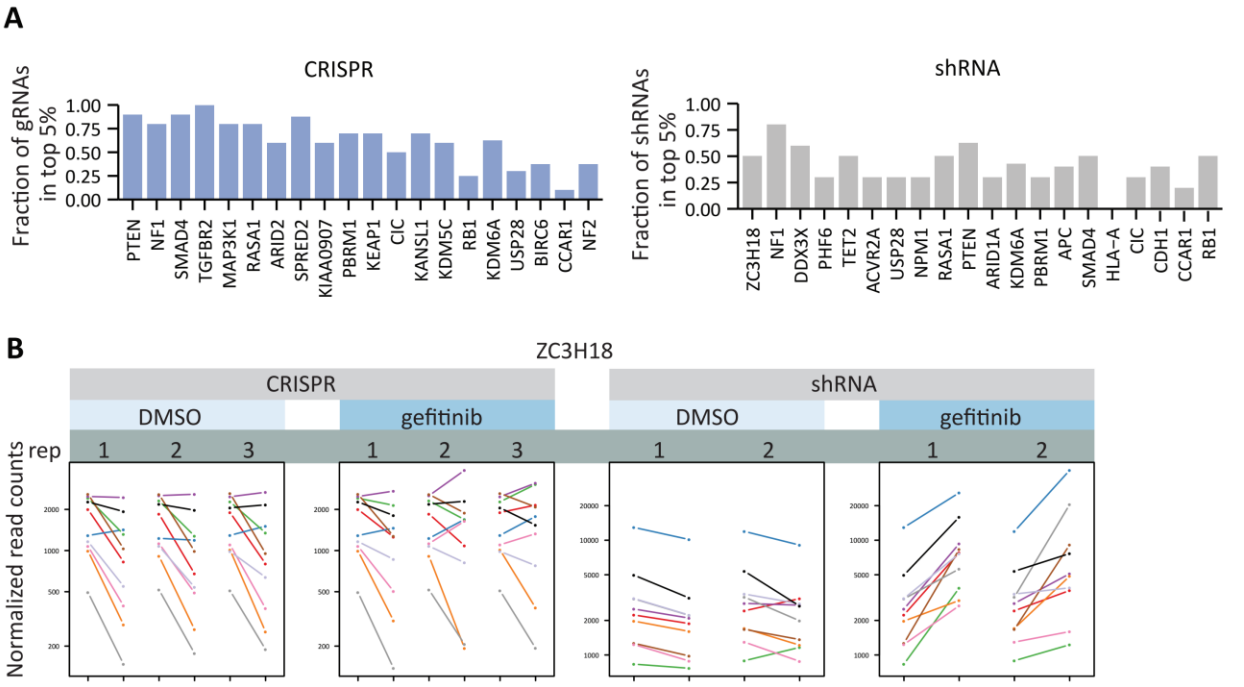

Figure 17. Comparison of CRISPR and shRNA screens. (A) For the top 20 genes of each screen, the fraction of unique gRNAs (left) or shRNAs (right) targeting each gene that is in the top 5% of all enriched gRNAs or shRNAs are shown. (B) Normalized raw read counts of gRNAs (left two plots) and shRNAs (right two plots) of *ZC3H18* in the gefitinib bypass screen. Each line represents the normalized read counts of individual gRNAs or shRNAs from start point to end point in each of the replicates (rep) of the CRISPR and shRNA screens, respectively.

2) In both the gefitinib bypass and JQ1 bypass screens, I found that the hits could be largely grouped based on the signaling pathways, protein complexes or biological functions to which they belong. For example, the SWI/SNF complexes in the gefitinib bypass screen and cell cycle

regulation in the JQ1 bypass screen. Such pathway analysis is very powerful. It informed us how to prioritize the hits and choose which ones to follow up. For example, I found that cell cycle regulation is a recurrent theme in mediating JQ1 resistance in both the TSG and OG screens, leading me to hypothesize that the endogenous CDK4/6–cyclin D/Rb axis may play an important role in modulating JQ1 sensitivity, which led me to the discovery of the synergy between CDK4/6 inhibition and BETis in NMC. In the present study, I essentially performed the pathway analysis manually given the small size of the TSG and OG libraries. In the future, we would like to perform genome-wide LOF screens to fully leverage the power of pathway analysis. Of course, the downside of performing a genome-wide screen is that it is more time-consuming and labor-intensive. This will gradually become less of an issue as the sgRNA design and statistical analysis algorithms improve so a smaller number of sgRNAs targeting each gene and replications are needed in the screen.

3) The fact that RRAS2^{Q72H}, N-Myc^{P44L}, Max^{R60Q} and mutants of many other OGs showed stronger phenotypes (i.e. greater fold changes) than their wild-type alleles in my screen confirmed the robustness of the TUSON Explorer algorithm to identify *bona fide* activating oncogenic mutations (Supplemental Table S3). Despite ongoing efforts in identifying cancer drivers, very little is known about which or how many mutations in those proto-oncogenes are truly activating mutations. This is a critical question because therapeutic decisions will more and more rely on accurate identification of which specific mutations drive that person's cancer as cancer genome sequencing moves into routine clinical practice (216). For example, *KRAS* mutation status has already been used as a biomarker to predict the therapeutic benefit of monoclonal antibody therapy against EGFR in metastatic colorectal cancer (217, 218), yet the functional impact of many of the rare alleles of *KRAS* mutations have not been studied (219). My results suggest that high-

throughput ORF screen can serve as a powerful tool to systematically interrogate the functional impact of each allele of OGs. We think that, as some other groups have already started doing (42, 219), the trends in the field will move from the gene-level characterization of cancer drivers towards in-depth characterization of individual mutations. This could be done eventually in an unbiased and saturated way as robotic screening platforms and efficient and cost-effective construction of ORF libraries with every possible amino acid substitution become more feasible.

4) In the present study, I only included the most recurrent mutation for each of the proto-oncogenes. One limitation of the OG library used in the current study is that most of the OGs are identified through their point mutational signatures in the exome. Many driver mutations likely lie within non-coding regions that have not yet been examined in sufficient detail due to limited sample sizes and availability of epigenomic datasets (220). Therefore, I propose that a small concentrated OG library could be very useful when the complexity of the library has to be constrained due to technical reasons, such as *in vivo* screens; While if time and resources permit, using a genome-wide ORF library will most likely capture the cancer driver genes that are missed in the list identified by the coding-sequence-based TUSON Explorer.

5) I discovered the synergy between CDK4/6 inhibition and BETis against NMC tumors and showed that the combination therapy can cause tumor shrinkage and significantly increase the median survival in an *in vivo* mouse model. Importantly, CDK4/6 inhibitors such as palbociclib, ribociclib, and abemaciclib have been approved in the clinic for the treatment of certain breast cancers. Therefore, the pharmacokinetic and pharmacodynamic profiles of the relevant drugs have been established. My results on synergy and the favorable clinical properties of the relevant inhibitors of these pathways suggest that this combination forms the basis of a clinical trial for

combination therapy of BET and CDK4/6 inhibitors on NMC. This has demonstrated the immediately translational value of studying genes that are druggable, namely GPCRs, ion channels, and protein kinases, which are currently targetable by small molecular inhibitors. Therefore, in the future, with the experience I have gained, I would prefer to perform more large-scale screens using libraries targeting the "druggable genome" rather than the TSG library.

Novels hits and interesting biological phenomena uncovered in the present study that are worthy of further investigation

My screens have uncovered many novel cancer driver genes that can genetically modify EGFR or BRD4-NUT dependency in NSCLC or NMC cancers, respectively. I have chosen a handful of them to characterize the underlying molecular mechanisms in-depth. Many other novel hits and interesting biological phenomena uncovered in the present study are worthy of further investigation in the future.

1) Two SWI/SNF subunits, *SMARCE1* and *ARID1A*, have been reported to confer resistance to MET and ALK inhibitors by regulating *EGFR* expression (138). However, we showed that loss of *PBRM1* does not affect EGFR levels. Instead, *PBRM1*-mutant NSCLC cells were able to restore activation of AKT in the presence of gefitinib after an initial inhibition. How *PBRM1* restrains AKT activation remains to be determined. Given the function of SWI/SNF complexes in transcriptional regulation, I propose to examine the transcriptional changes comparing *PBRM1* mutants with wild type during gefitinib treatment using RNA-seq. After identification of the potential candidate, depending on if it is a positive or negative regulator of

AKT signaling, we can test if knockdown/overexpression of the candidate can abolish the re-bound of AKT signaling in *PBRM1* mutants during gefitinib treatment. We will also perform chromatin immunoprecipitation (ChIP) experiments in PC9 cells treated with gefitinib or vehicle using an antibody against *PBRM1* to test if PBRM1 regulates the transcription of the candidate through direct interactions with its regulatory regions.

2) I have discovered that the Ets factors ETV1, 4 and 5 are transcriptionally up-regulated in the *CIC* mutants during gefitinib treatment and are likely to play an important role in the ability of *CIC* to modify PC9 cells' resistance to gefitinib. Unexpectedly, while we were able to express detectable levels of ETV5 from an exogenous promoter, inhibition of EGFR still extinguished ETV5 protein levels (Fig. 7C), suggesting that active EGFR is promoting the expression of ETV5 not only transcriptionally but also post-transcriptionally. More importantly, CIC knockdown sustained ETV5 protein levels under the gefitinib treatment (Fig. 7C), suggesting that the post-transcriptional regulation of ETV5 by EGFR signaling is partially mediated through CIC. Previously, in alveolar type 2 cells, ERK activation downstream of Ras was found to stabilize ETV5 through inactivation of the cullin-RING ubiquitin ligase $CRL4^{COP1/DET1}$ that targets ETV5 for proteasomal degradation (221). However, in PC9 cells, I found ERK phosphorylation is equally inhibited in *CIC* mutants compared to wild type under gefitinib treatment (Supplemental Fig. S4A). Also, *COP1* (*RFWD2*) did not show differential expression between *CIC* mutants and wild type cells under gefitinib treatment (Supplemental Table S2). Therefore, there might be another E3 ligase that is promoted by CIC targeting ETV5 for proteasomal degradation in PC9 cells or the down regulation of deubiquitinating enzyme. To confirm that ETV5 is targeted for proteasomal degradation under gefitinib treatment, I would express ETV5 in PC9 cells and treat the cells with gefitinib with and without a proteasome inhibitor to test if proteasome inhibitor can preserve ETV5

protein levels under gefitinib treatment. To identify which E3 ligase is responsible for the degradation of ETV5 under gefitinib treatment, I would express GFP-tagged ETV5 protein in PC9 cells. After making sure the tagged protein is regulated by EGFR signaling like the untagged one (i.e., gefitinib treatment should decrease GFP levels determined by FACS), I can use GFP-ETV5 expressing PC9 cells as a reporter cell line to do CRISPR screen using a sgRNA library targeting E3 ligases. After introduction of the CRISPR library to the reporter cell line, I would treat the cells with gefitinib and sort for high GFP-expressing cells and look for the sgRNAs that enrich in the GFP positive vs. negative cells. Because gefitinib quickly diminished ETV5 level at early time point (12 h) (Fig. 7C), sorting could be performed before cell survival is significantly affected by gefitinib.

3) The GPCR/cAMP/PKA signaling pathway is a major hit uncovered in my JQ bypass screen. I identified *GNAS* (c.2530C > T; p.R844C) in the OG screen (Fig. 10A). *GNAS* encodes the α subunit of the stimulatory G protein that transduces signals from GPCR signaling to the cAMP/PKA pathway. Activating mutations in *GNAS* promotes tumorigenesis through activation of PKA, resulting in up-regulation of Wnt and MAPK/ERK signaling (201-203). In agreement with the GOF screen, a negative regulator of PKA, *PRKAR1A*, was one of the top-scoring TSGs recovered in the LOF screen (Fig. 10A; Supplemental Table S3). *PRKAR1A* encodes the type 1a regulatory subunit (RIα) of PKA. LOF mutations of *PRKAR1A* are responsible for the Carney complex (CNC) (204, 205), a multiple neoplasia syndrome. Its inactivation acts as a tumorigenic signal through increasing PKA activity, resulting in ERK signaling activation, Wnt signaling activation, c-Myc activation, up-regulation of D-type cyclins and E2F1, increased cell cycle rates and decreased apoptosis (206-212). Given the important role that ERK signaling and cell cycle entry play in BETi resistance in my screens, their up-regulation through increased PKA activity

could be a plausible mechanism of *GNAS* and *PRKAR1A* loss-mediated BETi resistance in NMC and is worthy of further investigation. More importantly, as discussed above, since GPCRs and PKA are druggable, it would be worthy to test if GPCR or PKA inhibition might also show activity in combination therapy to further improve the efficacy of BETis in NMC.

4) One interesting observation from the OG screen was that expression of most of the OGs that provided enrichment in the presence of gefitinib resulted in a negative enrichment score when expressed in cells bearing activated *EGFR* without gefitinib (Fig. 3A). I refer to this phenomenon as "oncogenic overload" (Fig. 18). A similar observation was observed previously for expression of activated KRAS in *EGFR*-mutant tumors, suggesting that too much oncogenic signaling could be toxic and result in synthetic lethality (186). My results suggest that this observation may not be an isolated example but instead a general rule for OGs capable of suppressing EGFR loss. Large-scale sequencing of cancer genomes has revealed the apparent "mutual exclusivity" of oncogenic events in certain types of cancer (222-225). It is generally assumed such events are functionally redundant so that cells with both mutations have no advantages over cells with just one. However, the oncogenic overload model suggests that certain cancer driver pairs may be synthetic lethal, which provides a new perspective on how the cancer genome is shaped. Such lethality between oncogenic events may be further explored therapeutically by using signaling agonists to provoke events that are lethal only in the presence of another oncogenic event. Thus, the oncogenic overload model is worthy of further investigation in other OG addiction or TSG hypersensitivity models.

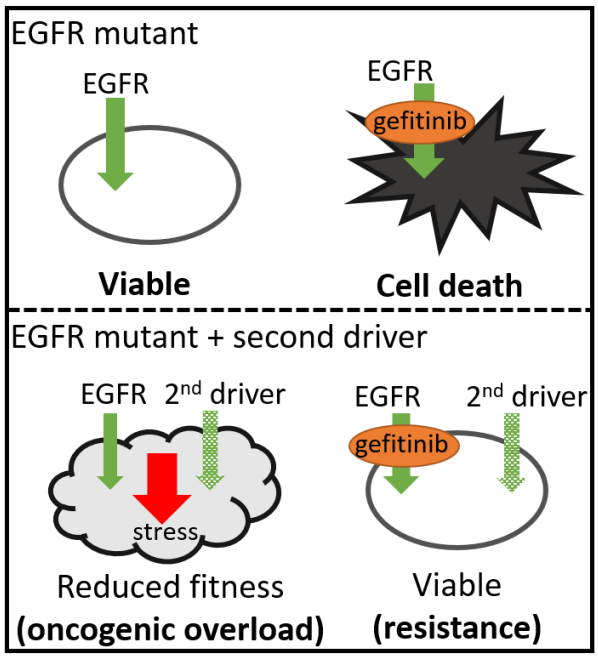

Figure 18. Schematic of oncogenic overload model.

Future directions

One key limitation of the present study is that the identified mechanisms of resistance may not be clinically relevant. The ability of the identified cancer drivers to mediate drug resistance needs to be further confirmed using *in vivo* mouse models. It needs to be further determined whether the novel drug resistance mechanisms identified here are operant in the clinical setting as pre-treatment and post-relapse tumor specimens from ongoing clinical trials become available.

My study suggests that it might be a general notion that cancer drivers can form a function network and genetically modify the dependency of each other. Thus, the TSGs and OGs identified by TUSON Explorer could serve as an ideal list to survey for the genetic modifiers that can partially replace the cancer driver of interest. While the positive selection pressure on those

putative cancer drivers based on *in silico* analysis suggests they play a role in cancer development, their biological functions in tumorigenesis and the underlying molecular mechanisms remain largely unknown for many. By interrogating their ability to regulate a well-characterized oncogenic signaling pathway, I have uncovered the potential functions of many of those cancer drivers in tumorigenesis – for example, the effects of PBRM1 on AKT signaling. My screens focused on anti-cancer drug bypass. This can be done virtually in the context of any hallmarks of cancer to further elucidate the biological functions of those novel cancer drivers: self-sufficiency in growth signals, insensitivity to anti-growth signals, evading apoptosis, limitless replicative potential, sustained angiogenesis, tissue invasion and metastasis, abnormal metabolic pathways and evading the immune system (13).

Appendix 1: Supplemental Tables

The following tables are provided separately as Excel spreadsheets:

Supplemental Table S1. Data analysis of gefitinib bypass screens

Supplemental Table S2. Transcriptional RNA-seq analysis of PC9 cells expressing control or CIC gRNAs treated with or without gefitinib

Supplemental Table S3. Data analysis of JQ1 bypass screens

Supplemental Table S4. Transcriptional RNA-seq analysis of NMC1015 cells containing an empty vector (EV) or expressing KLF4 treated with 200 nM JQ1 for 0 h, 6 h, 24 h or 7 d

Appendix 2: Supplemental Figures

Supplemental Figure 1
Mutual exclusivity analysis between the top 30 TSG hits with activating *EGFR* mutations. Three genes showed statistical significance in mutual exclusivity with activating *EGFR* mutations. The plots represent genomic alterations (legend) in specific genes (rows) affecting individual tumor samples (columns).

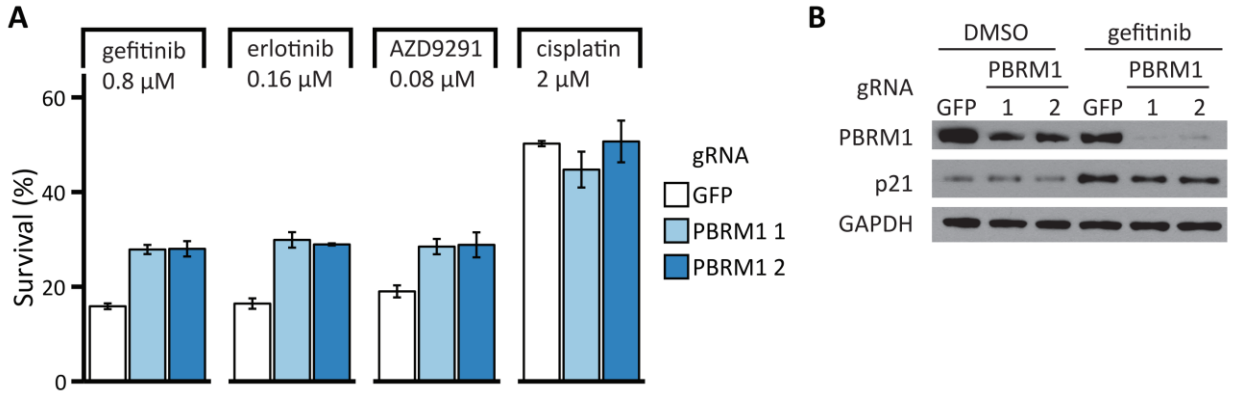

Supplemental Figure 2
(A) PBRM1 or GFP gRNA-expressing PC9 cells were treated with the indicated drugs for 72 h before cell viability was measured using an SRB assay and normalized to untreated controls. Data are means ± SD (n = 3).
(B) Immunoblot analysis with the indicated antibodies of PBRM1 or GFP gRNA-expressing, Cas9-expressing PC9 cells treated with 30 nM gefitinib or DMSO for 3 d.

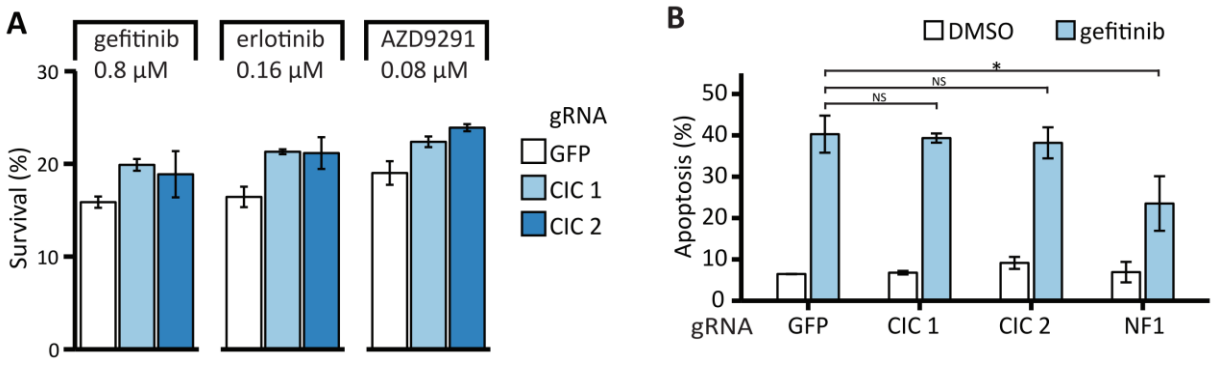

Supplemental Figure 3

(A) PC9 cells infected with a Cas9 and CIC- or GFP-gRNA expressing virus were treated with the indicated drugs for 72 h before cell viability was measured using an SRB assay and normalized to untreated controls. Data are means ± SD (n = 3).
(B) PI staining of PC9 cells infected with virus expressing Cas9 and the indicated gRNA treated with DMSO or 30 nM gefitinib for 48 h. Data are means ± SD (n = 3).

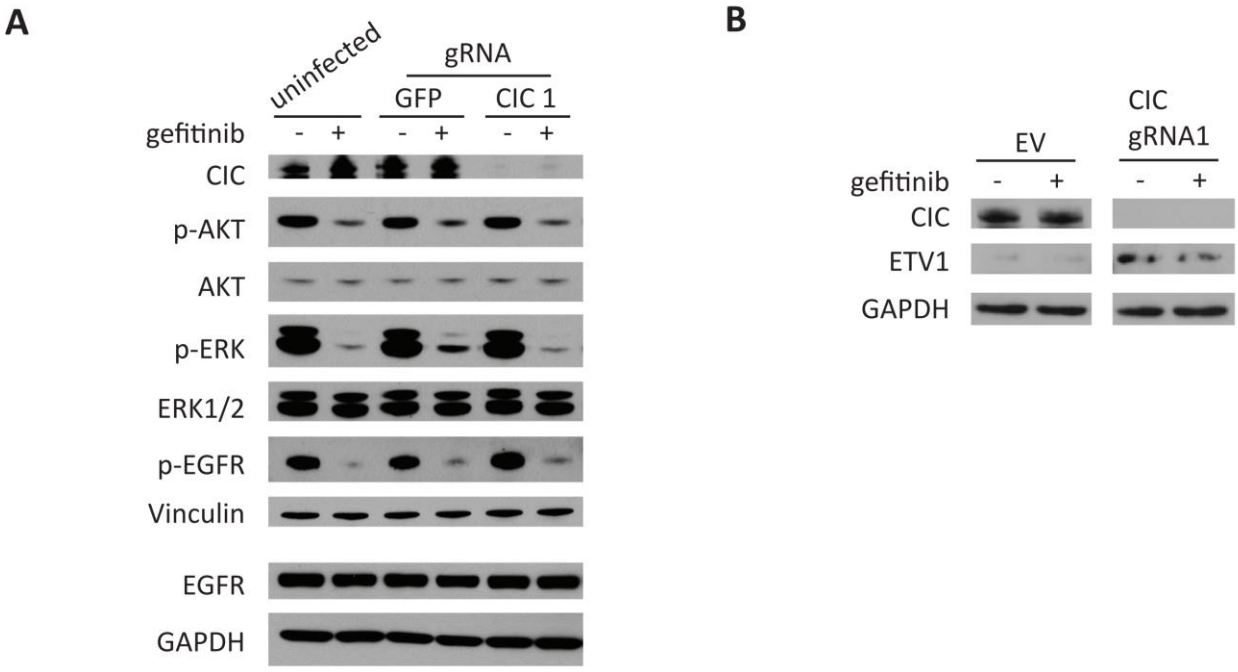

Supplemental Figure 4

(A) Immunoblot analysis of *CIC*-mutant PC9 cells treated with 30 nM gefitinib for 12 h.
(B) Immunoblot analysis of ETV1 levels in CIC-mutant and control PC9 cells during DMSO and gefitinib treatment. All samples were run on the same gel and exposed on the same membrane.

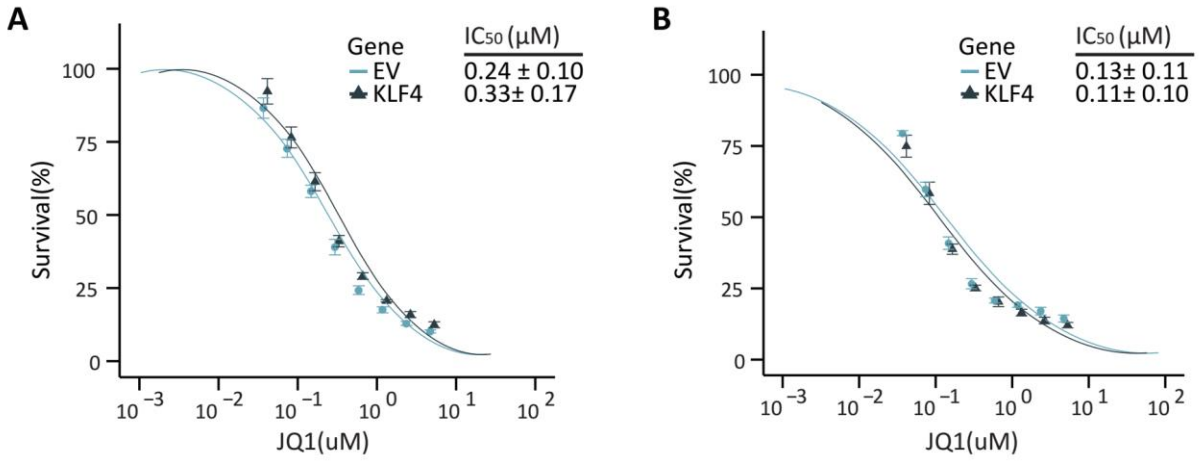

Supplemental Figure 5

(A and B) NMC797 cells (A) or NMC1015 cells (B) containing an empty vector (EV) or expressing KLF4 were treated with the indicated concentrations of JQ1 for 72 h before cell viability was measured using an SRB assay and normalized to untreated controls. Data are means ± SD (n = 3).

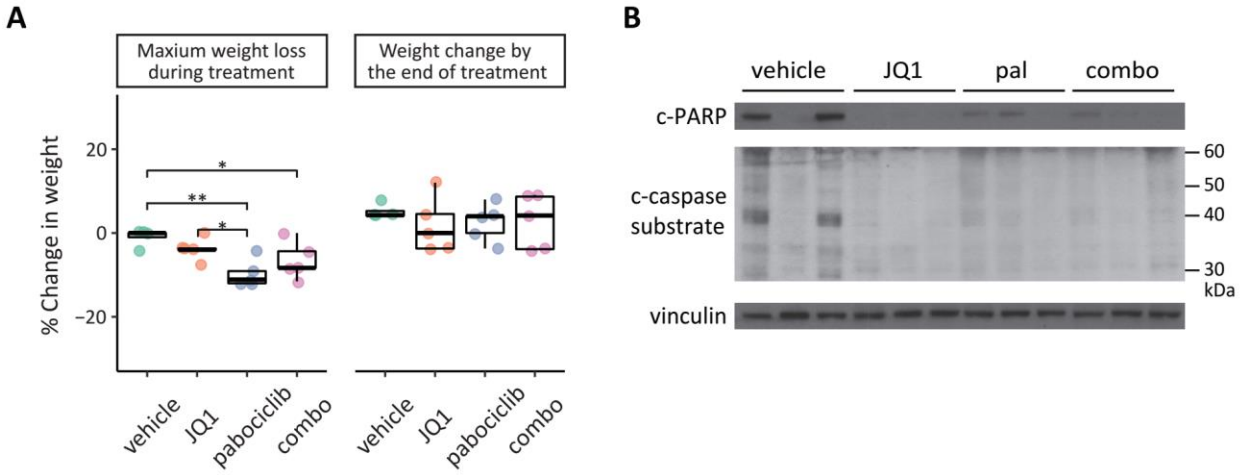

Supplemental Figure 6

(A) As in Fig. 15A. Left panel: The maximum weight loss of mice during treatment. Right panel: the weight change of mice at the end of treatment vs. start point or at the end of survival vs. start point if the tumor reached 1200 mm^3 (end of survival) before 21 d. Each dot represents an individual mouse. *$P < 0.05$, ** $P < 0.01$.

(B) As in Fig. 15A. Mice were treated with the indicated drugs for 3 d. Tumors were harvested 1 h after the last treatment and subjected to immunoblot analysis using the indicated antibodies. Each sample comes from an individual tumor. Pal stands for palbociclib.

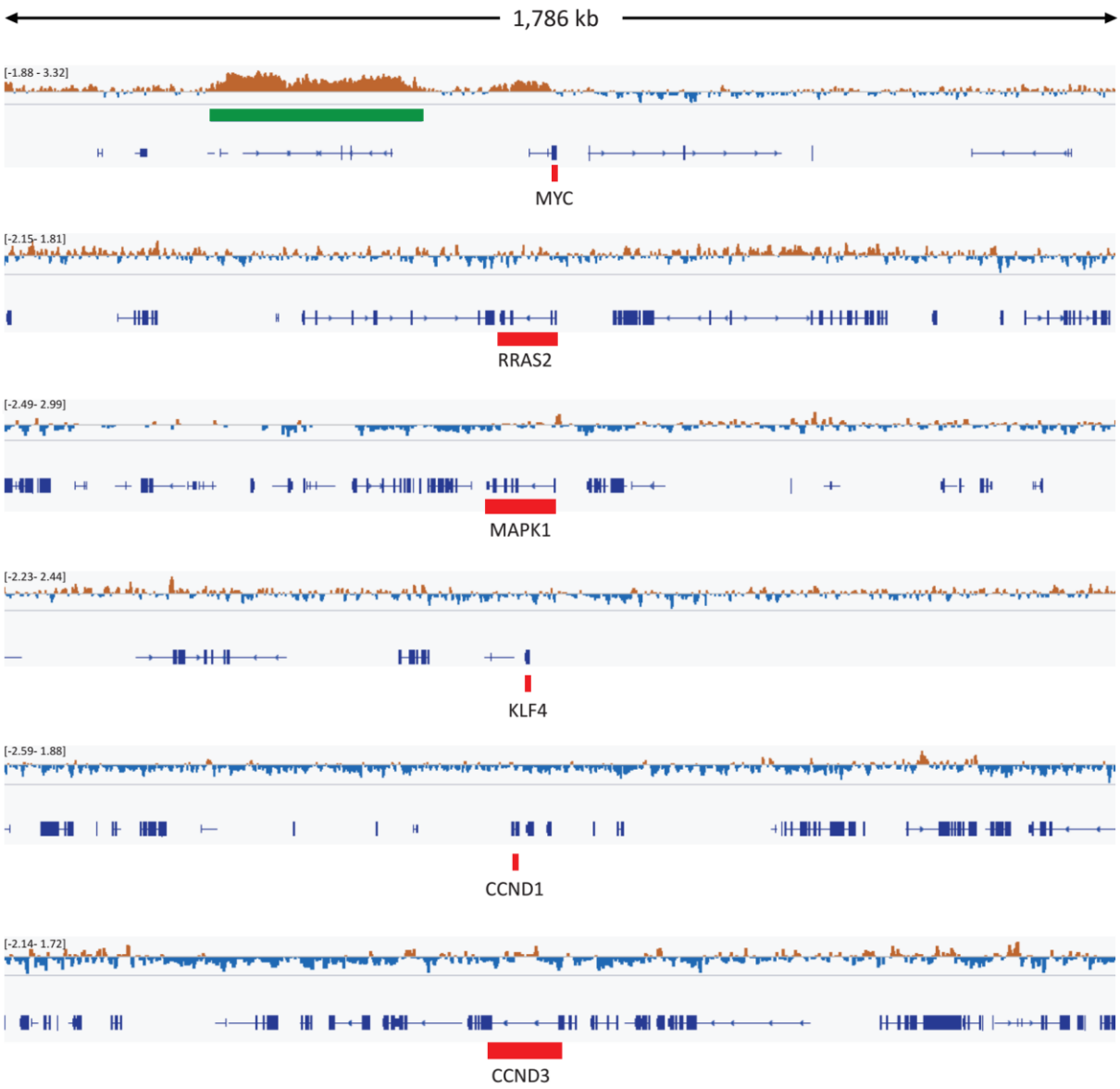

Supplemental Figure 7

ChIP profile of endogenous BRD4-NUT in NMC1015 cells using a highly specific monoclonal antibody to NUT from Alekseyenko et al. 2015. Red bars represent the gene body of the indicated gene. Green bar represents the region of BRD4-NUT megadomains. The scale of the $\log_2$ signal intensity of each track is shown on the upper left corner of each track.

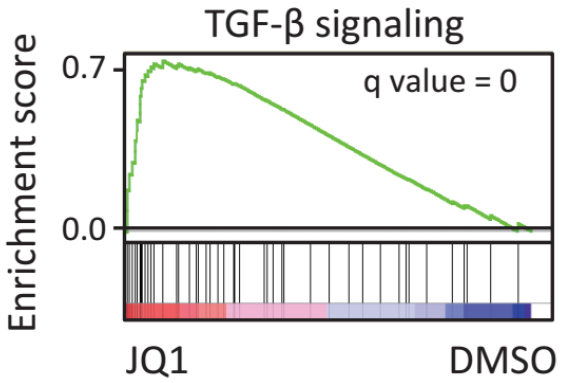

Supplemental Figure 8
As in Fig. 12B. Gene Set Enrichment Analysis plot. Plot indicates a significant upregulation of TGF-β signaling in NMC1015 cells containing an empty vector (EV) after treatment of 200 nM JQ1 for 7 d.

References

1. Ruddon RW. Cancer biology. 4th ed. Oxford ; New York: Oxford University Press; 2007. xiv, 530 p. p.

2. Hansemann D. Ueber asymmetrische Zelltheilung in Epithelkrebsen und deren biologische Bedeutung. Archiv für Pathologische Anatomie und Physiologie und für Klinische Medicin. 1890;119(2):299-326.

3. Boveri T. Zur Frage der Entstehung maligner Tumoren: Gustav Fischer; 1914.

4. Loeb LA, Harris CC. Advances in chemical carcinogenesis: a historical review and prospective. Cancer Res. 2008;68(17):6863-72.

5. Krontiris TG, Cooper GM. Transforming activity of human tumor DNAs. Proc Natl Acad Sci U S A. 1981;78(2):1181-4.

6. Shih C, Padhy LC, Murray M, Weinberg RA. Transforming genes of carcinomas and neuroblastomas introduced into mouse fibroblasts. Nature. 1981;290(5803):261-4.

7. Reddy EP, Reynolds RK, Santos E, Barbacid M. A point mutation is responsible for the acquisition of transforming properties by the T24 human bladder carcinoma oncogene. Nature. 1982;300(5888):149-52.

8. Tabin CJ, Bradley SM, Bargmann CI, Weinberg RA, Papageorge AG, Scolnick EM, et al. Mechanism of activation of a human oncogene. Nature. 1982;300(5888):143-9.

9. Vogelstein B, Papadopoulos N, Velculescu VE, Zhou S, Diaz LA, Jr., Kinzler KW. Cancer genome landscapes. Science. 2013;339(6127):1546-58.

10. Stratton MR, Campbell PJ, Futreal PA. The cancer genome. Nature. 2009;458(7239):719-24.

11. Chakravarthi BV, Nepal S, Varambally S. Genomic and Epigenomic Alterations in Cancer. Am J Pathol. 2016;186(7):1724-35.

12. Ley TJ, Mardis ER, Ding L, Fulton B, McLellan MD, Chen K, et al. DNA sequencing of a cytogenetically normal acute myeloid leukaemia genome. Nature. 2008;456(7218):66-72.

13. Hanahan D, Weinberg RA. Hallmarks of cancer: the next generation. Cell. 2011;144(5):646-74.

14. Martincorena I, Campbell PJ. Somatic mutation in cancer and normal cells. Science. 2015;349(6255):1483-9.

15. Negrini S, Gorgoulis VG, Halazonetis TD. Genomic instability--an evolving hallmark of cancer. Nat Rev Mol Cell Biol. 2010;11(3):220-8.

16. Meyerson M, Gabriel S, Getz G. Advances in understanding cancer genomes through second-generation sequencing. Nat Rev Genet. 2010;11(10):685-96.

17. Parmigiani G, Boca S, Lin J, Kinzler KW, Velculescu V, Vogelstein B. Design and analysis issues in genome-wide somatic mutation studies of cancer. Genomics. 2009;93(1):17-21.

18. Carter H, Chen S, Isik L, Tyekucheva S, Velculescu VE, Kinzler KW, et al. Cancer-specific high-throughput annotation of somatic mutations: computational prediction of driver missense mutations. Cancer Res. 2009;69(16):6660-7.

19. Youn A, Simon R. Identifying cancer driver genes in tumor genome sequencing studies. Bioinformatics. 2011;27(2):175-81.

20. Davoli T, Xu AW, Mengwasser KE, Sack LM, Yoon JC, Park PJ, et al. Cumulative haploinsufficiency and triplosensitivity drive aneuploidy patterns and shape the cancer genome. Cell. 2013;155(4):948-62.

21. Leiserson MD, Vandin F, Wu HT, Dobson JR, Eldridge JV, Thomas JL, et al. Pan-cancer network analysis identifies combinations of rare somatic mutations across pathways and protein complexes. Nat Genet. 2015;47(2):106-14.

22. Cho A, Shim JE, Kim E, Supek F, Lehner B, Lee I. MUFFINN: cancer gene discovery via network analysis of somatic mutation data. Genome Biol. 2016;17(1):129.

23. Wood LD, Parsons DW, Jones S, Lin J, Sjoblom T, Leary RJ, et al. The genomic landscapes of human breast and colorectal cancers. Science. 2007;318(5853):1108-13.

24. Roche B, Thomas F. Ecology and Evolution of Cancer: Elsevier Science; 2017.

25. Duval A, Hamelin R. Mutations at coding repeat sequences in mismatch repair-deficient human cancers: toward a new concept of target genes for instability. Cancer Res. 2002;62(9):2447-54.

26. Li J, Yen C, Liaw D, Podsypanina K, Bose S, Wang SI, et al. PTEN, a putative protein tyrosine phosphatase gene mutated in human brain, breast, and prostate cancer. Science. 1997;275(5308):1943-7.

27. Futreal PA, Coin L, Marshall M, Down T, Hubbard T, Wooster R, et al. A census of human cancer genes. Nat Rev Cancer. 2004;4(3):177-83.

28. Shalem O, Sanjana NE, Zhang F. High-throughput functional genomics using CRISPR-Cas9. Nat Rev Genet. 2015;16(5):299-311.

29. Fire A, Xu S, Montgomery MK, Kostas SA, Driver SE, Mello CC. Potent and specific genetic interference by double-stranded RNA in Caenorhabditis elegans. Nature. 1998;391(6669):806-11.

30. Ketting RF. The many faces of RNAi. Dev Cell. 2011;20(2):148-61.

31. Mohr S, Bakal C, Perrimon N. Genomic screening with RNAi: results and challenges. Annu Rev Biochem. 2010;79:37-64.

32. Horvath P, Barrangou R. CRISPR/Cas, the immune system of bacteria and archaea. Science. 2010;327(5962):167-70.

33. Barrangou R, Fremaux C, Deveau H, Richards M, Boyaval P, Moineau S, et al. CRISPR provides acquired resistance against viruses in prokaryotes. Science. 2007;315(5819):1709-12.

34. Marraffini LA, Sontheimer EJ. CRISPR interference limits horizontal gene transfer in staphylococci by targeting DNA. Science. 2008;322(5909):1843-5.

35. Cong L, Ran FA, Cox D, Lin S, Barretto R, Habib N, et al. Multiplex genome engineering using CRISPR/Cas systems. Science. 2013;339(6121):819-23.

36. Mali P, Yang L, Esvelt KM, Aach J, Guell M, DiCarlo JE, et al. RNA-guided human genome engineering via Cas9. Science. 2013;339(6121):823-6.

37. Wang H, La Russa M, Qi LS. CRISPR/Cas9 in Genome Editing and Beyond. Annu Rev Biochem. 2016;85:227-64.

38. Gilbert LA, Horlbeck MA, Adamson B, Villalta JE, Chen Y, Whitehead EH, et al. Genome-Scale CRISPR-Mediated Control of Gene Repression and Activation. Cell. 2014;159(3):647-61.

39. Gu Z, Steinmetz LM, Gu X, Scharfe C, Davis RW, Li WH. Role of duplicate genes in genetic robustness against null mutations. Nature. 2003;421(6918):63-6.

40. Liao S, Davoli T, Leng Y, Li MZ, Xu Q, Elledge SJ. A genetic interaction analysis identifies cancer drivers that modify EGFR dependency. Genes Dev. 2017;31(2):184-96.

41. Liao S, Maertens O, Cichowski K, Elledge SJ. Genetic modifiers of the BRD4-NUT dependency of NUT midline carcinoma uncovers a synergism between BETis and CDK4/6is. Genes Dev. 2018;32(17-18):1188-200.

42. Kim E, Ilic N, Shrestha Y, Zou L, Kamburov A, Zhu C, et al. Systematic Functional Interrogation of Rare Cancer Variants Identifies Oncogenic Alleles. Cancer Discov. 2016;6(7):714-26.

43. Papp B, Pal C, Hurst LD. Dosage sensitivity and the evolution of gene families in yeast. Nature. 2003;424(6945):194-7.

44. Vavouri T, Semple JI, Garcia-Verdugo R, Lehner B. Intrinsic protein disorder and interaction promiscuity are widely associated with dosage sensitivity. Cell. 2009;138(1):198-208.

45. Heinhuis KM, Ros W, Kok M, Steeghs N, Beijnen JH, Schellens JHM. Enhancing antitumor response by combining immune checkpoint inhibitors with chemotherapy in solid tumors. Ann Oncol. 2019;30(2):219-35.

46. Gerber DE. Targeted therapies: a new generation of cancer treatments. Am Fam Physician. 2008;77(3):311-9.

47. Housman G, Byler S, Heerboth S, Lapinska K, Longacre M, Snyder N, et al. Drug resistance in cancer: an overview. Cancers (Basel). 2014;6(3):1769-92.

48. Luo J, Solimini NL, Elledge SJ. Principles of cancer therapy: oncogene and non-oncogene addiction. Cell. 2009;136(5):823-37.

49. Folkman J. Tumor angiogenesis: therapeutic implications. N Engl J Med. 1971;285(21):1182-6.

50. Ye W. The Complexity of Translating Anti-angiogenesis Therapy from Basic Science to the Clinic. Dev Cell. 2016;37(2):114-25.

51. Chong CR, Janne PA. The quest to overcome resistance to EGFR-targeted therapies in cancer. Nat Med. 2013;19(11):1389-400.

52. Stewart EL, Tan SZ, Liu G, Tsao MS. Known and putative mechanisms of resistance to EGFR targeted therapies in NSCLC patients with EGFR mutations-a review. Transl Lung Cancer Res. 2015;4(1):67-81.

53. Shan Y, Eastwood MP, Zhang X, Kim ET, Arkhipov A, Dror RO, et al. Oncogenic mutations counteract intrinsic disorder in the EGFR kinase and promote receptor dimerization. Cell. 2012;149(4):860-70.

54. Red Brewer M, Yun CH, Lai D, Lemmon MA, Eck MJ, Pao W. Mechanism for activation of mutated epidermal growth factor receptors in lung cancer. Proc Natl Acad Sci U S A. 2013;110(38):E3595-604.

55. Mulloy R, Ferrand A, Kim Y, Sordella R, Bell DW, Haber DA, et al. Epidermal growth factor receptor mutants from human lung cancers exhibit enhanced catalytic activity and increased sensitivity to gefitinib. Cancer Res. 2007;67(5):2325-30.

56. Hynes NE, Lane HA. ERBB receptors and cancer: the complexity of targeted inhibitors. Nat Rev Cancer. 2005;5(5):341-54.

57. Maruyama R, Nishiwaki Y, Tamura T, Yamamoto N, Tsuboi M, Nakagawa K, et al. Phase III study, V-15-32, of gefitinib versus docetaxel in previously treated Japanese patients with non-small-cell lung cancer. J Clin Oncol. 2008;26(26):4244-52.

58. Kim ES, Hirsh V, Mok T, Socinski MA, Gervais R, Wu YL, et al. Gefitinib versus docetaxel in previously treated non-small-cell lung cancer (INTEREST): a randomised phase III trial. Lancet. 2008;372(9652):1809-18.

59. Thatcher N, Chang A, Parikh P, Rodrigues Pereira J, Ciuleanu T, von Pawel J, et al. Gefitinib plus best supportive care in previously treated patients with refractory advanced non-small-cell lung cancer: results from a randomised, placebo-controlled, multicentre study (Iressa Survival Evaluation in Lung Cancer). Lancet. 2005;366(9496):1527-37.

60. Gatzemeier U, Pluzanska A, Szczesna A, Kaukel E, Roubec J, De Rosa F, et al. Phase III study of erlotinib in combination with cisplatin and gemcitabine in advanced non-small-cell lung cancer: the Tarceva Lung Cancer Investigation Trial. J Clin Oncol. 2007;25(12):1545-52.

61. Herbst RS, Prager D, Hermann R, Fehrenbacher L, Johnson BE, Sandler A, et al. TRIBUTE: a phase III trial of erlotinib hydrochloride (OSI-774) combined with carboplatin and paclitaxel chemotherapy in advanced non-small-cell lung cancer. J Clin Oncol. 2005;23(25):5892-9.

62. Herbst RS, Giaccone G, Schiller JH, Natale RB, Miller V, Manegold C, et al. Gefitinib in combination with paclitaxel and carboplatin in advanced non-small-cell lung cancer: a phase III trial--INTACT 2. J Clin Oncol. 2004;22(5):785-94.

63. Giaccone G, Herbst RS, Manegold C, Scagliotti G, Rosell R, Miller V, et al. Gefitinib in combination with gemcitabine and cisplatin in advanced non-small-cell lung cancer: a phase III trial--INTACT 1. J Clin Oncol. 2004;22(5):777-84.

64. Miller VA, Riely GJ, Zakowski MF, Li AR, Patel JD, Heelan RT, et al. Molecular characteristics of bronchioloalveolar carcinoma and adenocarcinoma, bronchioloalveolar carcinoma subtype, predict response to erlotinib. J Clin Oncol. 2008;26(9):1472-8.

65. Fukuoka M, Yano S, Giaccone G, Tamura T, Nakagawa K, Douillard JY, et al. Multi-institutional randomized phase II trial of gefitinib for previously treated patients with advanced non-small-cell lung cancer (The IDEAL 1 Trial) [corrected]. J Clin Oncol. 2003;21(12):2237-46.

66. Lynch TJ, Bell DW, Sordella R, Gurubhagavatula S, Okimoto RA, Brannigan BW, et al. Activating mutations in the epidermal growth factor receptor underlying responsiveness of non-small-cell lung cancer to gefitinib. N Engl J Med. 2004;350(21):2129-39.

67. Paez JG, Janne PA, Lee JC, Tracy S, Greulich H, Gabriel S, et al. EGFR mutations in lung cancer: correlation with clinical response to gefitinib therapy. Science. 2004;304(5676):1497-500.

68. Pao W, Miller V, Zakowski M, Doherty J, Politi K, Sarkaria I, et al. EGF receptor gene mutations are common in lung cancers from "never smokers" and are associated with sensitivity of tumors to gefitinib and erlotinib. Proc Natl Acad Sci U S A. 2004;101(36):13306-11.

69. Rosell R, Moran T, Queralt C, Porta R, Cardenal F, Camps C, et al. Screening for epidermal growth factor receptor mutations in lung cancer. N Engl J Med. 2009;361(10):958-67.

70. Mitsudomi T, Morita S, Yatabe Y, Negoro S, Okamoto I, Tsurutani J, et al. Gefitinib versus cisplatin plus docetaxel in patients with non-small-cell lung cancer harbouring mutations of the epidermal growth factor receptor (WJTOG3405): an open label, randomised phase 3 trial. Lancet Oncol. 2010;11(2):121-8.

71. Mok TS, Wu YL, Thongprasert S, Yang CH, Chu DT, Saijo N, et al. Gefitinib or carboplatin-paclitaxel in pulmonary adenocarcinoma. N Engl J Med. 2009;361(10):947-57.

72. Thress KS, Paweletz CP, Felip E, Cho BC, Stetson D, Dougherty B, et al. Acquired EGFR C797S mutation mediates resistance to AZD9291 in non-small cell lung cancer harboring EGFR T790M. Nat Med. 2015;21(6):560-2.

73. Yun CH, Mengwasser KE, Toms AV, Woo MS, Greulich H, Wong KK, et al. The T790M mutation in EGFR kinase causes drug resistance by increasing the affinity for ATP. Proc Natl Acad Sci U S A. 2008;105(6):2070-5.

74. Yang JC, Ahn MJ, Kim DW, Ramalingam SS, Sequist LV, Su WC, et al. Osimertinib in Pretreated T790M-Positive Advanced Non-Small-Cell Lung Cancer: AURA Study Phase II Extension Component. J Clin Oncol. 2017;35(12):1288-96.

75. Oxnard GR, Hu Y, Mileham KF, Husain H, Costa DB, Tracy P, et al. Assessment of Resistance Mechanisms and Clinical Implications in Patients With EGFR T790M-

Positive Lung Cancer and Acquired Resistance to Osimertinib. JAMA Oncol. 2018;4(11):1527-34.

76. Engelman JA, Zejnullahu K, Mitsudomi T, Song Y, Hyland C, Park JO, et al. MET amplification leads to gefitinib resistance in lung cancer by activating ERBB3 signaling. Science. 2007;316(5827):1039-43.

77. Takezawa K, Pirazzoli V, Arcila ME, Nebhan CA, Song X, de Stanchina E, et al. HER2 amplification: a potential mechanism of acquired resistance to EGFR inhibition in EGFR-mutant lung cancers that lack the second-site EGFRT790M mutation. Cancer Discov. 2012;2(10):922-33.

78. Ercan D, Xu C, Yanagita M, Monast CS, Pratilas CA, Montero J, et al. Reactivation of ERK signaling causes resistance to EGFR kinase inhibitors. Cancer Discov. 2012;2(10):934-47.

79. Diaz LA, Jr., Williams RT, Wu J, Kinde I, Hecht JR, Berlin J, et al. The molecular evolution of acquired resistance to targeted EGFR blockade in colorectal cancers. Nature. 2012;486(7404):537-40.

80. Sartore-Bianchi A, Martini M, Molinari F, Veronese S, Nichelatti M, Artale S, et al. PIK3CA mutations in colorectal cancer are associated with clinical resistance to EGFR-targeted monoclonal antibodies. Cancer Res. 2009;69(5):1851-7.

81. Misale S, Yaeger R, Hobor S, Scala E, Janakiraman M, Liska D, et al. Emergence of KRAS mutations and acquired resistance to anti-EGFR therapy in colorectal cancer. Nature. 2012;486(7404):532-6.

82. Ohashi K, Sequist LV, Arcila ME, Moran T, Chmielecki J, Lin YL, et al. Lung cancers with acquired resistance to EGFR inhibitors occasionally harbor BRAF gene mutations but lack mutations in KRAS, NRAS, or MEK1. Proc Natl Acad Sci U S A. 2012;109(31):E2127-33.

83. Ng KP, Hillmer AM, Chuah CT, Juan WC, Ko TK, Teo AS, et al. A common BIM deletion polymorphism mediates intrinsic resistance and inferior responses to tyrosine kinase inhibitors in cancer. Nat Med. 2012;18(4):521-8.

84. Yu HA, Arcila ME, Rekhtman N, Sima CS, Zakowski MF, Pao W, et al. Analysis of tumor specimens at the time of acquired resistance to EGFR-TKI therapy in 155 patients with EGFR-mutant lung cancers. Clin Cancer Res. 2013;19(8):2240-7.

85. Uramoto H, Iwata T, Onitsuka T, Shimokawa H, Hanagiri T, Oyama T. Epithelial-mesenchymal transition in EGFR-TKI acquired resistant lung adenocarcinoma. Anticancer Res. 2010;30(7):2513-7.

86. Majem M, Remon J. Tumor heterogeneity: evolution through space and time in EGFR mutant non small cell lung cancer patients. Transl Lung Cancer Res. 2013;2(3):226-37.

87. Herbst RS, Baas P, Kim DW, Felip E, Perez-Gracia JL, Han JY, et al. Pembrolizumab versus docetaxel for previously treated, PD-L1-positive, advanced non-small-cell lung cancer (KEYNOTE-010): a randomised controlled trial. Lancet. 2016;387(10027):1540-50.

88. Brahmer J, Reckamp KL, Baas P, Crino L, Eberhardt WE, Poddubskaya E, et al. Nivolumab versus Docetaxel in Advanced Squamous-Cell Non-Small-Cell Lung Cancer. N Engl J Med. 2015;373(2):123-35.

89. Borghaei H, Paz-Ares L, Horn L, Spigel DR, Steins M, Ready NE, et al. Nivolumab versus Docetaxel in Advanced Nonsquamous Non-Small-Cell Lung Cancer. N Engl J Med. 2015;373(17):1627-39.

90. Gainor JF, Shaw AT, Sequist LV, Fu X, Azzoli CG, Piotrowska Z, et al. EGFR Mutations and ALK Rearrangements Are Associated with Low Response Rates to PD-1 Pathway Blockade in Non-Small Cell Lung Cancer: A Retrospective Analysis. Clin Cancer Res. 2016;22(18):4585-93.

91. Allis CD, Jenuwein T. The molecular hallmarks of epigenetic control. Nature Reviews Genetics. 2016;17:487.

92. Stathis A, Bertoni F. BET Proteins as Targets for Anticancer Treatment. Cancer Discov. 2018;8(1):24-36.

93. Dey A, Chitsaz F, Abbasi A, Misteli T, Ozato K. The double bromodomain protein Brd4 binds to acetylated chromatin during interphase and mitosis. Proc Natl Acad Sci U S A. 2003;100(15):8758-63.

94. Yang Z, Yik JHN, Chen R, He N, Jang MK, Ozato K, et al. Recruitment of P-TEFb for Stimulation of Transcriptional Elongation by the Bromodomain Protein Brd4. Molecular Cell. 2005;19(4):535-45.

95. Jang MK, Mochizuki K, Zhou M, Jeong H-S, Brady JN, Ozato K. The Bromodomain Protein Brd4 Is a Positive Regulatory Component of P-TEFb and Stimulates RNA Polymerase II-Dependent Transcription. Molecular Cell. 2005;19(4):523-34.

96. Marcotte R, Sayad A, Brown KR, Sanchez-Garcia F, Reimand J, Haider M, et al. Functional Genomic Landscape of Human Breast Cancer Drivers, Vulnerabilities, and Resistance. Cell. 2016;164(1-2):293-309.

97. Zuber J, Shi J, Wang E, Rappaport AR, Herrmann H, Sison EA, et al. RNAi screen identifies Brd4 as a therapeutic target in acute myeloid leukaemia. Nature. 2011;478(7370):524-8.

98. Toyoshima M, Howie HL, Imakura M, Walsh RM, Annis JE, Chang AN, et al. Functional genomics identifies therapeutic targets for MYC-driven cancer. Proc Natl Acad Sci U S A. 2012;109(24):9545-50.

99. Baratta MG, Schinzel AC, Zwang Y, Bandopadhayay P, Bowman-Colin C, Kutt J, et al. An in-tumor genetic screen reveals that the BET bromodomain protein, BRD4, is a potential therapeutic target in ovarian carcinoma. Proc Natl Acad Sci U S A. 2015;112(1):232-7.

100. Loven J, Hoke HA, Lin CY, Lau A, Orlando DA, Vakoc CR, et al. Selective inhibition of tumor oncogenes by disruption of super-enhancers. Cell. 2013;153(2):320-34.

101. Fong CY, Gilan O, Lam EY, Rubin AF, Ftouni S, Tyler D, et al. BET inhibitor resistance emerges from leukaemia stem cells. Nature. 2015;525(7570):538-42.

102. Rathert P, Roth M, Neumann T, Muerdter F, Roe JS, Muhar M, et al. Transcriptional plasticity promotes primary and acquired resistance to BET inhibition. Nature. 2015;525(7570):543-7.

103. Kumar K, Raza SS, Knab LM, Chow CR, Kwok B, Bentrem DJ, et al. GLI2-dependent c-MYC upregulation mediates resistance of pancreatic cancer cells to the BET bromodomain inhibitor JQ1. Sci Rep. 2015;5:9489.

104. Shu S, Lin CY, He HH, Witwicki RM, Tabassum DP, Roberts JM, et al. Response and resistance to BET bromodomain inhibitors in triple-negative breast cancer. Nature. 2016;529(7586):413-7.

105. Kurimchak AM, Shelton C, Duncan KE, Johnson KJ, Brown J, O'Brien S, et al. Resistance to BET Bromodomain Inhibitors Is Mediated by Kinome Reprogramming in Ovarian Cancer. Cell Rep. 2016;16(5):1273-86.

106. Jang JE, Eom JI, Jeung HK, Cheong JW, Lee JY, Kim JS, et al. AMPK-ULK1-Mediated Autophagy Confers Resistance to BET Inhibitor JQ1 in Acute Myeloid Leukemia Stem Cells. Clin Cancer Res. 2017;23(11):2781-94.

107. Zhao Y, Liu Q, Acharya P, Stengel KR, Sheng Q, Zhou X, et al. High-Resolution Mapping of RNA Polymerases Identifies Mechanisms of Sensitivity and Resistance to BET Inhibitors in t(8;21) AML. Cell Rep. 2016;16(7):2003-16.

108. Shi X, Mihaylova VT, Kuruvilla L, Chen F, Viviano S, Baldassarre M, et al. Loss of TRIM33 causes resistance to BET bromodomain inhibitors through MYC- and TGF-beta-dependent mechanisms. Proc Natl Acad Sci U S A. 2016;113(31):E4558-66.

109. Janouskova H, El Tekle G, Bellini E, Udeshi ND, Rinaldi A, Ulbricht A, et al. Opposing effects of cancer-type-specific SPOP mutants on BET protein degradation and sensitivity to BET inhibitors. Nat Med. 2017;23(9):1046-54.

110. French CA, Miyoshi I, Kubonishi I, Grier HE, Perez-Atayde AR, Fletcher JA. BRD4-NUT fusion oncogene: a novel mechanism in aggressive carcinoma. Cancer Res. 2003;63(2):304-7.

111. French CA, Ramirez CL, Kolmakova J, Hickman TT, Cameron MJ, Thyne ME, et al. BRD-NUT oncoproteins: a family of closely related nuclear proteins that block epithelial differentiation and maintain the growth of carcinoma cells. Oncogene. 2008;27(15):2237-42.

112. Alekseyenko AA, Walsh EM, Wang X, Grayson AR, Hsi PT, Kharchenko PV, et al. The oncogenic BRD4-NUT chromatin regulator drives aberrant transcription within large topological domains. Genes Dev. 2015;29(14):1507-23.

113. Grayson AR, Walsh EM, Cameron MJ, Godec J, Ashworth T, Ambrose JM, et al. MYC, a downstream target of BRD-NUT, is necessary and sufficient for the blockade of differentiation in NUT midline carcinoma. Oncogene. 2014;33(13):1736-42.

114. Bauer DE, Mitchell CM, Strait KM, Lathan CS, Stelow EB, Luer SC, et al. Clinicopathologic features and long-term outcomes of NUT midline carcinoma. Clin Cancer Res. 2012;18(20):5773-9.

115. Stathis A, Zucca E, Bekradda M, Gomez-Roca C, Delord JP, de La Motte Rouge T, et al. Clinical Response of Carcinomas Harboring the BRD4-NUT Oncoprotein to the Targeted Bromodomain Inhibitor OTX015/MK-8628. Cancer Discov. 2016;6(5):492-500.

116. Neel DS, Bivona TG. Resistance is futile: overcoming resistance to targeted therapies in lung adenocarcinoma. NPJ Precis Oncol. 2017;1.

117. Eberlein CA, Stetson D, Markovets AA, Al-Kadhimi KJ, Lai Z, Fisher PR, et al. Acquired Resistance to the Mutant-Selective EGFR Inhibitor AZD9291 Is Associated with Increased Dependence on RAS Signaling in Preclinical Models. Cancer Res. 2015;75(12):2489-500.

118. Tricker EM, Xu C, Uddin S, Capelletti M, Ercan D, Ogino A, et al. Combined EGFR/MEK Inhibition Prevents the Emergence of Resistance in EGFR-Mutant Lung Cancer. Cancer Discov. 2015;5(9):960-71.

119. Hrustanovic G, Olivas V, Pazarentzos E, Tulpule A, Asthana S, Blakely CM, et al. RAS-MAPK dependence underlies a rational polytherapy strategy in EML4-ALK-positive lung cancer. Nat Med. 2015;21(9):1038-47.

120. Planchard D, Besse B, Groen HJM, Souquet PJ, Quoix E, Baik CS, et al. Dabrafenib plus trametinib in patients with previously treated BRAF(V600E)-mutant metastatic non-small cell lung cancer: an open-label, multicentre phase 2 trial. Lancet Oncol. 2016;17(7):984-93.

121. Johnson DB, Flaherty KT, Weber JS, Infante JR, Kim KB, Kefford RF, et al. Combined BRAF (Dabrafenib) and MEK inhibition (Trametinib) in patients with BRAFV600-mutant melanoma experiencing progression with single-agent BRAF inhibitor. J Clin Oncol. 2014;32(33):3697-704.

122. Flaherty KT, Infante JR, Daud A, Gonzalez R, Kefford RF, Sosman J, et al. Combined BRAF and MEK inhibition in melanoma with BRAF V600 mutations. N Engl J Med. 2012;367(18):1694-703.

123. Karachaliou N, Gonzalez-Cao M, Sosa A, Berenguer J, Bracht JWP, Ito M, et al. The combination of checkpoint immunotherapy and targeted therapy in cancer. Ann Transl Med. 2017;5(19):388.

124. Chen N, Fang W, Zhan J, Hong S, Tang Y, Kang S, et al. Upregulation of PD-L1 by EGFR Activation Mediates the Immune Escape in EGFR-Driven NSCLC: Implication

for Optional Immune Targeted Therapy for NSCLC Patients with EGFR Mutation. J Thorac Oncol. 2015;10(6):910-23.

125. Suda K, Rozeboom L, Rivard C, Yu H, Melnick MA, Hinz T, et al. MA15.11 Acquired Resistance Mechanisms to EGFR Kinase Inhibitors Alter PD-L1 Expression Status in Lung Cancer. Journal of Thoracic Oncology. 2017;12(1):S433-S4.

126. Topalian SL, Hodi FS, Brahmer JR, Gettinger SN, Smith DC, McDermott DF, et al. Safety, activity, and immune correlates of anti-PD-1 antibody in cancer. N Engl J Med. 2012;366(26):2443-54.

127. Herbst RS, Soria JC, Kowanetz M, Fine GD, Hamid O, Gordon MS, et al. Predictive correlates of response to the anti-PD-L1 antibody MPDL3280A in cancer patients. Nature. 2014;515(7528):563-7.

128. Garon EB, Rizvi NA, Hui R, Leighl N, Balmanoukian AS, Eder JP, et al. Pembrolizumab for the treatment of non-small-cell lung cancer. N Engl J Med. 2015;372(21):2018-28.

129. Wang X, Goldstein D, Crowe PJ, Yang JL. Next-generation EGFR/HER tyrosine kinase inhibitors for the treatment of patients with non-small-cell lung cancer harboring EGFR mutations: a review of the evidence. Onco Targets Ther. 2016;9:5461-73.

130. Sharifnia T, Rusu V, Piccioni F, Bagul M, Imielinski M, Cherniack AD, et al. Genetic modifiers of EGFR dependence in non-small cell lung cancer. Proc Natl Acad Sci U S A. 2014;111(52):18661-6.

131. de Bruin EC, Cowell C, Warne PH, Jiang M, Saunders RE, Melnick MA, et al. Reduced NF1 expression confers resistance to EGFR inhibition in lung cancer. Cancer Discov. 2014;4(5):606-19.

132. Sos ML, Koker M, Weir BA, Heynck S, Rabinovsky R, Zander T, et al. PTEN loss contributes to erlotinib resistance in EGFR-mutant lung cancer by activation of Akt and EGFR. Cancer Res. 2009;69(8):3256-61.

133. Yamamoto C, Basaki Y, Kawahara A, Nakashima K, Kage M, Izumi H, et al. Loss of PTEN expression by blocking nuclear translocation of EGR1 in gefitinib-resistant lung cancer cells harboring epidermal growth factor receptor-activating mutations. Cancer Res. 2010;70(21):8715-25.

134. Li W, Xu H, Xiao T, Cong L, Love MI, Zhang F, et al. MAGeCK enables robust identification of essential genes from genome-scale CRISPR/Cas9 knockout screens. Genome Biol. 2014;15(12):554.

135. Helming KC, Wang X, Roberts CW. Vulnerabilities of mutant SWI/SNF complexes in cancer. Cancer Cell. 2014;26(3):309-17.

136. Xia W, Nagase S, Montia AG, Kalachikov SM, Keniry M, Su T, et al. BAF180 is a critical regulator of p21 induction and a tumor suppressor mutated in breast cancer. Cancer Res. 2008;68(6):1667-74.

137. Lee H, Dai F, Zhuang L, Xiao ZD, Kim J, Zhang Y, et al. BAF180 regulates cellular senescence and hematopoietic stem cell homeostasis through p21. Oncotarget. 2016;7(15):19134-46.

138. Papadakis AI, Sun C, Knijnenburg TA, Xue Y, Grernrum W, Holzel M, et al. SMARCE1 suppresses EGFR expression and controls responses to MET and ALK inhibitors in lung cancer. Cell Res. 2015;25(4):445-58.

139. Roch F, Jimenez G, Casanova J. EGFR signalling inhibits Capicua-dependent repression during specification of Drosophila wing veins. Development. 2002;129(4):993-1002.

140. Tseng AS, Tapon N, Kanda H, Cigizoglu S, Edelmann L, Pellock B, et al. Capicua regulates cell proliferation downstream of the receptor tyrosine kinase/ras signaling pathway. Curr Biol. 2007;17(8):728-33.

141. Kobayashi S, Shimamura T, Monti S, Steidl U, Hetherington CJ, Lowell AM, et al. Transcriptional profiling identifies cyclin D1 as a critical downstream effector of mutant epidermal growth factor receptor signaling. Cancer Res. 2006;66(23):11389-98.

142. Oh S, Shin S, Janknecht R. ETV1, 4 and 5: an oncogenic subfamily of ETS transcription factors. Biochim Biophys Acta. 2012;1826(1):1-12.

143. Hollenhorst PC, Ferris MW, Hull MA, Chae H, Kim S, Graves BJ. Oncogenic ETS proteins mimic activated RAS/MAPK signaling in prostate cells. Genes Dev. 2011;25(20):2147-57.

144. Pirazzoli V, Nebhan C, Song X, Wurtz A, Walther Z, Cai G, et al. Acquired resistance of EGFR-mutant lung adenocarcinomas to afatinib plus cetuximab is associated with activation of mTORC1. Cell Rep. 2014;7(4):999-1008.

145. Cheng H, Fertig EJ, Ozawa H, Hatakeyama H, Howard JD, Perez J, et al. Decreased SMAD4 expression is associated with induction of epithelial-to-mesenchymal transition and cetuximab resistance in head and neck squamous cell carcinoma. Cancer Biol Ther. 2015;16(8):1252-8.

146. Rishi AK, Zhang L, Yu Y, Jiang Y, Nautiyal J, Wali A, et al. Cell cycle- and apoptosis-regulatory protein-1 is involved in apoptosis signaling by epidermal growth factor receptor. J Biol Chem. 2006;281(19):13188-98.

147. Takekawa M, Tatebayashi K, Itoh F, Adachi M, Imai K, Saito H. Smad-dependent GADD45beta expression mediates delayed activation of p38 MAP kinase by TGF-beta. EMBO J. 2002;21(23):6473-82.

148. Niederst MJ, Sequist LV, Poirier JT, Mermel CH, Lockerman EL, Garcia AR, et al. RB loss in resistant EGFR mutant lung adenocarcinomas that transform to small-cell lung cancer. Nat Commun. 2015;6:6377.

149. Stalinska L, Ferenc T. [The role of TGF-beta in cell cycle regulation]. Postepy Hig Med Dosw (Online). 2005;59:441-9.

150. Schiewer MJ, Augello MA, Knudsen KE. The AR dependent cell cycle: mechanisms and cancer relevance. Mol Cell Endocrinol. 2012;352(1-2):34-45.

151. VanArsdale T, Boshoff C, Arndt KT, Abraham RT. Molecular Pathways: Targeting the Cyclin D-CDK4/6 Axis for Cancer Treatment. Clin Cancer Res. 2015;21(13):2905-10.

152. O'Leary B, Finn RS, Turner NC. Treating cancer with selective CDK4/6 inhibitors. Nat Rev Clin Oncol. 2016;13(7):417-30.

153. Liu X, Su L, Liu X. Loss of CDH1 up-regulates epidermal growth factor receptor via phosphorylation of YBX1 in non-small cell lung cancer cells. FEBS Lett. 2013;587(24):3995-4000.

154. Yamadori T, Ishii Y, Homma S, Morishima Y, Kurishima K, Itoh K, et al. Molecular mechanisms for the regulation of Nrf2-mediated cell proliferation in non-small-cell lung cancers. Oncogene. 2012;31(45):4768-77.

155. Schwartz S, Wongvipat J, Trigwell CB, Hancox U, Carver BS, Rodrik-Outmezguine V, et al. Feedback suppression of PI3Kalpha signaling in PTEN-mutated tumors is relieved by selective inhibition of PI3Kbeta. Cancer Cell. 2015;27(1):109-22.

156. Costa C, Ebi H, Martini M, Beausoleil SA, Faber AC, Jakubik CT, et al. Measurement of PIP3 levels reveals an unexpected role for p110beta in early adaptive responses to p110alpha-specific inhibitors in luminal breast cancer. Cancer Cell. 2015;27(1):97-108.

157. Jimenez G, Shvartsman SY, Paroush Z. The Capicua repressor--a general sensor of RTK signaling in development and disease. J Cell Sci. 2012;125(Pt 6):1383-91.

158. Dissanayake K, Toth R, Blakey J, Olsson O, Campbell DG, Prescott AR, et al. ERK/p90(RSK)/14-3-3 signalling has an impact on expression of PEA3 Ets transcription factors via the transcriptional repressor capicua. Biochem J. 2011;433(3):515-25.

159. Li MZ, Elledge SJ. SLIC: a method for sequence- and ligation-independent cloning. Methods Mol Biol. 2012;852:51-9.

160. Adzhubei IA, Schmidt S, Peshkin L, Ramensky VE, Gerasimova A, Bork P, et al. A method and server for predicting damaging missense mutations. Nat Methods. 2010;7(4):248-9.

161. Vichai V, Kirtikara K. Sulforhodamine B colorimetric assay for cytotoxicity screening. Nat Protoc. 2006;1(3):1112-6.

162. Pertea M, Kim D, Pertea GM, Leek JT, Salzberg SL. Transcript-level expression analysis of RNA-seq experiments with HISAT, StringTie and Ballgown. Nat Protoc. 2016;11(9):1650-67.

163. Liao Y, Smyth GK, Shi W. The Subread aligner: fast, accurate and scalable read mapping by seed-and-vote. Nucleic Acids Res. 2013;41(10):e108.

164. Robinson MD, McCarthy DJ, Smyth GK. edgeR: a Bioconductor package for differential expression analysis of digital gene expression data. Bioinformatics. 2010;26(1):139-40.

165. Subramanian A, Tamayo P, Mootha VK, Mukherjee S, Ebert BL, Gillette MA, et al. Gene set enrichment analysis: a knowledge-based approach for interpreting genome-wide expression profiles. Proc Natl Acad Sci U S A. 2005;102(43):15545-50.

166. Kuleshov MV, Jones MR, Rouillard AD, Fernandez NF, Duan Q, Wang Z, et al. Enrichr: a comprehensive gene set enrichment analysis web server 2016 update. Nucleic Acids Res. 2016;44(W1):W90-7.

167. Sanjana NE, Shalem O, Zhang F. Improved vectors and genome-wide libraries for CRISPR screening. Nat Methods. 2014;11(8):783-4.

168. De Raedt T, Beert E, Pasmant E, Luscan A, Brems H, Ortonne N, et al. PRC2 loss amplifies Ras-driven transcription and confers sensitivity to BRD4-based therapies. Nature. 2014;514(7521):247-51.

169. Hogg SJ, Newbold A, Vervoort SJ, Cluse LA, Martin BP, Gregory GP, et al. BET Inhibition Induces Apoptosis in Aggressive B-Cell Lymphoma via Epigenetic Regulation of BCL-2 Family Members. Mol Cancer Ther. 2016;15(9):2030-41.

170. Harbinski F, Craig VJ, Sanghavi S, Jeffery D, Liu L, Sheppard KA, et al. Rescue screens with secreted proteins reveal compensatory potential of receptor tyrosine kinases in driving cancer growth. Cancer Discov. 2012;2(10):948-59.

171. Wilson TR, Fridlyand J, Yan Y, Penuel E, Burton L, Chan E, et al. Widespread potential for growth-factor-driven resistance to anticancer kinase inhibitors. Nature. 2012;487(7408):505-9.

172. Santarius T, Shipley J, Brewer D, Stratton MR, Cooper CS. A census of amplified and overexpressed human cancer genes. Nat Rev Cancer. 2010;10(1):59-64.

173. Sack LM, Davoli T, Li MZ, Li Y, Xu Q, Naxerova K, et al. Profound Tissue Specificity in Proliferation Control Underlies Cancer Drivers and Aneuploidy Patterns. Cell. 2018;173(2):499-514 e23.

174. Pavlova NN, Pallasch C, Elia AE, Braun CJ, Westbrook TF, Hemann M, et al. A role for PVRL4-driven cell-cell interactions in tumorigenesis. Elife. 2013;2:e00358.

175. Taube JH, Herschkowitz JI, Komurov K, Zhou AY, Gupta S, Yang J, et al. Core epithelial-to-mesenchymal transition interactome gene-expression signature is associated

with claudin-low and metaplastic breast cancer subtypes. Proc Natl Acad Sci U S A. 2010;107(35):15449-54.

176. Chan AM, Miki T, Meyers KA, Aaronson SA. A human oncogene of the RAS superfamily unmasked by expression cDNA cloning. Proc Natl Acad Sci U S A. 1994;91(16):7558-62.

177. Graham SM, Cox AD, Drivas G, Rush MG, D'Eustachio P, Der CJ. Aberrant function of the Ras-related protein TC21/R-Ras2 triggers malignant transformation. Mol Cell Biol. 1994;14(6):4108-15.

178. Movilla N, Crespo P, Bustelo XR. Signal transduction elements of TC21, an oncogenic member of the R-Ras subfamily of GTP-binding proteins. Oncogene. 1999;18(43):5860-9.

179. Murphy GA, Graham SM, Morita S, Reks SE, Rogers-Graham K, Vojtek A, et al. Involvement of phosphatidylinositol 3-kinase, but not RalGDS, in TC21/R-Ras2-mediated transformation. J Biol Chem. 2002;277(12):9966-75.

180. Rosario M, Paterson HF, Marshall CJ. Activation of the Ral and phosphatidylinositol 3' kinase signaling pathways by the ras-related protein TC21. Mol Cell Biol. 2001;21(11):3750-62.

181. Hunter JC, Manandhar A, Carrasco MA, Gurbani D, Gondi S, Westover KD. Biochemical and Structural Analysis of Common Cancer-Associated KRAS Mutations. Mol Cancer Res. 2015;13(9):1325-35.

182. Toretsky JA, Jenson J, Sun CC, Eskenazi AE, Campbell A, Hunger SP, et al. Translocation (11;15;19): a highly specific chromosome rearrangement associated with poorly differentiated thymic carcinoma in young patients. Am J Clin Oncol. 2003;26(3):300-6.

183. Rowland BD, Peeper DS. KLF4, p21 and context-dependent opposing forces in cancer. Nat Rev Cancer. 2006;6(1):11-23.

184. Farrugia MK, Sharma SB, Lin CC, McLaughlin SL, Vanderbilt DB, Ammer AG, et al. Regulation of anti-apoptotic signaling by Kruppel-like factors 4 and 5 mediates lapatinib resistance in breast cancer. Cell Death Dis. 2015;6:e1699.

185. Lund RJ, Huhtinen K, Salmi J, Rantala J, Nguyen EV, Moulder R, et al. DNA methylation and Transcriptome Changes Associated with Cisplatin Resistance in Ovarian Cancer. Sci Rep. 2017;7(1):1469.

186. Polo JM, Anderssen E, Walsh RM, Schwarz BA, Nefzger CM, Lim SM, et al. A molecular roadmap of reprogramming somatic cells into iPS cells. Cell. 2012;151(7):1617-32.

187. McCleland ML, Mesh K, Lorenzana E, Chopra VS, Segal E, Watanabe C, et al. CCAT1 is an enhancer-templated RNA that predicts BET sensitivity in colorectal cancer. J Clin Invest. 2016;126(2):639-52.

188. Xiang JF, Yin QF, Chen T, Zhang Y, Zhang XO, Wu Z, et al. Human colorectal cancer-specific CCAT1-L lncRNA regulates long-range chromatin interactions at the MYC locus. Cell Res. 2014;24(5):513-31.

189. Dyson NJ. RB1: a prototype tumor suppressor and an enigma. Genes Dev. 2016;30(13):1492-502.

190. Schulze A, Zerfass K, Spitkovsky D, Middendorp S, Berges J, Helin K, et al. Cell cycle regulation of the cyclin A gene promoter is mediated by a variant E2F site. Proc Natl Acad Sci U S A. 1995;92(24):11264-8.

191. Schmitz R, Young RM, Ceribelli M, Jhavar S, Xiao W, Zhang M, et al. Burkitt lymphoma pathogenesis and therapeutic targets from structural and functional genomics. Nature. 2012;490(7418):116-20.

192. Koepp DM, Schaefer LK, Ye X, Keyomarsi K, Chu C, Harper JW, et al. Phosphorylation-dependent ubiquitination of cyclin E by the SCFFbw7 ubiquitin ligase. Science. 2001;294(5540):173-7.

193. Welcker M, Orian A, Jin J, Grim JE, Harper JW, Eisenman RN, et al. The Fbw7 tumor suppressor regulates glycogen synthase kinase 3 phosphorylation-dependent c-Myc protein degradation. Proc Natl Acad Sci U S A. 2004;101(24):9085-90.

194. Yada M, Hatakeyama S, Kamura T, Nishiyama M, Tsunematsu R, Imaki H, et al. Phosphorylation-dependent degradation of c-Myc is mediated by the F-box protein Fbw7. EMBO J. 2004;23(10):2116-25.

195. Chou TC, Talalay P. Quantitative analysis of dose-effect relationships: the combined effects of multiple drugs or enzyme inhibitors. Adv Enzyme Regul. 1984;22:27-55.

196. Liu S, Edgerton SM, Moore DH, 2nd, Thor AD. Measures of cell turnover (proliferation and apoptosis) and their association with survival in breast cancer. Clin Cancer Res. 2001;7(6):1716-23.

197. Rickman DS, Schulte JH, Eilers M. The Expanding World of N-MYC-Driven Tumors. Cancer Discov. 2018;8(2):150-63.

198. Dela Cruz FS, Diolaiti D, Turk AT, Rainey AR, Ambesi-Impiombato A, Andrews SJ, et al. A case study of an integrative genomic and experimental therapeutic approach for rare tumors: identification of vulnerabilities in a pediatric poorly differentiated carcinoma. Genome Med. 2016;8(1):116.

199. Ohba Y, Mochizuki N, Yamashita S, Chan AM, Schrader JW, Hattori S, et al. Regulatory proteins of R-Ras, TC21/R-Ras2, and M-Ras/R-Ras3. J Biol Chem. 2000;275(26):20020-6.

200. Carlino MS, Fung C, Shahheydari H, Todd JR, Boyd SC, Irvine M, et al. Preexisting MEK1P124 mutations diminish response to BRAF inhibitors in metastatic melanoma patients. Clin Cancer Res. 2015;21(1):98-105.

201. Regard JB, Cherman N, Palmer D, Kuznetsov SA, Celi FS, Guettier JM, et al. Wnt/beta-catenin signaling is differentially regulated by Galpha proteins and contributes to fibrous dysplasia. Proc Natl Acad Sci U S A. 2011;108(50):20101-6.

202. Wilson CH, McIntyre RE, Arends MJ, Adams DJ. The activating mutation R201C in GNAS promotes intestinal tumourigenesis in Apc(Min/+) mice through activation of Wnt and ERK1/2 MAPK pathways. Oncogene. 2010;29(32):4567-75.

203. Nomura R, Saito T, Mitomi H, Hidaka Y, Lee SY, Watanabe S, et al. GNAS mutation as an alternative mechanism of activation of the Wnt/beta-catenin signaling pathway in gastric adenocarcinoma of the fundic gland type. Hum Pathol. 2014;45(12):2488-96.

204. Bertherat J, Horvath A, Groussin L, Grabar S, Boikos S, Cazabat L, et al. Mutations in regulatory subunit type 1A of cyclic adenosine 5'-monophosphate-dependent protein kinase (PRKAR1A): phenotype analysis in 353 patients and 80 different genotypes. J Clin Endocrinol Metab. 2009;94(6):2085-91.

205. Horvath A, Bertherat J, Groussin L, Guillaud-Bataille M, Tsang K, Cazabat L, et al. Mutations and polymorphisms in the gene encoding regulatory subunit type 1-alpha of protein kinase A (PRKAR1A): an update. Hum Mutat. 2010;31(4):369-79.

206. Almeida MQ, Muchow M, Boikos S, Bauer AJ, Griffin KJ, Tsang KM, et al. Mouse Prkar1a haploinsufficiency leads to an increase in tumors in the Trp53+/- or Rb1+/- backgrounds and chemically induced skin papillomas by dysregulation of the cell cycle and Wnt signaling. Hum Mol Genet. 2010;19(8):1387-98.

207. Basso F, Rocchetti F, Rodriguez S, Nesterova M, Cormier F, Stratakis CA, et al. Comparison of the effects of PRKAR1A and PRKAR2B depletion on signaling pathways, cell growth, and cell cycle control of adrenocortical cells. Horm Metab Res. 2014;46(12):883-8.

208. Nadella KS, Kirschner LS. Disruption of protein kinase a regulation causes immortalization and dysregulation of D-type cyclins. Cancer Res. 2005;65(22):10307-15.

209. Nesterova M, Bossis I, Wen F, Horvath A, Matyakhina L, Stratakis CA. An immortalized human cell line bearing a PRKAR1A-inactivating mutation: effects of overexpression of the wild-type Allele and other protein kinase A subunits. J Clin Endocrinol Metab. 2008;93(2):565-71.

210. Robinson-White A, Hundley TR, Shiferaw M, Bertherat J, Sandrini F, Stratakis CA. Protein kinase-A activity in PRKAR1A-mutant cells, and regulation of mitogen-activated protein kinases ERK1/2. Hum Mol Genet. 2003;12(13):1475-84.

211. Robinson-White A, Meoli E, Stergiopoulos S, Horvath A, Boikos S, Bossis I, et al. PRKAR1A Mutations and protein kinase A interactions with other signaling pathways in the adrenal cortex. J Clin Endocrinol Metab. 2006;91(6):2380-8.

212. Robinson-White AJ, Leitner WW, Aleem E, Kaldis P, Bossis I, Stratakis CA. PRKAR1A inactivation leads to increased proliferation and decreased apoptosis in human B lymphocytes. Cancer Res. 2006;66(21):10603-12.

213. Inman GJ. Switching TGFbeta from a tumor suppressor to a tumor promoter. Curr Opin Genet Dev. 2011;21(1):93-9.

214. Shalem O, Sanjana NE, Hartenian E, Shi X, Scott DA, Mikkelsen TS, et al. Genome-scale CRISPR-Cas9 knockout screening in human cells. Science. 2014;343(6166):84-7.

215. Blomen VA, Majek P, Jae LT, Bigenzahn JW, Nieuwenhuis J, Staring J, et al. Gene essentiality and synthetic lethality in haploid human cells. Science. 2015;350(6264):1092-6.

216. Martincorena I, Raine KM, Gerstung M, Dawson KJ, Haase K, Van Loo P, et al. Universal Patterns of Selection in Cancer and Somatic Tissues. Cell. 2017;171(5):1029-41 e21.

217. Weber J, McCormack PL. Panitumumab: in metastatic colorectal cancer with wild-type KRAS. BioDrugs. 2008;22(6):403-11.

218. Peeters M, Douillard JY, Van Cutsem E, Siena S, Zhang K, Williams R, et al. Mutant KRAS codon 12 and 13 alleles in patients with metastatic colorectal cancer: assessment as prognostic and predictive biomarkers of response to panitumumab. J Clin Oncol. 2013;31(6):759-65.

219. Kim E. Functional characterization of genetic alterations in cancer: Harvard University; 2016.

220. Cuykendall TN, Rubin MA, Khurana E. Non-coding genetic variation in cancer. Curr Opin Syst Biol. 2017;1:9-15.

221. Zhang Z, Newton K, Kummerfeld SK, Webster J, Kirkpatrick DS, Phu L, et al. Transcription factor Etv5 is essential for the maintenance of alveolar type II cells. Proc Natl Acad Sci U S A. 2017;114(15):3903-8.

222. Ding L, Getz G, Wheeler DA, Mardis ER, McLellan MD, Cibulskis K, et al. Somatic mutations affect key pathways in lung adenocarcinoma. Nature. 2008;455(7216):1069-75.

223. Ciriello G, Cerami E, Sander C, Schultz N. Mutual exclusivity analysis identifies oncogenic network modules. Genome Res. 2012;22(2):398-406.

224. Cancer Genome Atlas Research N. Comprehensive genomic characterization defines human glioblastoma genes and core pathways. Nature. 2008;455(7216):1061-8.

225. Yeang CH, McCormick F, Levine A. Combinatorial patterns of somatic gene mutations in cancer. FASEB J. 2008;22(8):2605-22.